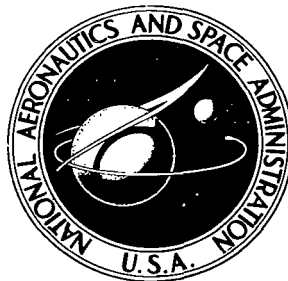


NASA TECHNICAL NOTE



NASA TN D-6425

2.1

NASA TN D-6425

LOAN COPY: RETURN
AFWL (DOGL)
KIRTLAND AFB, N



STATIC FORCE TESTS OF A MODEL OF
A TWIN-JET FIGHTER AIRPLANE FOR
ANGLES OF ATTACK FROM -10° TO 110°
AND SIDESLIP ANGLES FROM -40° TO 40°

by Ernie L. Anglin
Langley Research Center
Hampton, Va. 23365



0132839

1. Report No. NASA TN D-6425	2. Government Accession No.	3. Recipit	0132839	
4. Title and Subtitle STATIC FORCE TESTS OF A MODEL OF A TWIN-JET FIGHTER AIRPLANE FOR ANGLES OF ATTACK FROM -10° TO 110° AND SIDESLIP ANGLES FROM -40° TO 40°		5. Report Date August 1971	6. Performing Organization Code	
		8. Performing Organization Report No. L-7808	10. Work Unit No. 136-63-02-04	
7. Author(s) Ernie L. Anglin		11. Contract or Grant No.		
		13. Type of Report and Period Covered Technical Note		
9. Performing Organization Name and Address NASA Langley Research Center Hampton, Va. 23365		14. Sponsoring Agency Code		
		12. Sponsoring Agency Name and Address National Aeronautics and Space Administration Washington, D.C. 20546		
15. Supplementary Notes				
16. Abstract <p>An investigation was conducted to obtain a set of static-force-test data for use as aerodynamic inputs to theoretical spin studies. Control-effectiveness tests were made for each control individually and for a full left pro-spin combination of controls. The results are presented without detailed analysis, but are analyzed in terms of factors which would affect their applicability for use in spin theory. Several data characteristics are indicated that are deemed to be of significance with regard to their intended use in theoretical spin studies.</p>				
17. Key Words (Suggested by Author(s)) Static force tests Twin-jet fighter airplane Control effectiveness		18. Distribution Statement Unclassified - Unlimited		
19. Security Classif. (of this report) Unclassified	20. Security Classif. (of this page) Unclassified	21. No. of Pages 89	22. Price* \$3.00	

STATIC FORCE TESTS OF A MODEL OF A TWIN-JET FIGHTER
AIRPLANE FOR ANGLES OF ATTACK FROM -10° TO 110°
AND SIDESLIP ANGLES FROM -40° TO 40°

By Ernie L. Anglin
Langley Research Center

SUMMARY

A wind-tunnel investigation was conducted on a 0.13-scale model of a twin-jet fighter airplane to obtain a set of static longitudinal and lateral-directional aerodynamic coefficients for use as inputs to a theoretical spin study. The tests were made for an angle-of-attack range of -10° to 110° and a sideslip-angle range of $\pm 40^{\circ}$. Control-effectiveness tests were made for each control deflected individually and for a full left pro-spin combination of control deflections.

The data are analyzed with respect to their intended use in spin theory. It was found that the data were repeatable and had no significant hysteresis effects. The lateral data had large nonlinear variations with sideslip angle over at least a portion of the angle-of-attack range. Deflection of the horizontal tail to the maximum stick-back position had significant effects on the yawing stability derivative in the spin-entry and developed-spin angle-of-attack ranges. The lateral control effectiveness for full left pro-spin control deflections was not the same as the sum of the effectiveness of each control individually deflected. The longitudinal control effectiveness was the same for the full left pro-spin control deflections as for horizontal tail alone.

INTRODUCTION

The Langley Research Center of the National Aeronautics and Space Administration is currently engaged in a research program to develop and validate theoretical methods for prediction of airplane spin characteristics. A large part of this program involves correlation between spin motions based on theoretical spin calculation and experimental spin motions obtained with dynamically scaled radio-controlled models. Theoretical spin calculations are at present normally made by using aerodynamic inputs and equations of motion similar to those described in references 1 and 2. A previous attempt was made to validate these theoretical spin methods with the use of a model of a variable-sweep fighter airplane with a long pointed nose; the results of that investigation are presented in detail in reference 3. For that configuration, the results showed very poor

correlation between theoretical and experimental spin motions because large random asymmetric yawing moments were produced by flow separation off the pointed nose at high angles of attack.

An investigation was undertaken to obtain a set of static aerodynamic data on a second configuration, a twin-jet swept-wing fighter airplane, for potential use as aerodynamic inputs for spin theory so that further efforts could be made to correlate theoretical spin motions with experimental spin motions. Preliminary force tests of this configuration indicated that the data obtained were repeatable and showed no large variations of yawing moment, such as occurred for the model of reference 3. Several additional investigations have been made regarding the stall and/or spin characteristics of this particular configuration. Some factors affecting the lateral-directional characteristics at the stall have been reported in reference 4. The aerodynamic factors affecting flat-spin tendencies are presented in reference 5.

The current series of wind-tunnel tests were conducted for the purpose of obtaining a set of static- and dynamic-force-test aerodynamic data with the use of the same individual model which is intended to be used for the free-flight radio-controlled experimental spin work. The results of the dynamic force tests for this particular model have been reported in reference 6. The investigation reported herein consisted of the static wind-tunnel force tests for this particular configuration over the angle-of-attack and sideslip-angle ranges associated with spinning. The study included control-effectiveness tests to determine the effects of each individual control. In addition, at angles of attack beyond the stall, the effects of combinations of controls that would correspond to pro-spin and/or recommended spin-recovery controls were determined. The present tests were conducted at a tunnel velocity approximately equal to the expected velocity of the proposed free-flight model during spins.

The present tests were conducted only to provide aerodynamic data for theoretical spin studies. Thus, the test results are presented with brief analyses or comments only on those data characteristics that are deemed to be of significance with regard to their intended use in theoretical spin studies.

SYMBOLS

All forces and moments presented herein are referred to the body system of axes, as shown in figure 1. The moment data are referred to a center-of-gravity position of 33 percent of the wing mean aerodynamic chord. In order to facilitate international usage of the aerodynamic data presented, dimensional quantities are presented both in the International System of Units (SI) and in the U.S. Customary Units. Measurements

were made in U.S. Customary Units and equivalent dimensions were determined by using the conversion factors given in reference 7.

b wing span, m (ft)

\bar{c} mean aerodynamic chord of wing, m (ft)

\bar{c}_t mean aerodynamic chord of horizontal tail, m (ft)

C_l rolling-moment coefficient, $\frac{M_X}{q_\infty S b}$

$C_{l_\beta} = \frac{\partial C_l}{\partial \beta}$, per deg or per rad

C_m pitching-moment coefficient, $\frac{M_Y}{q_\infty S \bar{c}}$

C_n yawing-moment coefficient, $\frac{M_Z}{q_\infty S b}$

$C_{n_\beta} = \frac{\partial C_n}{\partial \beta}$, per deg or per rad

$C_{n_{\delta_a}}$ yawing-moment coefficient due to aileron deflection, per deg

$C_{n_{\delta_r}}$ yawing-moment coefficient due to rudder deflection, per deg

C_X longitudinal-force coefficient, $\frac{F_X}{q_\infty S}$

C_Y side-force coefficient, $\frac{F_Y}{q_\infty S}$

$C_{Y_\beta} = \frac{\partial C_Y}{\partial \beta}$, per deg or per rad

C_Z normal-force coefficient, $\frac{F_Z}{q_\infty S}$

F_X	longitudinal force acting along X body axis, N (lb)
F_Y	lateral force acting along Y body axis, N (lb)
F_Z	normal force acting along Z body axis, N (lb)
I_X, I_Y, I_Z	moments of inertia about X, Y, and Z body axes, respectively, kg-m ² (slug-ft ²)
M_X	rolling moment acting about X body axis, m-N (ft-lb)
M_Y	pitching moment acting about Y body axis, m-N (ft-lb)
M_Z	yawing moment acting about Z body axis, m-N (ft-lb)
p, q, r	angular velocities about X, Y, and Z body axes, respectively, rad/sec
q_∞	free-stream dynamic pressure, $\rho V^2/2$, N/m ² (lb/ft ²)
S	wing area, m ² (ft ²)
u, v, w	linear velocities along X, Y, and Z body axes, respectively, m/sec (ft/sec)
V	free-stream velocity, m/sec (ft/sec)
V_R	resultant linear velocity, m/sec (ft/sec)
X, Y, Z	body reference axes
X_e, Y_e, Z_e	earth reference axes
α	angle of attack, deg or rad
β	angle of sideslip, deg or rad
$\delta_{a,L}, \delta_{a,R}$	left and right aileron deflection, respectively, with respect to chord line of wing, positive when trailing edge of aileron is down, deg

- δ_h horizontal-tail (elevator) deflection with respect to fuselage reference line, positive when trailing edge of elevator is down, deg
- δ_r rudder deflection with respect to vertical tail, positive when trailing edge is to left, deg
- $\delta_{s,L}, \delta_{s,R}$ left and right spoiler deflection, respectively, with respect to wing surface, positive when trailing edge of spoiler is down, deg
- ρ air density, kg/m³ (slugs/ft³)
- θ angle of pitch, deg or rad
- ϕ angle of roll, deg or rad
- ψ angle of yaw, deg or rad

A Δ with a coefficient represents an incremental difference between a control-deflected value and a control-neutral value of that coefficient; for example,

$$\Delta C_Y = (C_Y)_{\text{control deflected}} - (C_Y)_{\text{control neutral}}$$

MODEL

The force-test investigation was conducted with a 0.13-scale model of a two-place twin-jet high-performance fighter airplane designed for land and carrier-based operations. A three-view sketch showing the general layout of the model is presented in figure 2, a photograph of the model is shown in figure 3, and the geometric characteristics of the full-scale airplane are listed in table I. The longitudinal control system of the configuration consists of an all-movable horizontal tail which incorporates 23° of negative dihedral to satisfy longitudinal stability requirements in the normal operational flight range. Lateral control is provided by spoilers and ailerons in combination. The ailerons deflect downward only whereas the spoilers deflect upward only. The left aileron and right spoiler operate simultaneously as do the right aileron and left spoiler. The directional-control system consists of a conventional rudder. The maximum control-surface deflections are as follows:

Horizontal-tail (elevator) deflection (trailing edge), deg	21 up, 9 down
Aileron deflection, deg	0 up, 30 down
Spoiler deflection, deg	45 up, 0 down
Rudder deflection, deg	±30

TUNNEL AND TEST APPARATUS

The investigation was conducted in the 9.1- by 18.3-meter (30- by 60-foot) open-throat test section of the Langley full-scale tunnel. The model was so small in proportion to the tunnel test section that no wind-tunnel jet-boundary or blockage corrections were required.

The tests were made with the model mounted in the tunnel on the sting-support system as shown in figure 4. For angles of attack from -10° to 22.5° , the model was mounted on the sting as shown in figure 4(a). For the higher angles of attack, the model was mounted with the sting through the top of the model and the nose of the model toward the base of the sting support. (See fig. 4(b).) The angle of sideslip is varied by changing the yaw angle of the support strut about the vertical axis. The forces and moments were measured with a six-component internal strain-gage balance; 10 values were recorded and averaged to obtain the final value of each data point presented herein.

TESTS

The force tests were conducted in the Langley full-scale tunnel at a speed of approximately 30.78 meters per second (101 ft/sec) which corresponds to a Reynolds number of about 1.35×10^6 based on wing mean aerodynamic chord.

Tests were made for the complete model at angles of attack from -10° to 22.5° over a sideslip-angle range of $\pm 20^{\circ}$. In this relatively low angle-of-attack range, control effectiveness was measured, with the effect of each control being determined separately. For the higher angles of attack (25° to 110°), the sideslip-angle range was extended to $\pm 40^{\circ}$. In the high angle-of-attack range, control effectiveness was also measured for each control separately and, in addition, the effectiveness of a set of combination controls was investigated. Some brief tests were conducted with horizontal tails removed. Some repeat runs were made to investigate the repeatability of the data (or data scatter) and hysteresis effects.

Typical loading conditions for this configuration result in most of the mass being distributed along the fuselage, with values of I_Y and I_Z more than five times as great as I_X . For a mass loading of this type, the recommended spin-recovery control technique is simultaneous movement of the ailerons to full with the spin (stick right in a right spin), rudder to full against the direction of rotation, and elevators remaining in the original elevator-up setting (stick full back). (See ref. 1.) The set of combination controls investigated herein may be interpreted as pro-spin controls for a left spin or recovery controls for a right spin.

PRESENTATION OF RESULTS

The results of the wind-tunnel tests are presented in figures 5 to 13 as indicated in the following table:

Figure	Data presented	Effects of -
5	C_Z, C_X, C_m plotted against α	β, δ_h , and hysteresis
6	$\Delta C_Z, \Delta C_X, \Delta C_m$ plotted against α	Comparison of effectiveness of different control combinations on static longitudinal coefficients
7	C_Y, C_n, C_l plotted against β	α and δ_r
8	C_Y, C_n, C_l plotted against α	Asymmetries at $\beta = 0^\circ$
9	C_Y, C_n, C_l plotted against β	α and δ_a
10	C_Y, C_n, C_l plotted against β	α and combined left pro-spin controls
11	C_Y, C_n, C_l plotted against β	α and δ_h
12	$C_{Y\beta}, C_{n\beta}, C_{l\beta}$ plotted against α	δ_h
13	$\Delta C_Y, \Delta C_n, \Delta C_l$ plotted against α	Comparison of effectiveness of different control combinations on static lateral coefficients

DISCUSSION OF RESULTS

The present wind-tunnel investigation was made to obtain a set of longitudinal and lateral-directional static-force-test aerodynamic data with the use of the same individual model which is intended to be used for free-flight radio-controlled experimental spin work. The investigation was conducted solely to provide aerodynamic data for use as inputs for theoretical spin studies. The aerodynamic data thus obtained and presented herein is believed to be an excellent overall set of force-test data in that all the data, including specifically the data above the stall and at developed-spin angles of attack, were highly repeatable, as can be seen from the many repeat points shown in figures 5 to 13. The test results are presented with only brief analyses or comments on those data characteristics that are deemed to be of significance with regard to their intended use in theoretical spin studies.

Longitudinal Characteristics

Variation with angle of attack.- The static longitudinal coefficients of the model as functions of angles of attack and sideslip are presented in figure 5. Some static longitudinal tests for controls neutral ($\delta_h = 0^\circ$) were made with angle of attack increasing

and some tests were made with angle of attack decreasing. A comparison of the longitudinal data from these two tests shows no significant differences. This result indicates that there are no significant hysteresis effects nor any significant scatter in the longitudinal data for this configuration.

Results are also shown in figure 5 for the model with horizontal-tail deflection angles of -21° and 7° and with horizontal tails off. The variation of longitudinal- and normal-force coefficients presented in figure 5(g), for zero sideslip angle and neutral controls ($\delta_h = 0^{\circ}$), indicates that flow separation and stall begin to appear at an angle of attack of about 12° to 15° . An examination of the pitching-moment variation in figure 5(g) indicates that the model is mildly unstable over a small angle-of-attack range just at the onset of the stall ($\alpha = 12^{\circ}$ to 18°), but is thereafter statically stable throughout the higher angle-of-attack range. The results obtained also show that the same region of static instability near the stall is present with the horizontal tails off as with the horizontal tail on and, therefore, this instability is apparently related to wing stall.

Variation with sideslip angle.- A comparison of the pitching-moment results presented in figure 5 indicates that throughout the developed-spin angle-of-attack range ($\alpha = 45^{\circ}$ to 85°), there is generally no effect of sideslip angle on the pitching moment over a sideslip-angle range of $\pm 20^{\circ}$. The pitching moment becomes only very slightly more nose-up in magnitude at the larger sideslip angles. Thus, for this configuration, the wind-tunnel data show no significant difference in the static pitching moments which would be acting during either the steady developed spin, where the sideslip angles remain small, or during the oscillatory developed spin, where the sideslip angles may exceed $\pm 30^{\circ}$. (See ref. 8 for spin-tunnel test results.)

Elevator effectiveness.- The longitudinal data shown in figure 5(g) indicate that the elevator control effectiveness is sufficient with stick full back ($\delta_h = -21^{\circ}$) to trim the model at an angle of attack of approximately 28° , which is well above the stall. The stick-back control effectiveness decreases to a minimum at about $\alpha = 60^{\circ}$, but then increases with further increases in α . Control effectiveness for stick full forward ($\delta_h = 7^{\circ}$) decreases to near zero at $\alpha = 60^{\circ}$ and remains near zero at all higher angles of attack.

Effects of different control combinations.- A comparison of the longitudinal effects of two different control combinations, horizontal tail alone and full left pro-spin controls, is presented in figure 6. These results show that there are only small differences evidenced in normal-force and pitching-moment coefficients when full left pro-spin controls are used instead of horizontal tail alone. Some larger differences do exist in the longitudinal-force coefficient. It is believed, however, that these differences in longitudinal-force coefficient would not significantly affect the developed-spin characteristics.

Lateral-Directional Characteristics

Variation with angle of attack.- The static lateral-directional stability coefficients of the model as functions of angles of attack and sideslip are presented in figure 7. These results indicate that with all controls neutral ($\delta_r = 0^\circ$) the model is directionally stable (positive slope of C_n plotted against β for small values of β) up to an angle of attack of 20° and directionally unstable at all higher angles of attack. In addition, the effective dihedral (negative slope of C_l plotted against β for small values of β) increases from $\alpha = 0^\circ$ to $\alpha = 15^\circ$. But, where the longitudinal data show flow separation and stall to begin, at about $\alpha = 15^\circ$, a reduction in effective dihedral occurs, with the slope of C_l against β becoming positive at $\alpha = 30^\circ$. This combination of directional instability and lack of effective dihedral at angles of attack just beyond the stall are conducive to directional-divergence problems which could lead to inadvertent spin entries. A more detailed discussion regarding the directional divergence of this configuration is presented in reference 4.

An examination of the lateral coefficients presented in figure 7 shows that each of the coefficients exhibit nonlinearities with respect to sideslip angle over at least a portion of the angle-of-attack range. Near the stall angle of attack, these nonlinearities generally occur at $\beta = \pm 10^\circ$ or $\beta = \pm 15^\circ$. At angles of attack representative of those for the developed spin ($\alpha = 45^\circ$ to 85°), these nonlinearities do not generally occur until the sideslip angles exceed $\pm 20^\circ$. The spin-tunnel test results, reported in reference 8, show that this configuration has an oscillatory developed spin with roll angles of over $\pm 30^\circ$. Since spin recoveries are normally even more oscillatory than the equilibrium developed spin, it will be necessary to include all aerodynamic nonlinearities with respect to sideslip in any theoretical spin study for this configuration.

The lateral force tests of a different configuration, reported in reference 3, showed the existence of large asymmetric yawing moments but they were random and nonrepeatable at high angles of attack (α approximately 60° to 70°) and zero sideslip. These nonrepeatable yawing moments contributed to a lack of correlation between spin theory and experimental flight results for the configuration. The data of figure 7 show that the present configuration also has some lateral asymmetries, but that all the lateral data, including the asymmetries, were closely repeatable. The asymmetries of the present model are summarized in figure 8, where the lateral-directional coefficients at zero sideslip are presented as a function of angle of attack. As can be seen, only small asymmetries occurred in C_n , with a maximum value of 0.024 occurring at $\alpha = 85^\circ$.

Rudder effectiveness.- The rudder control effectiveness is also shown in figure 7 for both left (30°) and right (-30°) rudder deflections. The rudder shows very good effectiveness in producing yawing moment up to $\alpha = 30^\circ$. But, at all higher angles of

attack, the rudder effectiveness dropped off until it became zero and it remained near zero, as would be expected.

It should be noted that the rudder effectiveness in particular, and indeed all combinations of lateral controls investigated, showed a variation in the magnitude of control effectiveness with sideslip angle. If the control effectiveness data as reported herein were obtained in a normal manner, only a control effectiveness coefficient in the form of, for example, $C_{n\delta_r}$ or $C_{n\delta_a}$ at $\beta = 0^\circ$ would be obtained. To use this type of aerodynamic control input in a theoretical spin study as has normally been done in the past (see refs. 1 and 2) would presume no control effectiveness variations with sideslip. Although nothing is presently known concerning the significance of these variations in magnitude of control effectiveness with sideslip on the spin entry, developed spin, or recovery motions, it would seem to be advisable to include these variations in any proposed theoretical spin study.

Aileron and spoiler effectiveness.- The effect of roll control deflections (combined aileron and spoiler) on the lateral-directional stability coefficients is shown in figure 9. The magnitude of the effectiveness of the roll control on C_l at $\alpha = 0^\circ$ decreases by approximately 50 percent at $\alpha = 15^\circ$. The roll effectiveness remains near that magnitude from $\alpha = 15^\circ$ to $\alpha = 30^\circ$, the angle-of-attack range within which the directional divergence will occur. At all angles of attack above 40° , the roll control effectiveness on C_l drops off to zero and remains near zero.

The effect of roll control deflections on C_n is practically zero at angles of attack from -10° to 12.5° ; then an adverse effect occurs around $\alpha = 20^\circ$ to 25° . At higher angles of attack, the trends are not consistent in magnitude or even direction.

Full left pro-spin control effectiveness.- The effects on the lateral-directional stability coefficients of deflecting all controls to their full left pro-spin deflections is shown in figure 10. Through the developed-spin angle-of-attack range ($\alpha = 45^\circ$ to 85°), only C_n shows any effect due to the left pro-spin control deflections. The effects on C_n , however, again do not show any consistent pattern with regard to magnitude or even direction. At flat-spin angles of attack of $\alpha = 85^\circ$ to $\alpha = 90^\circ$, even these combined pro-spin controls show very little effects on C_n and practically zero effects on C_l . This near-zero control effectiveness would explain the poor spin-recovery characteristics of this configuration from these flat spins. (See refs. 5 and 8.)

Effect of horizontal-tail position.- The effect of horizontal-tail position on the static lateral-directional stability coefficients is presented in figure 11. The horizontal-tail position has some effect on yawing moment at larger sideslip angles over the entire angle-of-attack range. In the angle-of-attack range from $\alpha = 50^\circ$ to $\alpha = 70^\circ$, the stick-full-back position ($\delta_h = -21^\circ$) causes some relatively large differences in yawing

moment at small sideslip angles. These effects of horizontal-tail position at small sideslip angles are summarized in figure 12, where the static lateral-directional stability derivatives are presented as a function of angle of attack. Figure 12 shows that deflection of the horizontal tail to stick-full-back position ($\delta_h = -21^\circ$) caused the directional instability above the stall to be much more severe up to an angle of attack of about 60° , and again at angles of attack above 85° . These results indicate the probability of an interference effect between the horizontal and vertical tails at these angles of attack. Horizontal-tail position had very little effect on $C_{Y\beta}$ or $C_{l\beta}$.

Effects of different control combinations.- A comparison of the effectiveness of different control combinations on the static lateral-directional stability coefficients for $\beta = 0^\circ$ is presented in figure 13. The data points shown in figure 13 are taken directly from the data shown in figures 7 to 12. The relative magnitudes of the effectiveness of rudder and roll controls on the lateral-directional coefficients are indicated. As can be seen, at developed-spin angles of attack, several combinations of controls would have some small effect on C_n whereas no combination of controls would produce any significant rolling moment.

If the control effectiveness data as reported herein were reduced to the usual form of $C_{n\delta_a}$ and $C_{n\delta_r}$, as mentioned previously, and used as inputs in a theoretical spin study, their use in a normal manner would mean that the effectiveness of two or more controls individually would be added to account for these controls being deflected simultaneously. Figure 13 shows that the lateral control effectiveness for full left pro-spin control deflections is not the same as the sum of the effectiveness of each control individually deflected. Since rolling moment is the primary spin-recovery moment for this configuration and since the measured magnitudes of rolling moment in the developed-spin angle-of-attack range are so small (essentially zero), even a relatively small rolling-moment error in that angle-of-attack range could give an erroneous picture of the spin-recovery potential. Therefore, it is deemed advisable to include these control effectiveness variations in any proposed theoretical spin study.

CONCLUDING REMARKS

Static wind-tunnel force tests were made on a 0.13-scale model of a twin-jet fighter airplane over an angle-of-attack range of -10° to 110° and a sideslip-angle range of $\pm 40^\circ$ to obtain aerodynamic input data for use in a theoretical spin study. An analysis of the data thus obtained indicates that the following data characteristics are deemed to be of particular significance with regard to their intended use in theoretical spin studies:

1. The data were highly consistent (i.e., repeatable) and had no significant hysteresis effects.

2. There was no significant effect of sideslip angle on the longitudinal data.
3. There were no significant differences evidenced in longitudinal control effectiveness when full left pro-spin controls were used instead of horizontal tail alone.
4. The model had large nonlinear variations of all lateral stability coefficients with sideslip angle over at least a portion of the angle-of-attack range.
5. Deflection of the horizontal tail to the stick-full-back position had significant effects on the yawing stability derivative in the spin-entry and developed-spin angle-of-attack ranges.
6. Lateral control effectiveness for full left pro-spin control deflections was not the same as the sum of the effectiveness of each control individually deflected.

Langley Research Center,
National Aeronautics and Space Administration,
Hampton, Va., July 2, 1971.

REFERENCES

1. Anglin, Ernie L.: Analytical Study of Effects of Product of Inertia on Airplane Spin Entries, Developed Spins, and Spin Recoveries. NASA TN D-2754, 1965.
2. Anglin, Ernie L.: Relationship Between Magnitude of Applied Spin Recovery Moment and Ensuing Number of Recovery Turns. NASA TN D-4077, 1967.
3. Chambers, Joseph R.; Anglin, Ernie L.; and Bowman, James S., Jr.: Effects of a Pointed Nose on Spin Characteristics of a Fighter Airplane Model Including Correlation With Theoretical Calculations. NASA TN D-5921, 1970.
4. Chambers, Joseph R.; and Anglin, Ernie L.: Analysis of Lateral-Directional Stability Characteristics of a Twin-Jet Fighter Airplane at High Angles of Attack. NASA TN D-5361, 1969.
5. Chambers, Joseph R.; Bowman, James S., Jr.; and Anglin, Ernie L.: Analysis of the Flat-Spin Characteristics of a Twin-Jet Swept-Wing Fighter Airplane. NASA TN D-5409, 1969.
6. Grafton, Sue B.; and Libbey, Charles E.: Dynamic Stability Derivatives of a Twin-Jet Fighter Model for Angles of Attack From -10° to 110° . NASA TN D-6091, 1971.
7. Mechtly, E. A.: The International System of Units - Physical Constants and Conversion Factors (Revised). NASA SP-7012, 1969.
8. Bowman, James S., Jr.; and White, William L.: Spin-Tunnel Investigation of a 1/30-Scale Model of the Fighter and Reconnaissance Versions of the McDonnell F-4B Airplane (Revised). NASA TM SX-1744, Naval Air Systems Command, 1969.

TABLE I.- GEOMETRIC CHARACTERISTICS OF AIRPLANE

Overall length	17.55 m (57.59 ft)
Wing:	
Span	11.71 m (38.41 ft)
Area (including leading-edge extension)	50.01 m ² (538.34 ft ²)
Root chord	716.28 cm (282.00 in.)
Tip chord	119.38 cm (47.00 in.)
Mean aerodynamic chord, \bar{c}	488.95 cm (192.50 in.)
Leading edge of \bar{c} rearward of leading edge of root chord	281.33 cm (110.76 in.)
Aspect ratio	2.82
Taper ratio	0.167
Sweepback of 25-percent-chord line	45.00°
Dihedral (inboard 69.5 percent b/2)	0°
Dihedral (outboard 69.5 percent b/2)	12.00°
Incidence	1.00°
Airfoil section:	
Root	NACA 0006.4-64 (modified)
Tip	NACA 0003.0-64 (modified)
Aileron:	
Area (one side)	1.23 m ² (13.26 ft ²)
Area (one side) rearward of hinge line	1.22 m ² (13.08 ft ²)
Span (one aileron) (from 44.5 to 67.0 percent b/2)	1.33 m (4.35 ft) or 22.5 percent b/2
Inboard end chord (base line 103.24 in. (262.23 cm))	96.04 cm (37.81 in.) or 21.3 percent \bar{c}
Outboard end chord (base line 155.44 in. (394.82 cm))	87.33 cm (34.38 in.) or 27.6 percent \bar{c}
Spoilers:	
Area (one side)	0.54 m ² (5.84 ft ²)
Area (one side) rearward of hinge line	0.50 m ² (5.44 ft ²)
Span (from 45.3 to 67.0 percent b/2)	1.28 m (4.19 ft)
Inboard end chord	0.42 m (1.39 ft)
Outboard end chord	0.32 m (1.04 ft)

TABLE I.- GEOMETRIC CHARACTERISTICS OF AIRPLANE – Concluded

Horizontal tail:		
Area (in chord plane)	8.80 m ²	(94.70 ft ²)
Movable area	7.19 m ²	(77.40 ft ²)
Span	5.40 m	(17.705 ft)
Aspect ratio		3.30
Taper ratio		0.20
Sweepback of 25-percent-chord line		35.50 ^o
Dihedral		-23.00 ^o
Root chord (at airplane center line)	271.78 cm	(107.00 in.)
Tip chord (theoretical)	54.36 cm	(21.40 in.)
Airfoil section:		
Root (airplane center line)	NACA 0003.7-64 (modified)	
Tip (theoretical)	NACA 0003.0-64 (modified)	
Hinge-line location, percent \bar{c}_t		41.00
Vertical tail:		
Area	6.27 m ²	(67.50 ft ²)
Span	1.94 m	(6.38 ft)
Taper ratio		0.227
Root chord	526.16 cm	(207.15 in.)
Tip chord	119.63 cm	(47.10 in.)
Sweepback of 25-percent-chord line		58.30 ^o
Airfoil section:		
Root	NACA 0004.0-64 (modified)	
Tip	NACA 0002.5-64 (modified)	
Rudder:		
Area (rearward of hinge line)	1.03 m ²	(11.07 ft ²)
Hinge-line location, percent chord		80.00

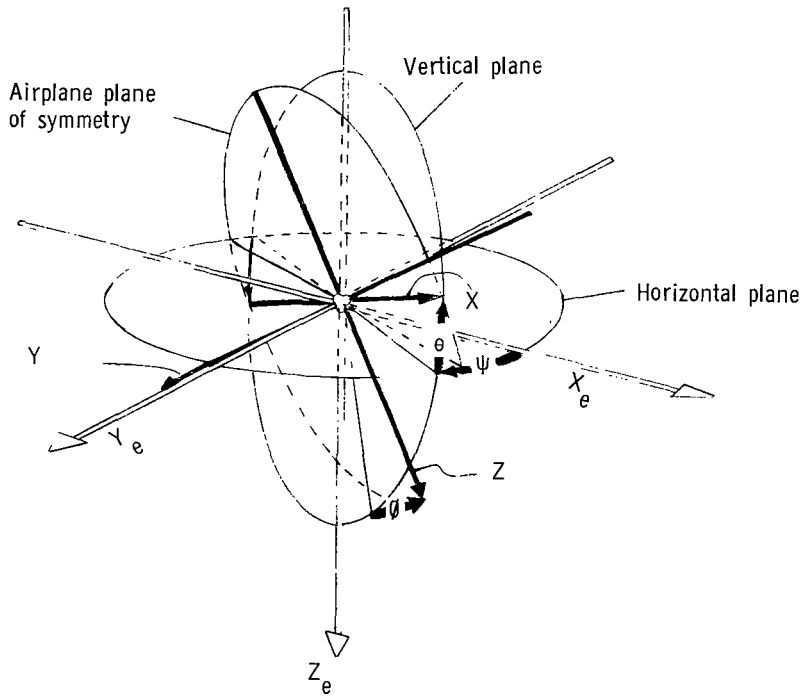
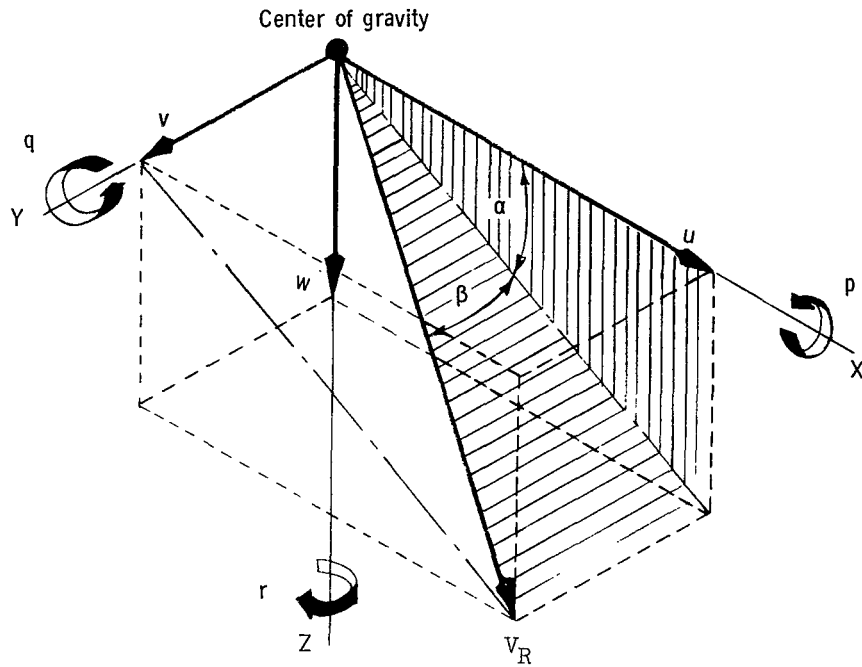


Figure 1.- Body system of axes and related angles.
Arrows indicate positive directions.

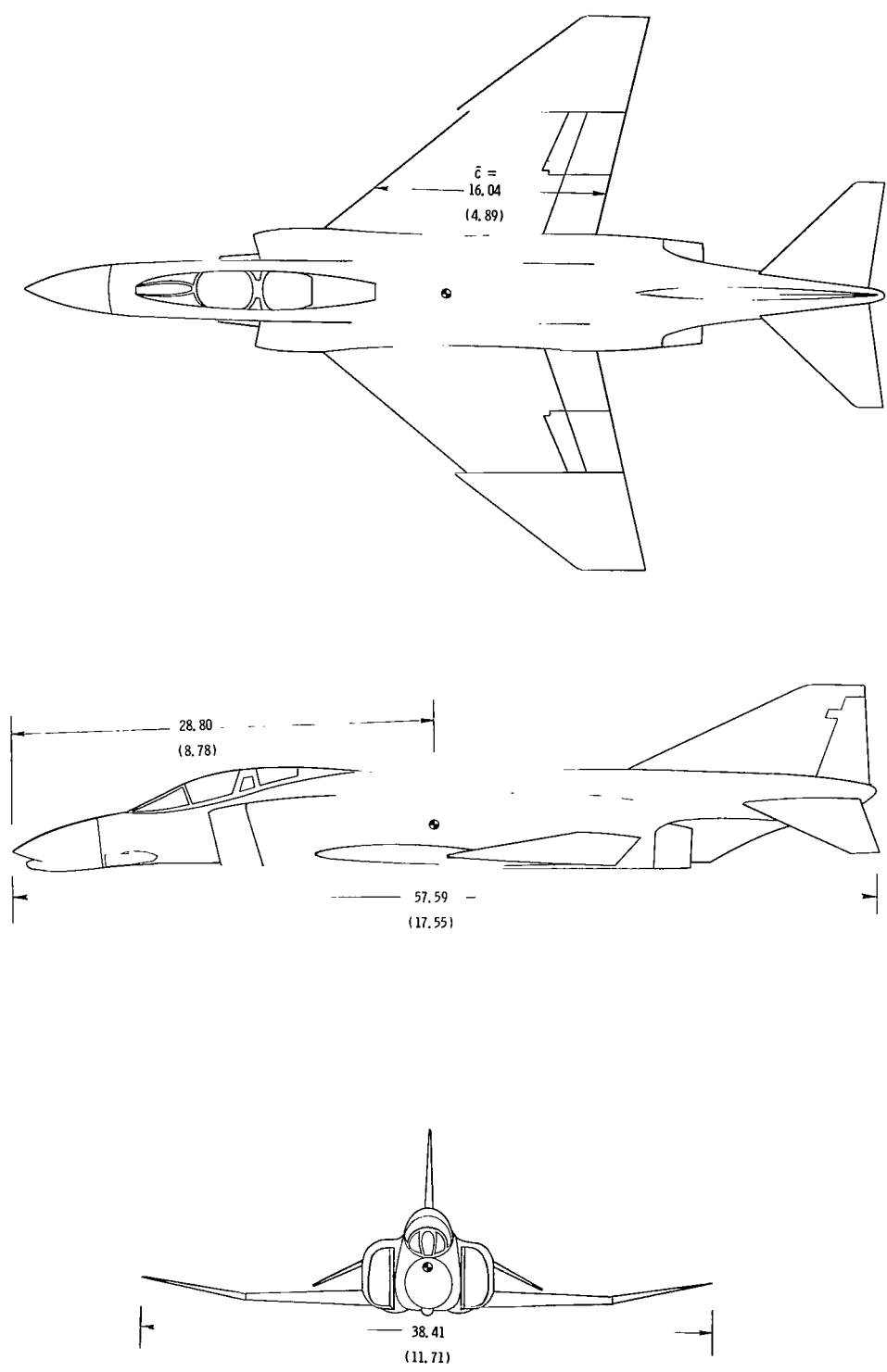
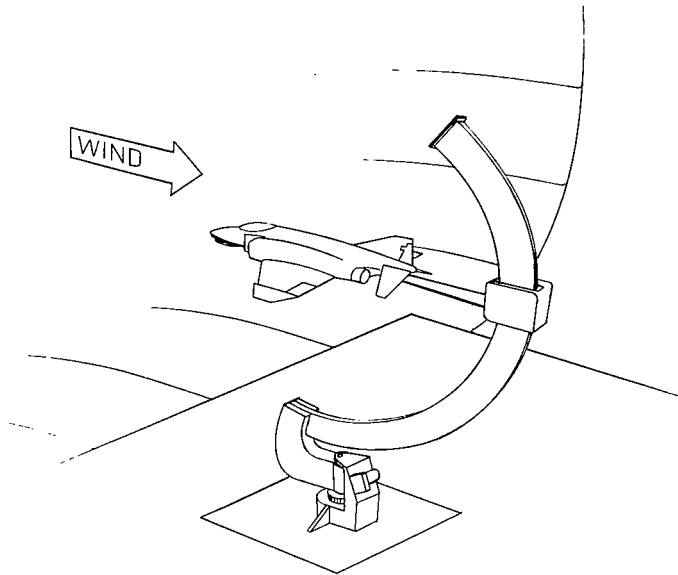


Figure 2.- Three-view sketch of airplane. All dimensions are in feet (meters).

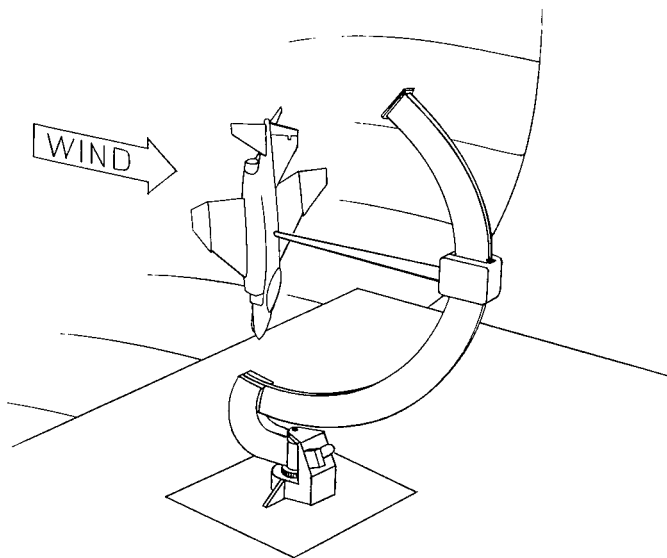


Figure 3.- Photograph of the 0.13-scale model of the twin-jet fighter airplane.

L-70-3313

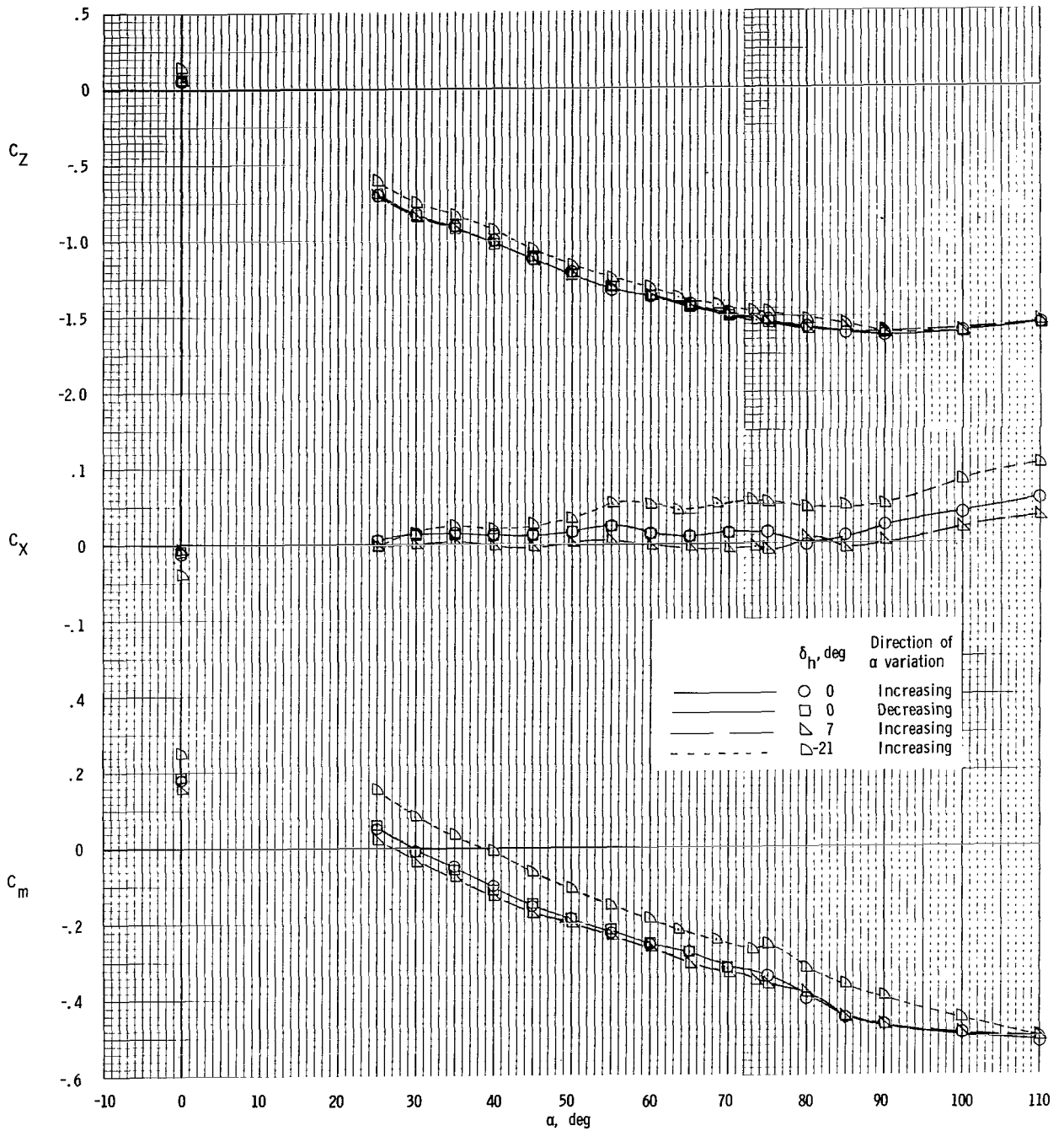


(a) Low angle-of-attack tests.



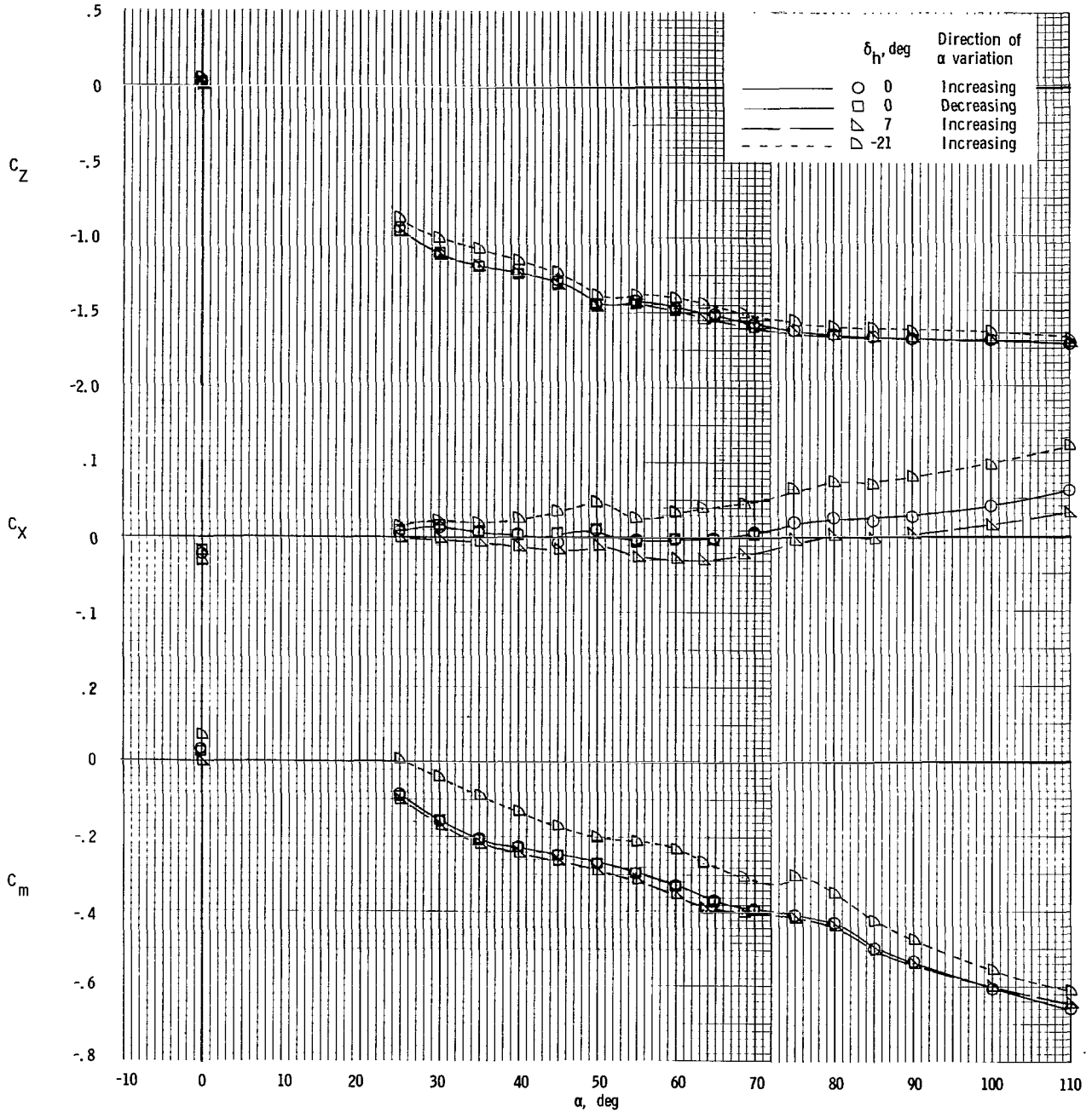
(b) High angle-of-attack tests.

Figure 4.- Sketches of the model as mounted in tunnel for static force tests.



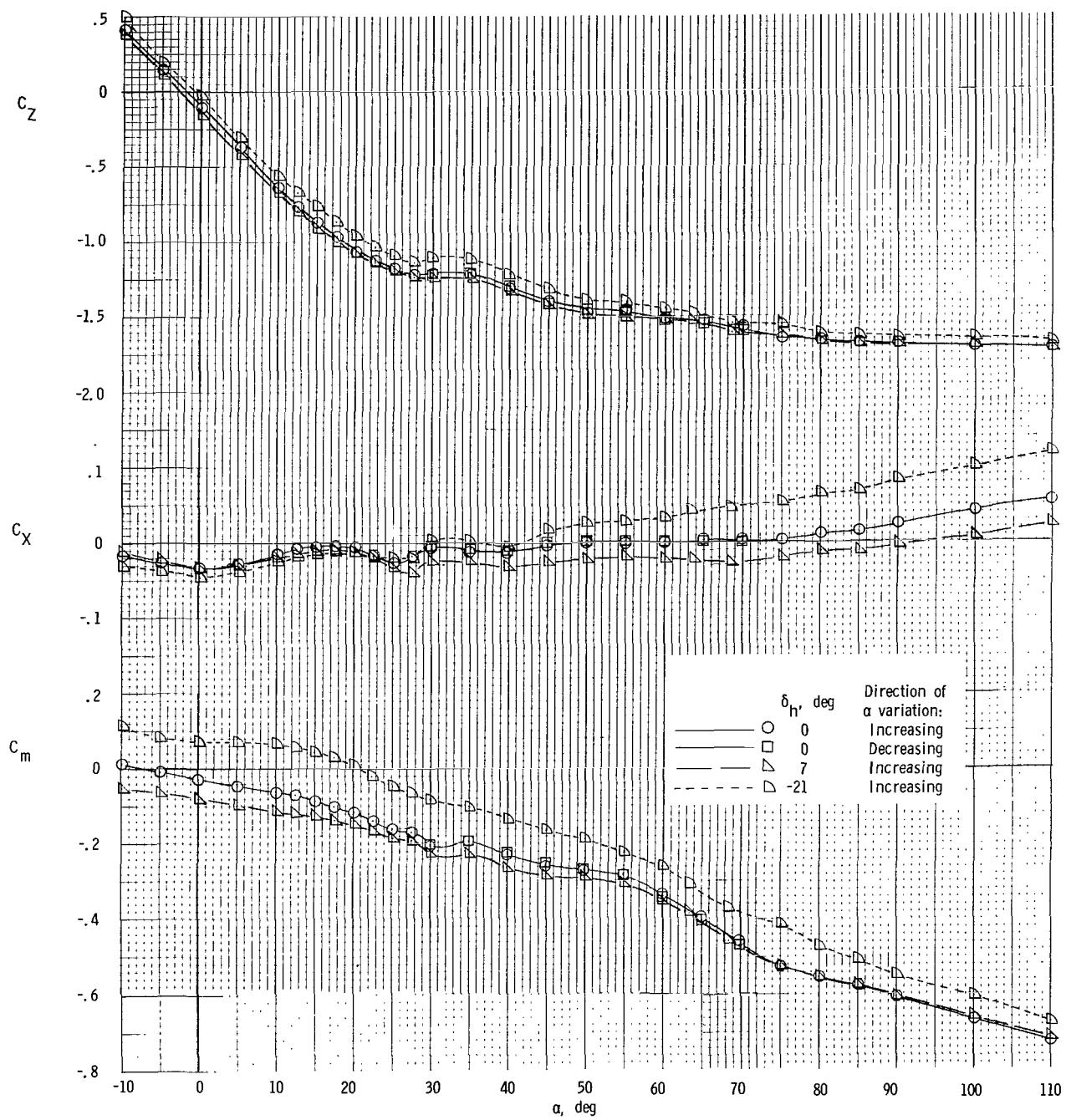
(a) $\beta = -40^\circ$.

Figure 5.- Effect of horizontal-tail deflection on the static longitudinal coefficients as functions of angle of attack and sideslip angle.



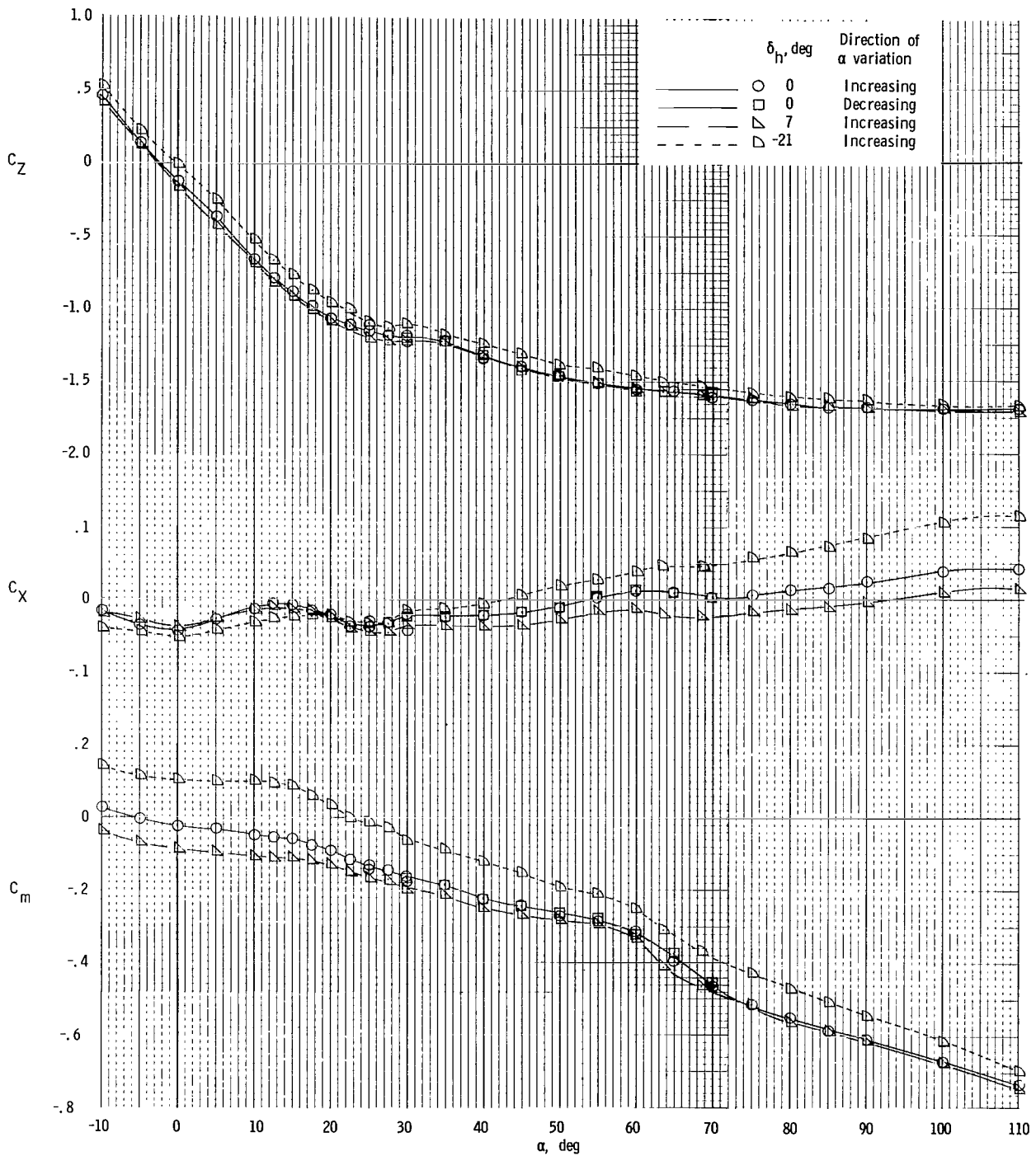
(b) $\beta = -30^\circ$.

Figure 5.- Continued.



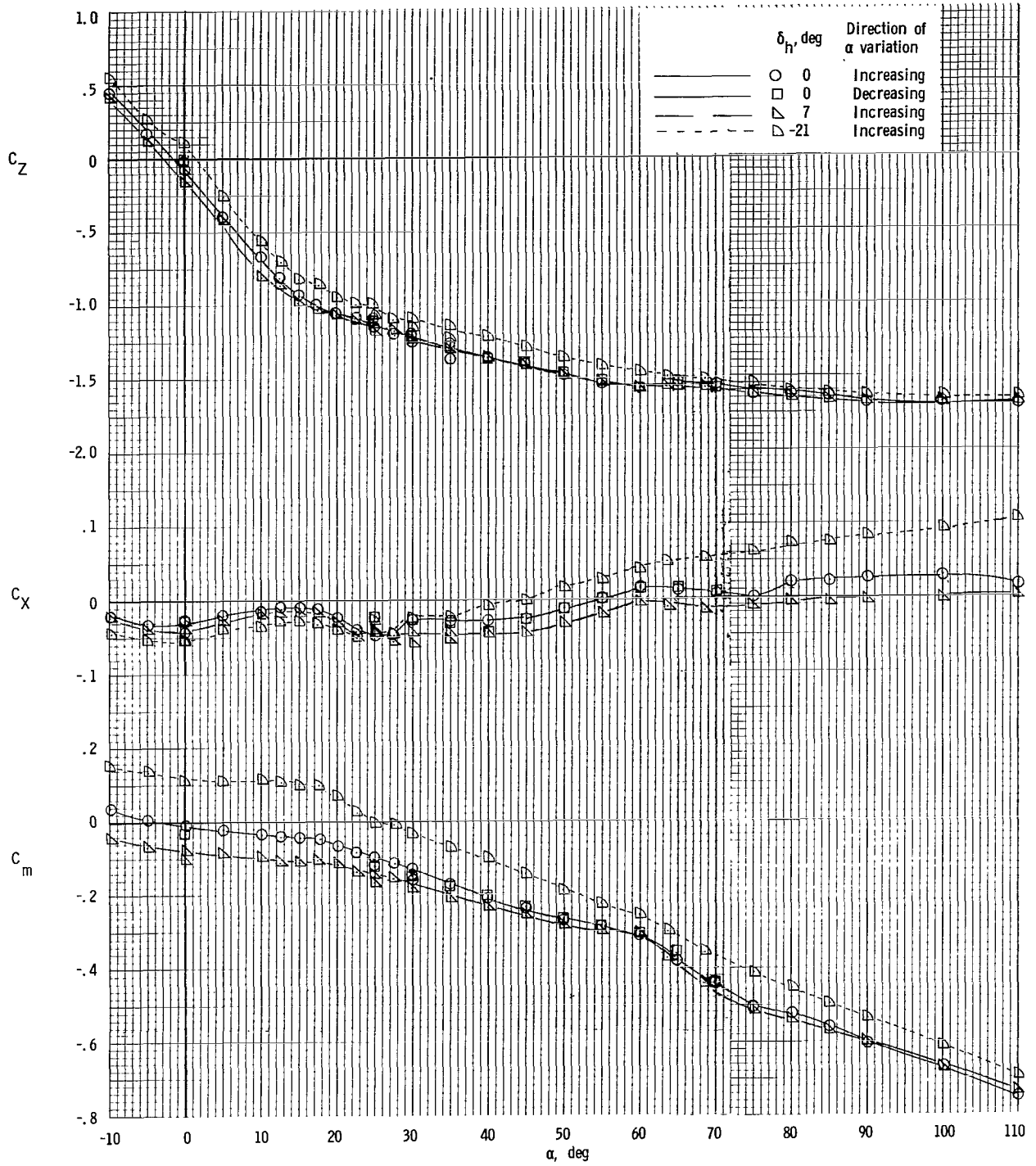
(c) $\beta = -20^\circ$.

Figure 5.- Continued.



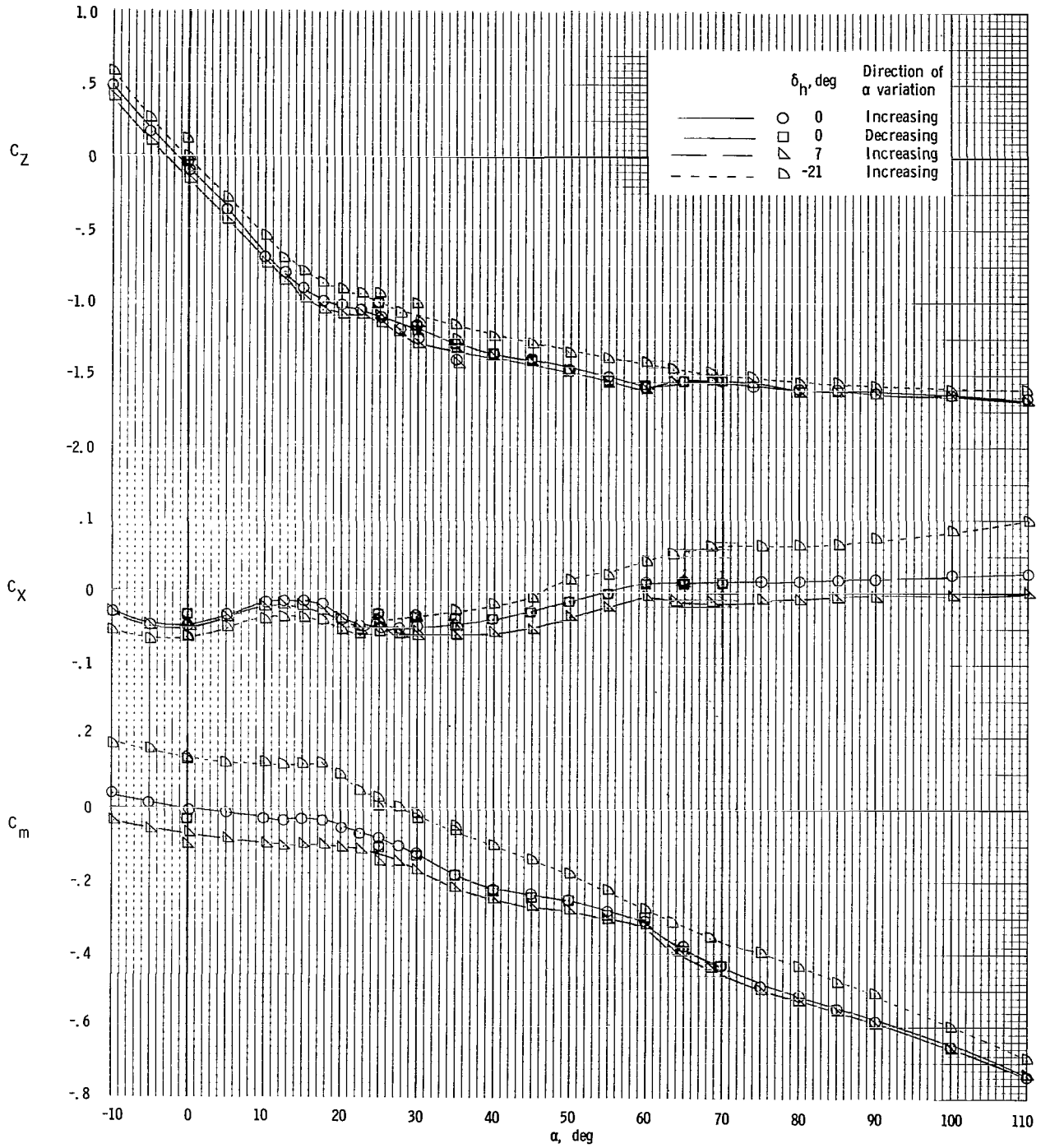
(d) $\beta = -15^\circ$.

Figure 5.- Continued.



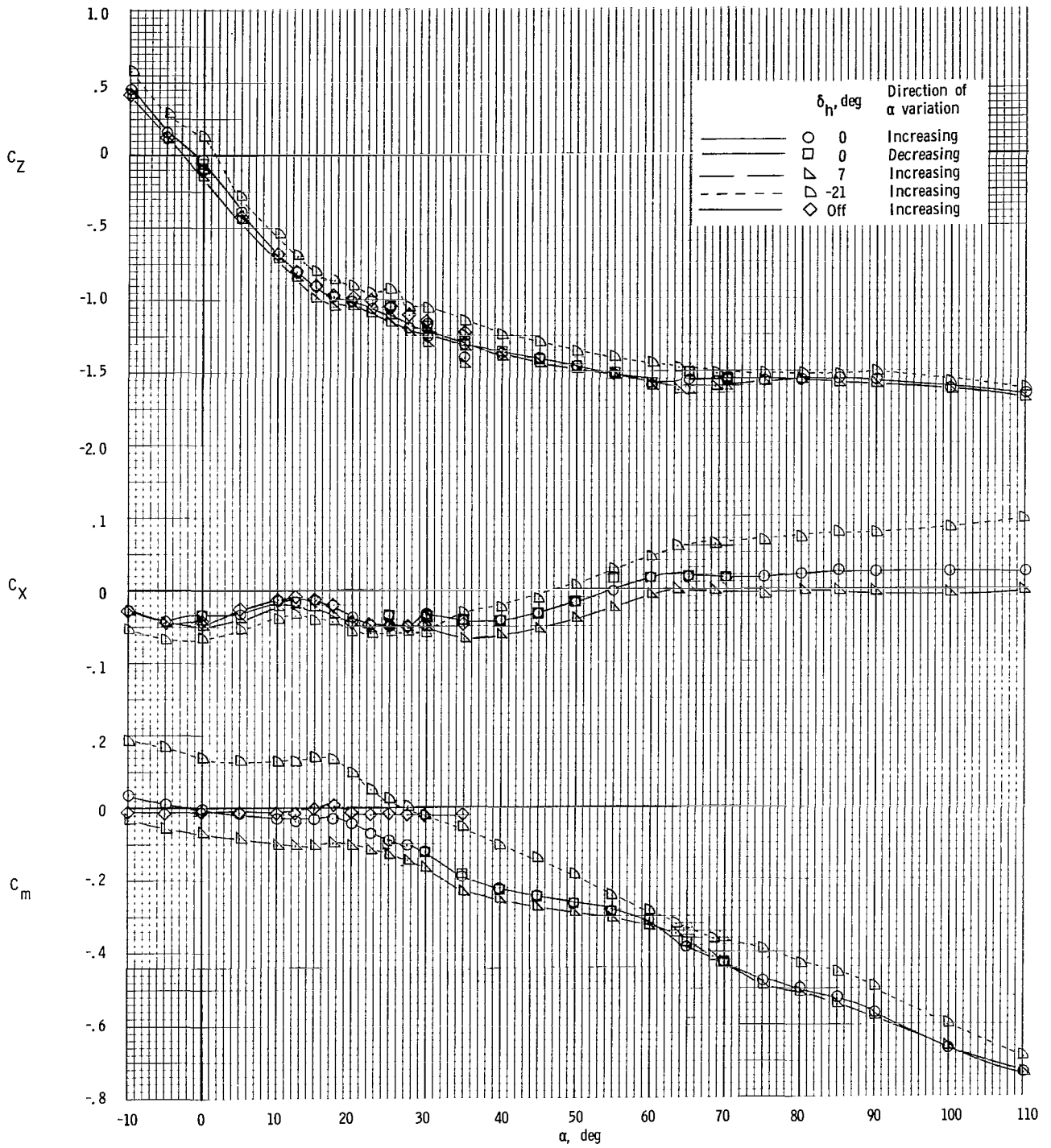
(e) $\beta = -10^0$.

Figure 5.- Continued.



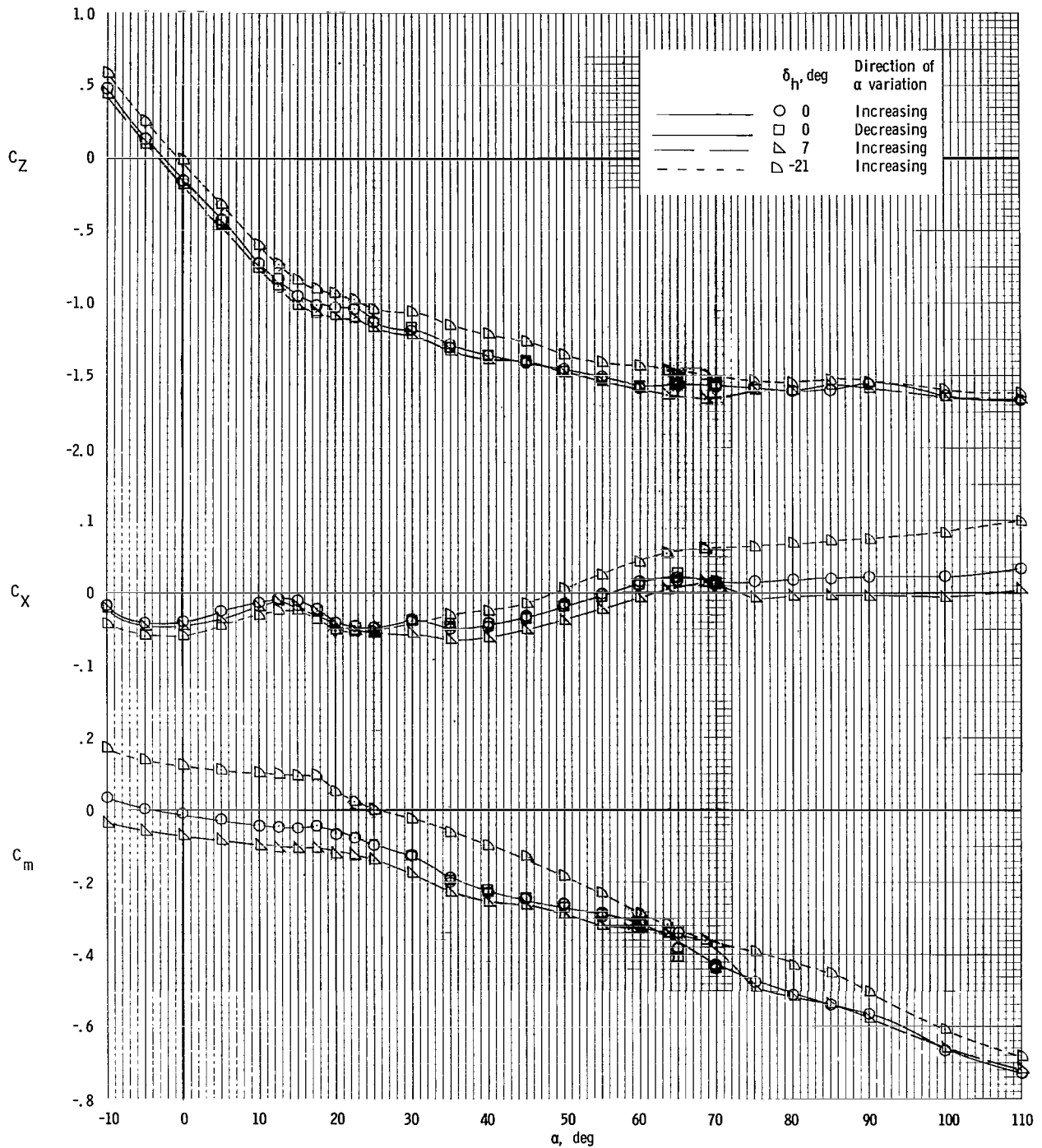
(f) $\beta = -5^\circ$.

Figure 5.- Continued.



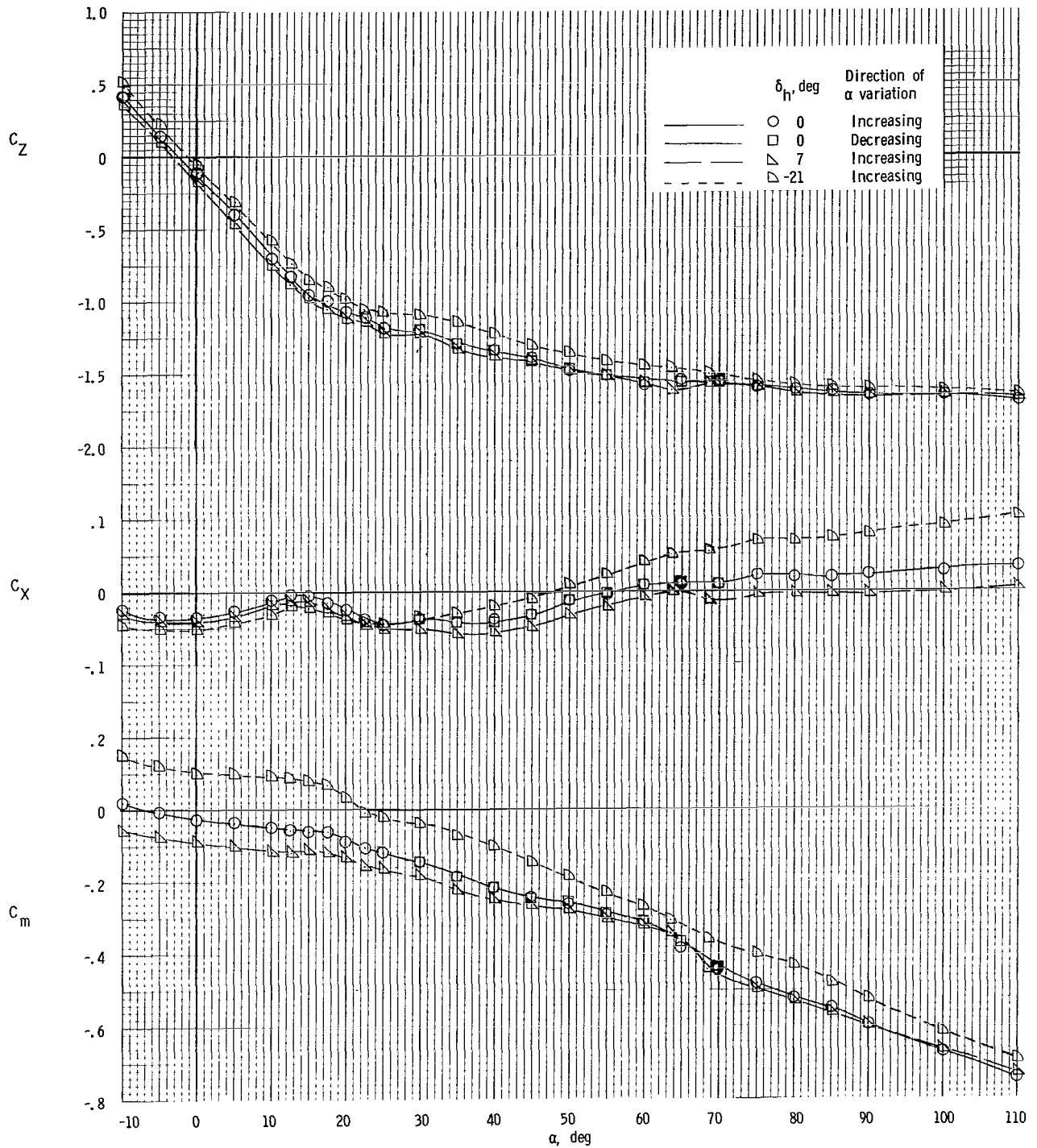
(g) $\beta = 0^\circ$.

Figure 5.- Continued.



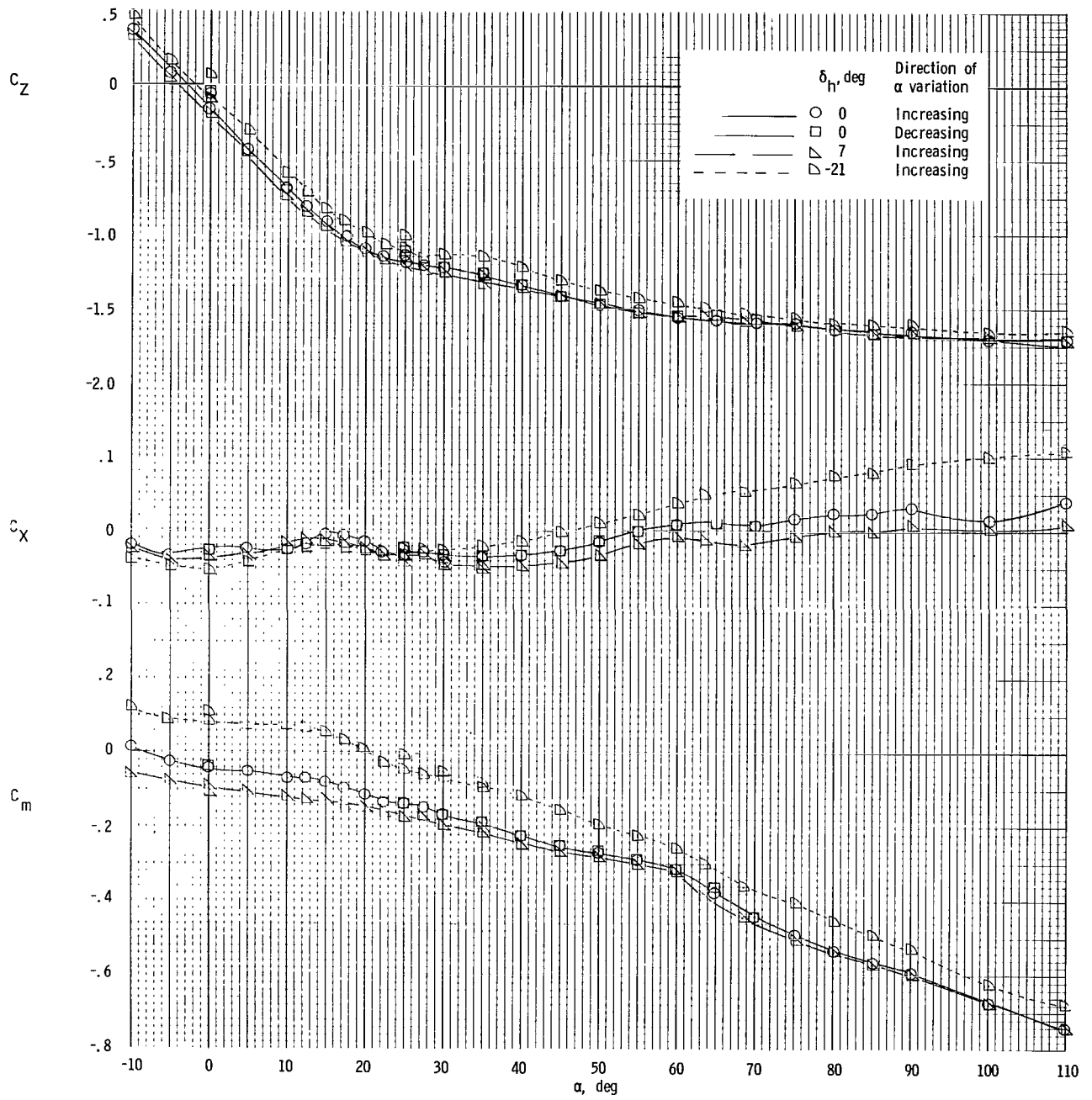
(h) $\beta = 5^\circ$.

Figure 5.- Continued.



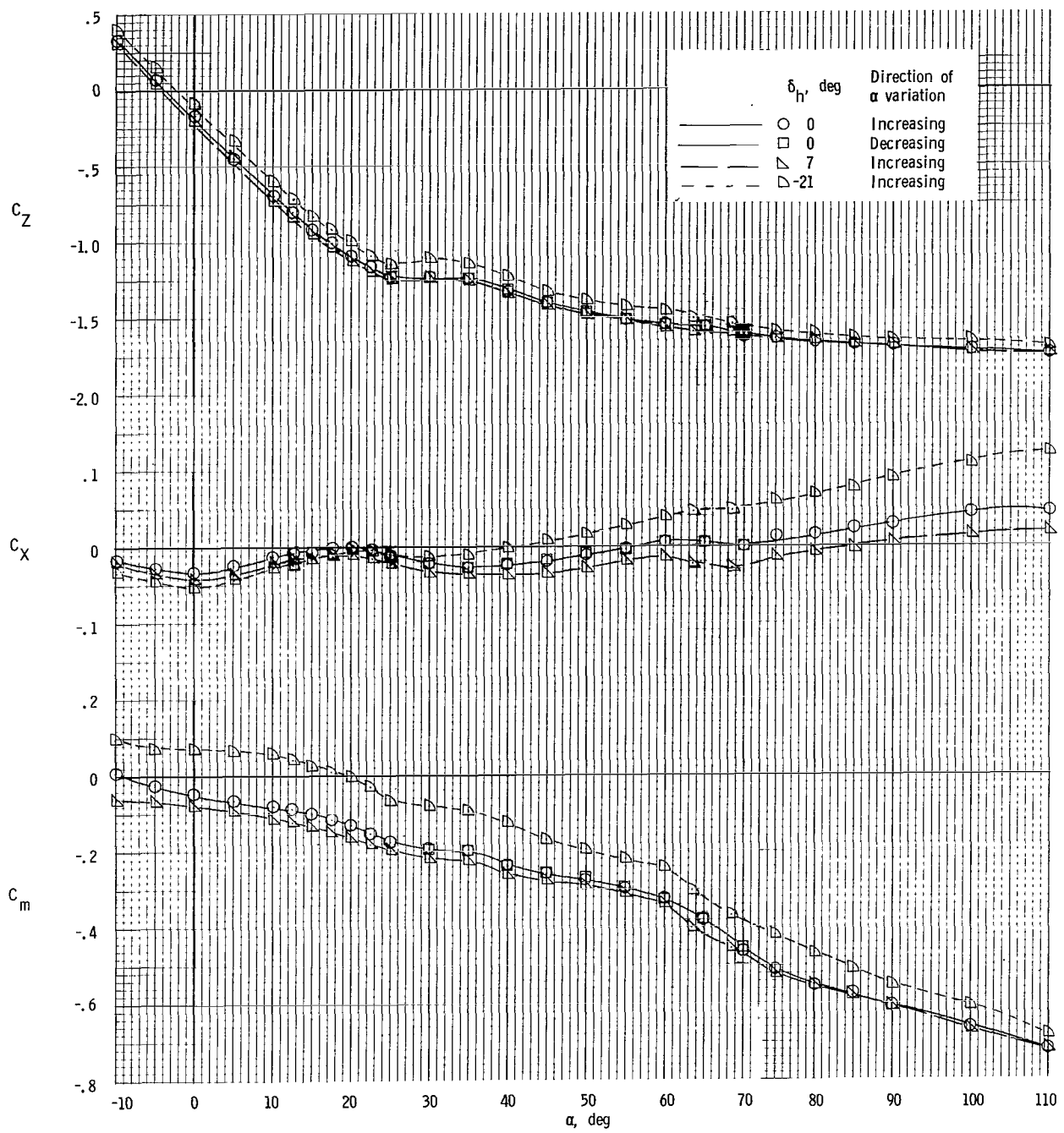
(i) $\beta = 10^{\circ}$.

Figure 5.- Continued.



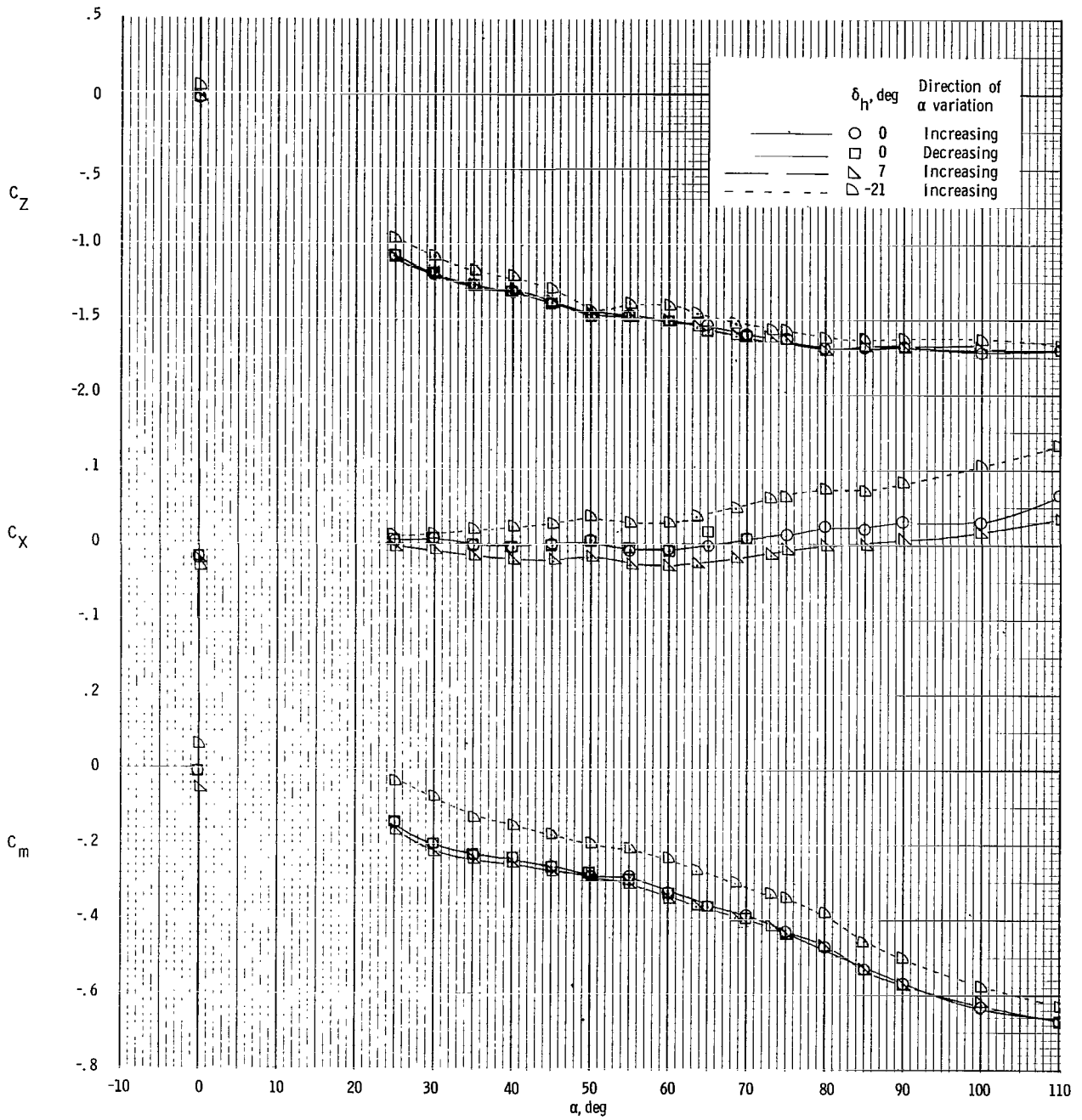
(j) $\beta = 15^\circ$.

Figure 5.- Continued.



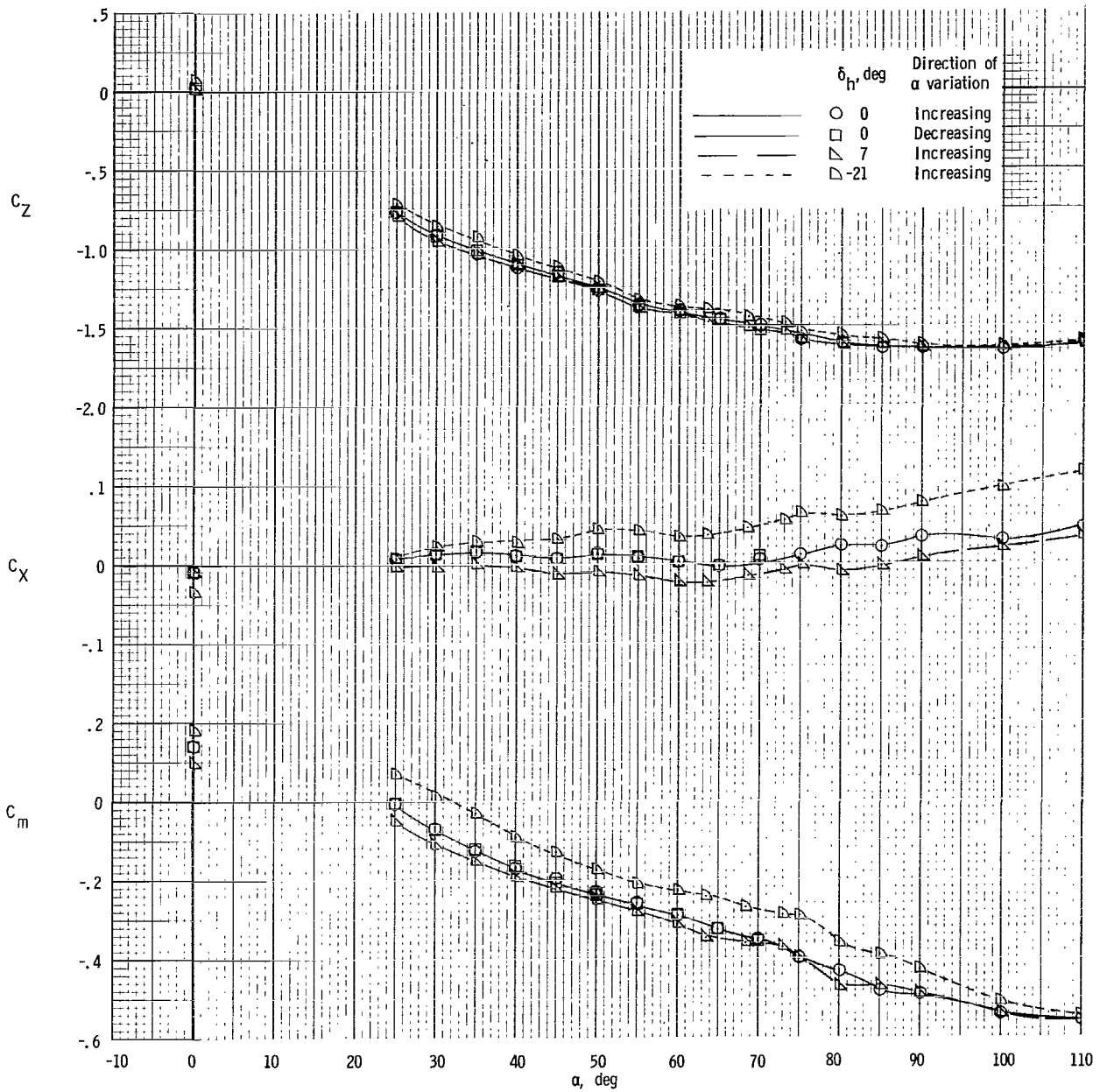
(k) $\beta = 20^\circ$.

Figure 5.- Continued.



(2) $\beta = 30^\circ$.

Figure 5.- Continued.



(m) $\beta = 40^\circ$.

Figure 5.- Concluded.

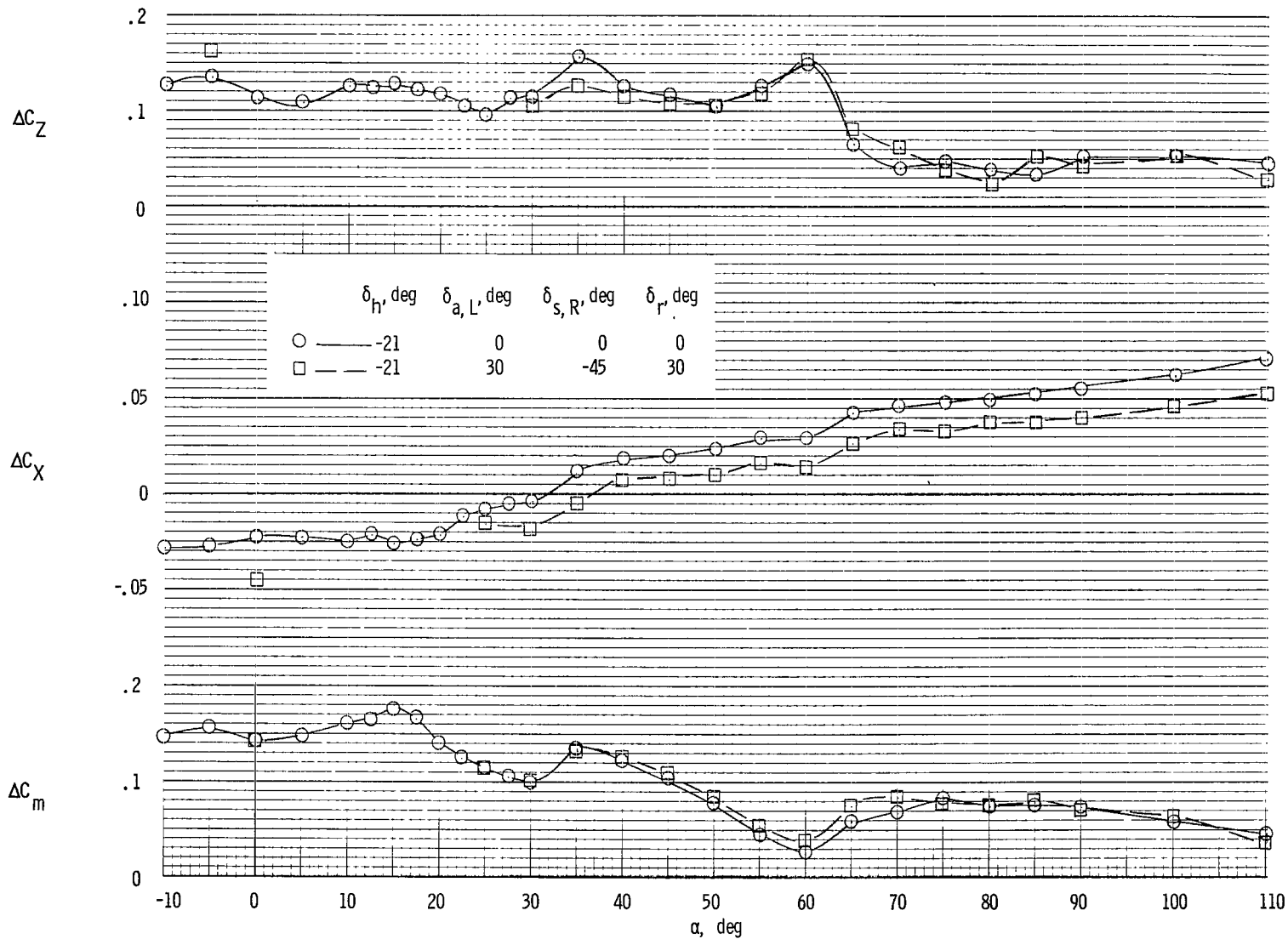
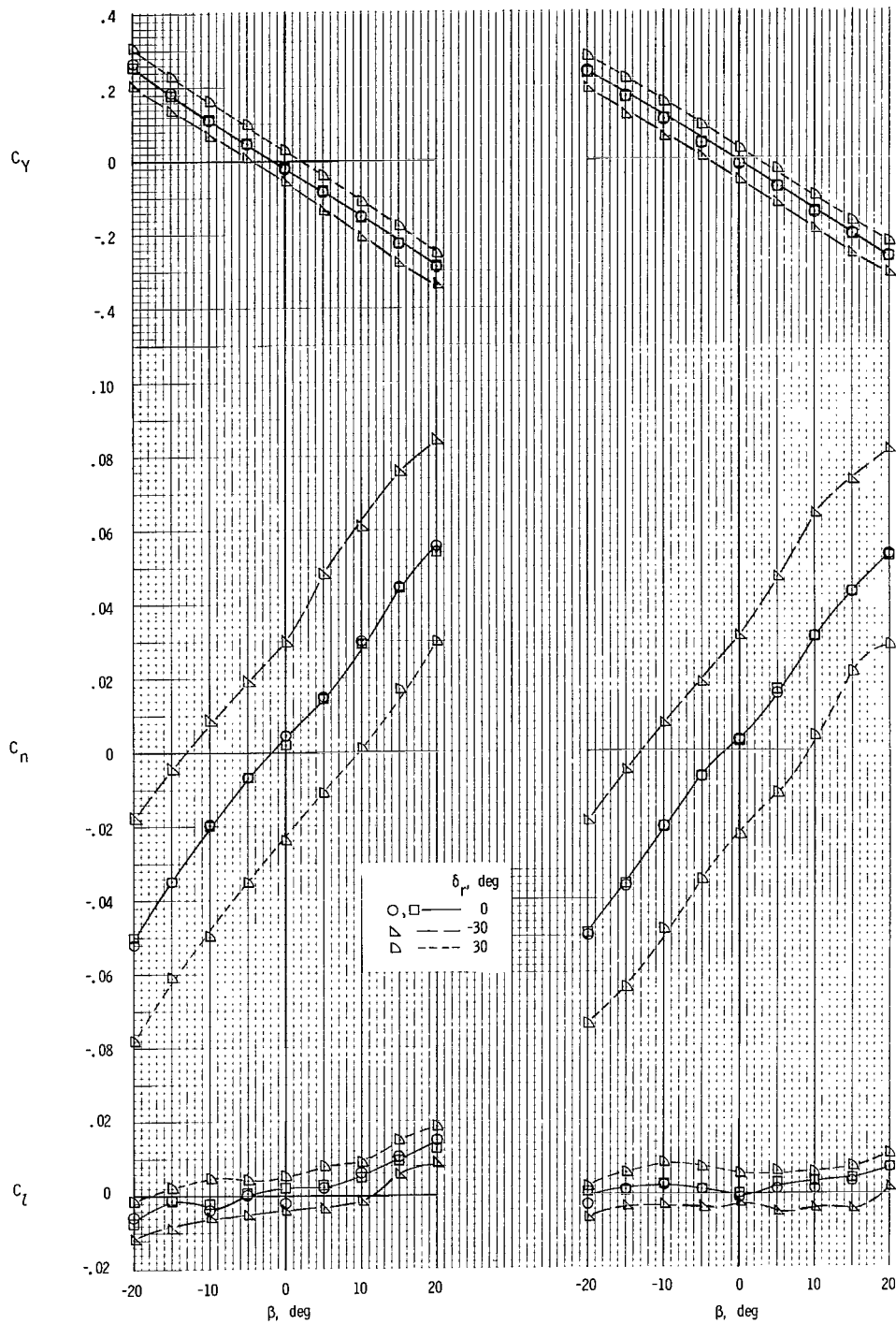


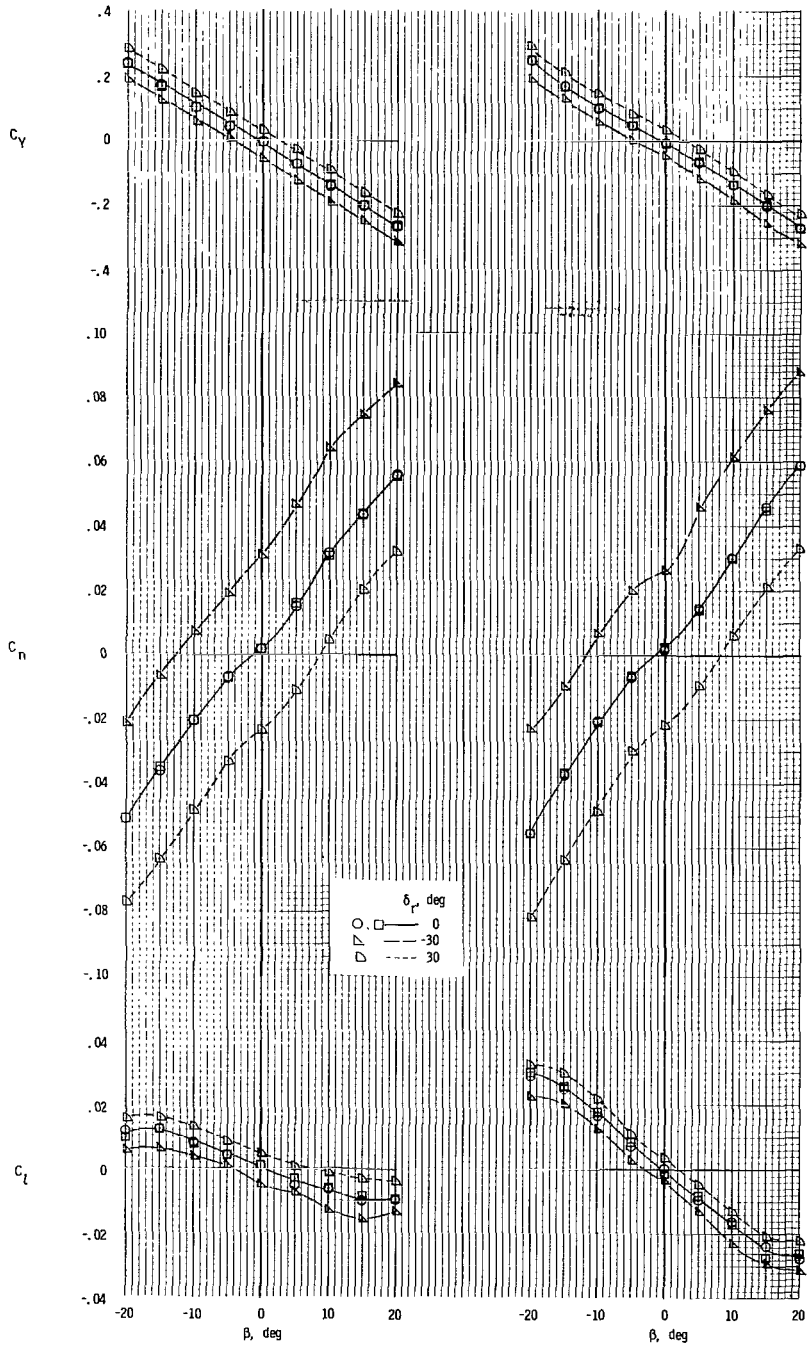
Figure 6.- Comparison of effectiveness of different control combinations on the static longitudinal characteristics at $\beta = 0^\circ$.



(a) $\alpha = -10^\circ$.

(b) $\alpha = -5^\circ$.

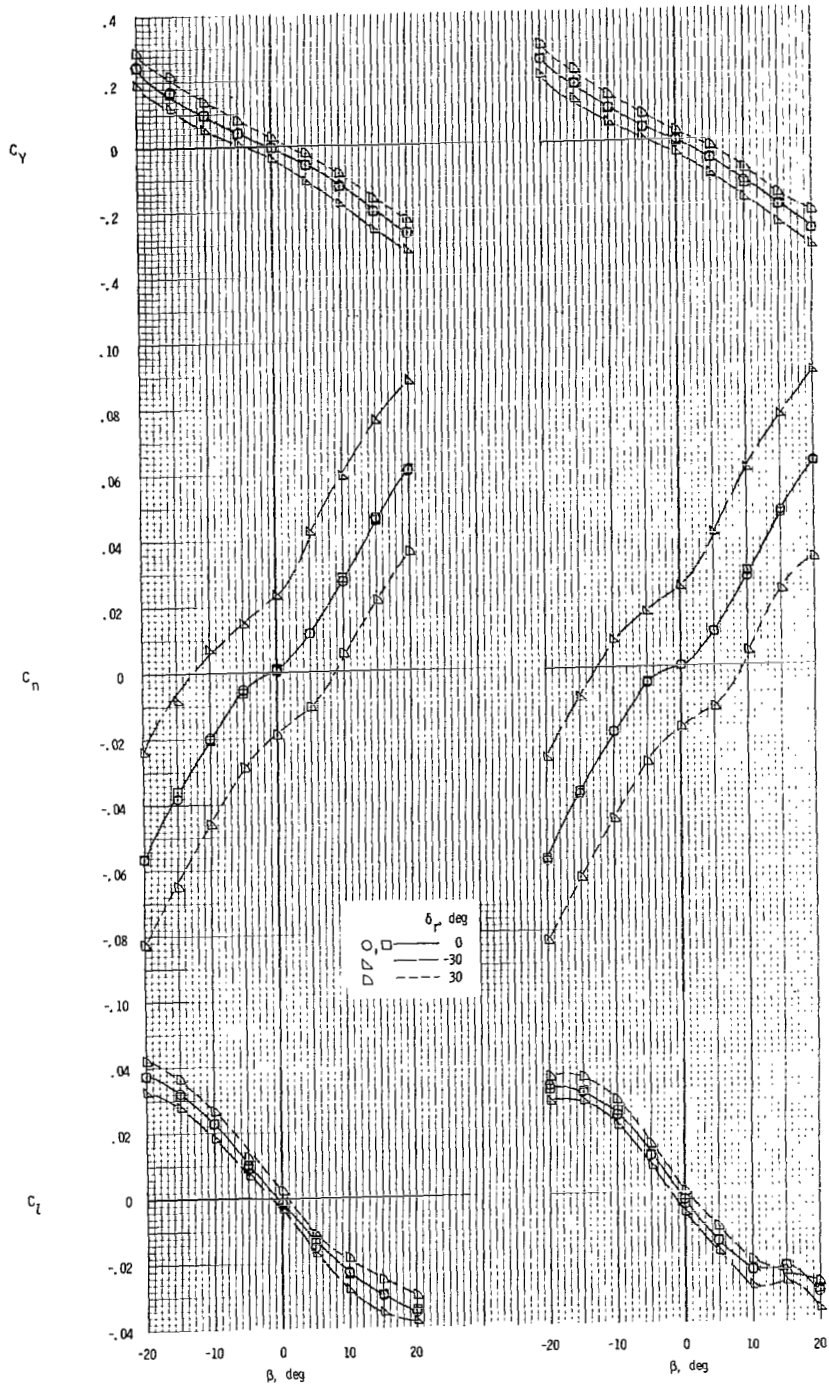
Figure 7.- Effect of rudder deflection on the static lateral-directional stability coefficients as a function of angle of attack and sideslip angle. $\delta_h = 0^\circ$. (Double symbols, when used, show repeat tests.)



(c) $\alpha = 0^\circ$.

(d) $\alpha = 5^\circ$.

Figure 7.- Continued.



(e) $\alpha = 10^\circ$.

(f) $\alpha = 12.5^\circ$.

Figure 7.- Continued.

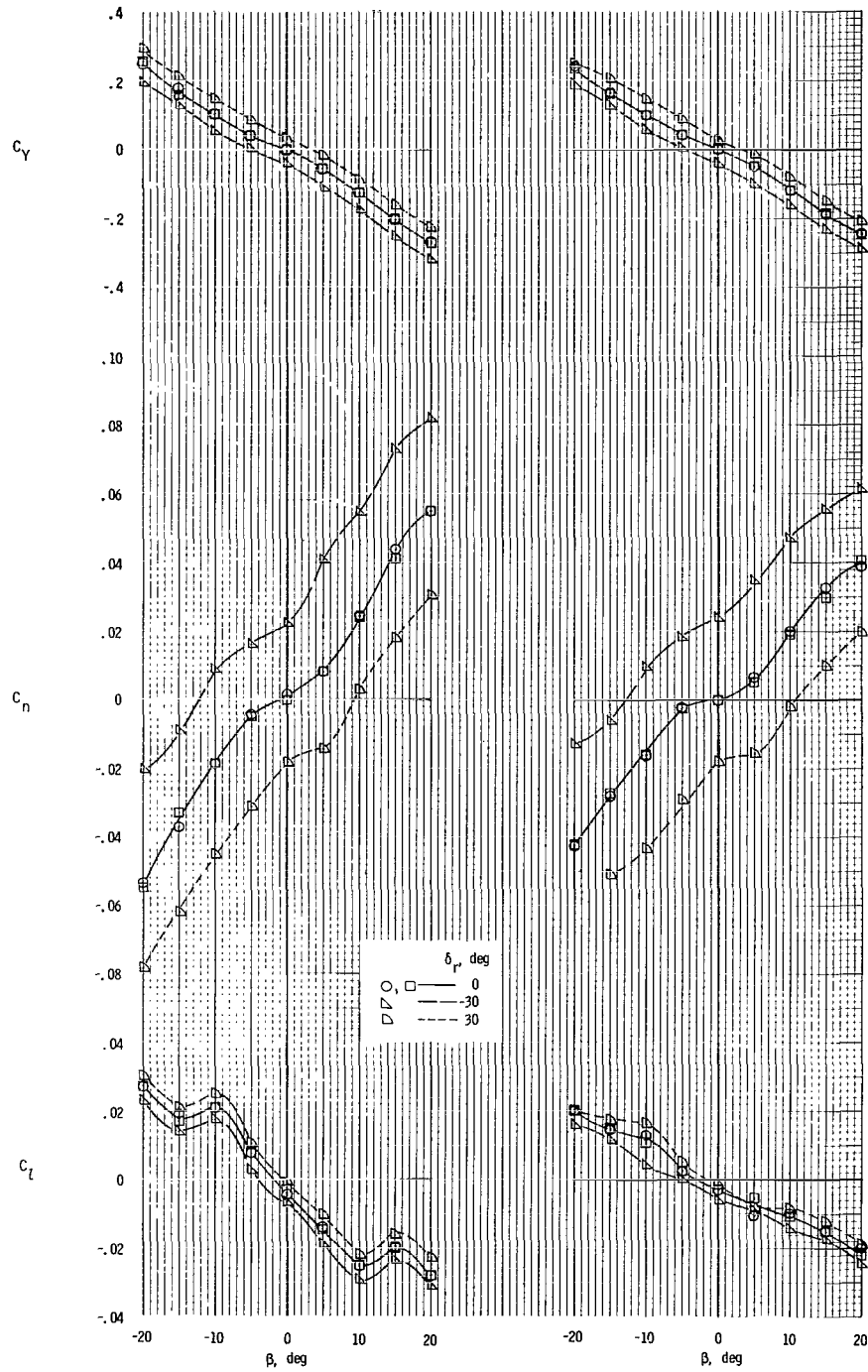
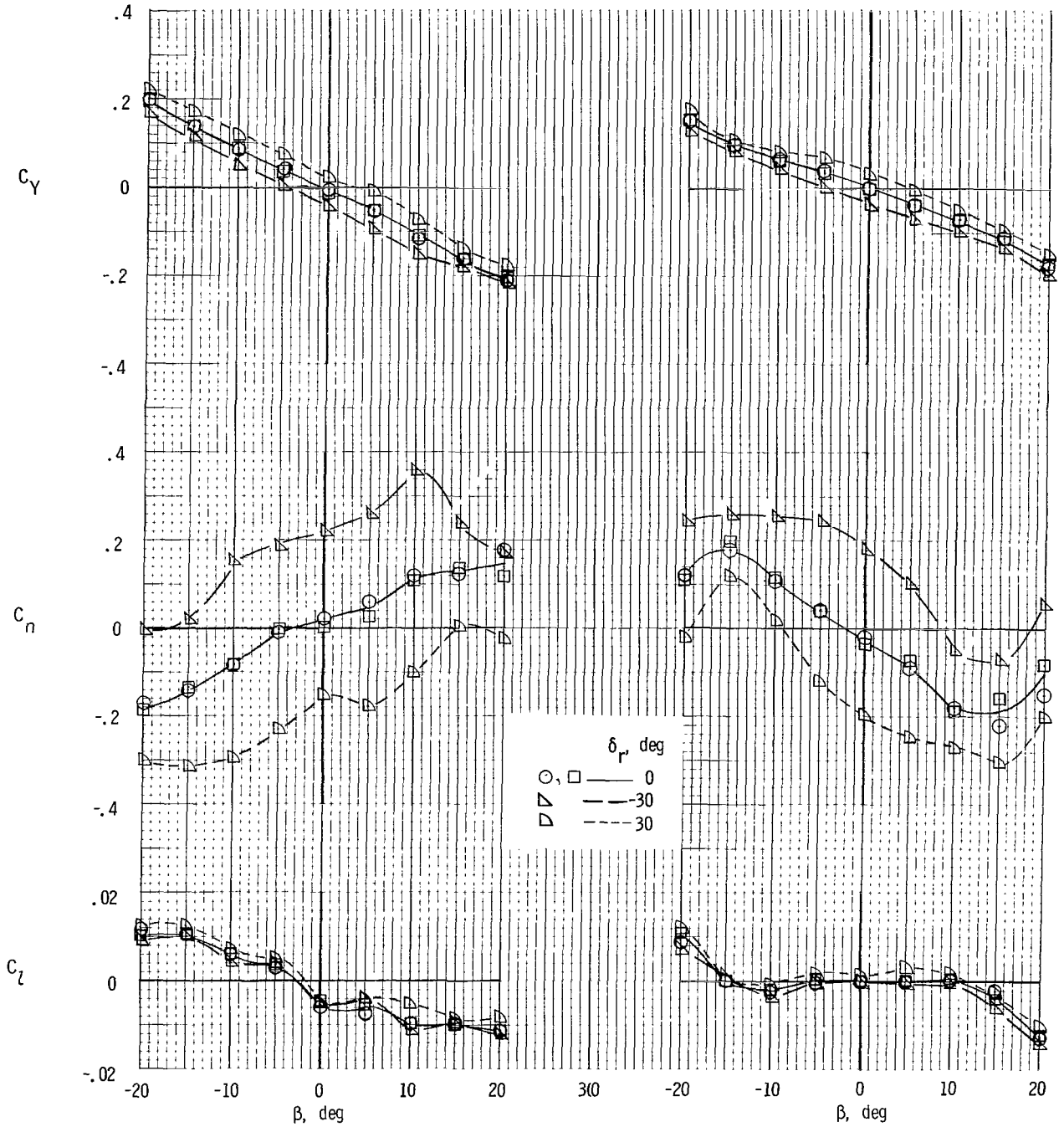


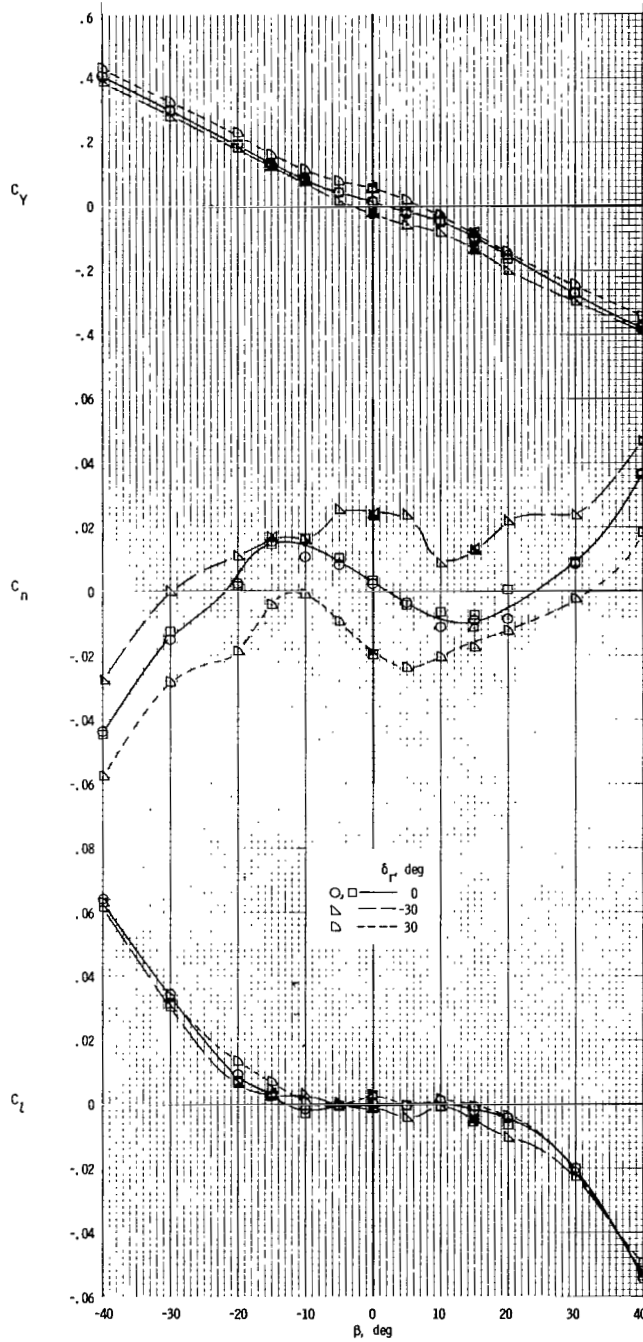
Figure 7.- Continued.



(i) $\alpha = 20^\circ$.

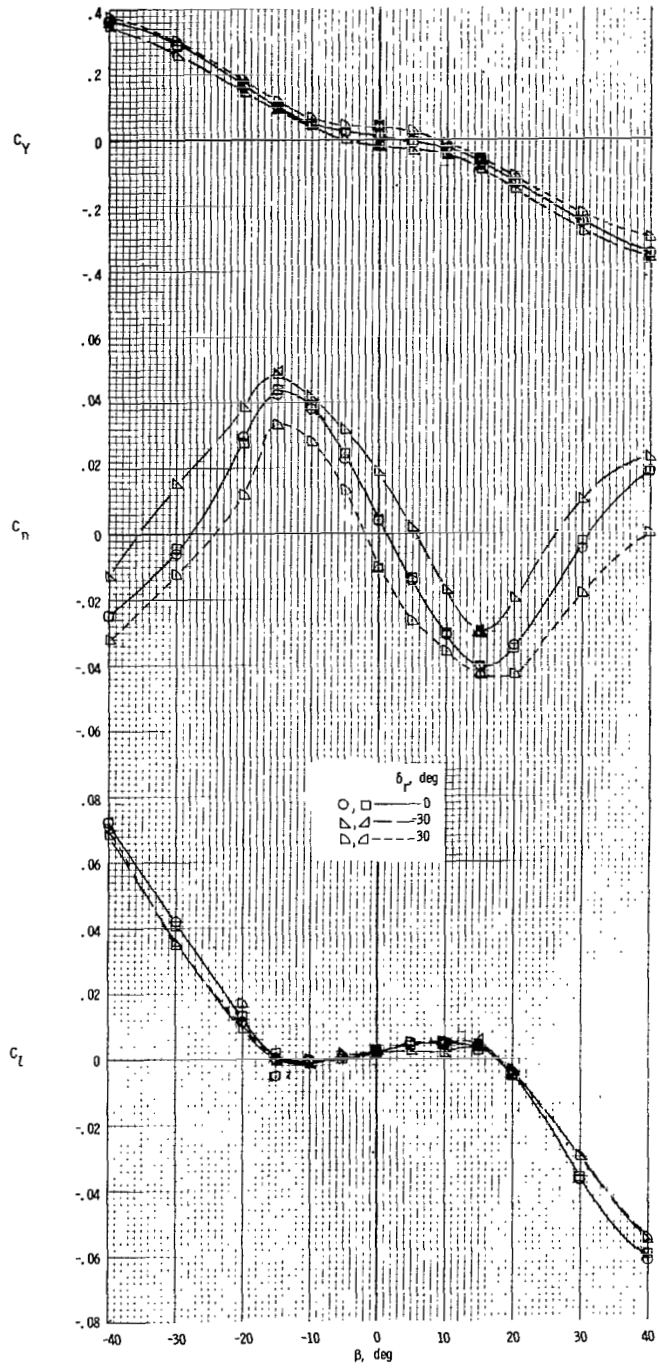
(j) $\alpha = 22.5^\circ$.

Figure 7.- Continued.



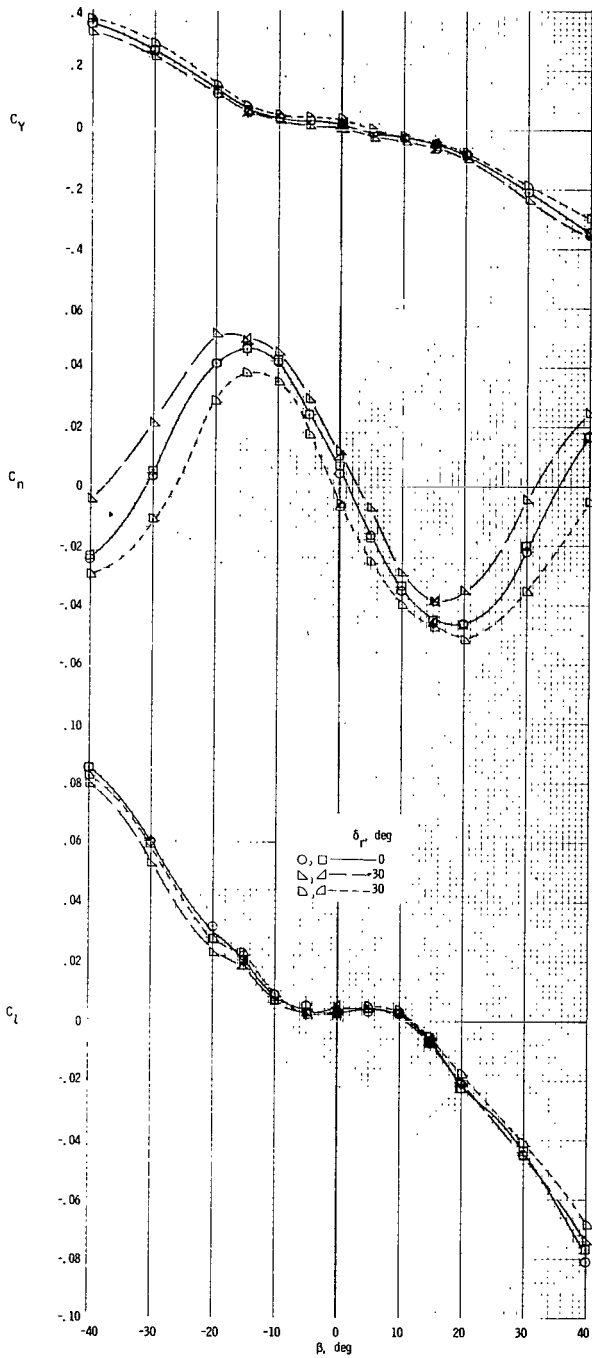
(k) $\alpha = 25^\circ$.

Figure 7.- Continued.

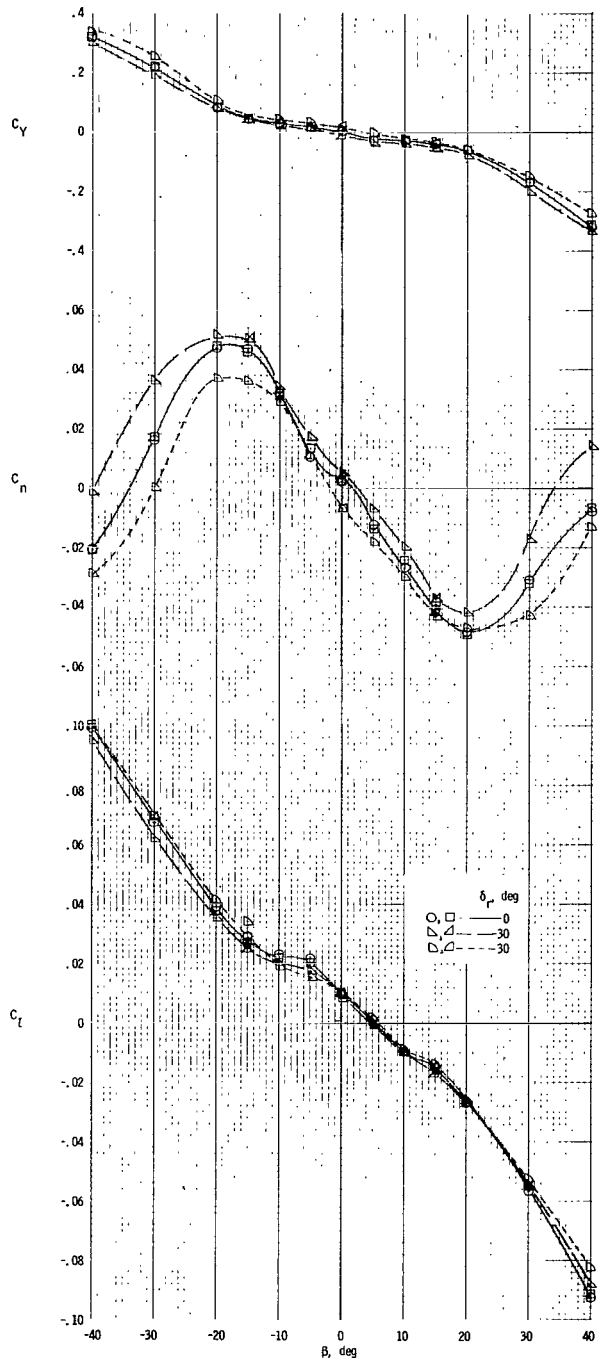


(l) $\alpha = 30^\circ$.

Figure 7.- Continued.

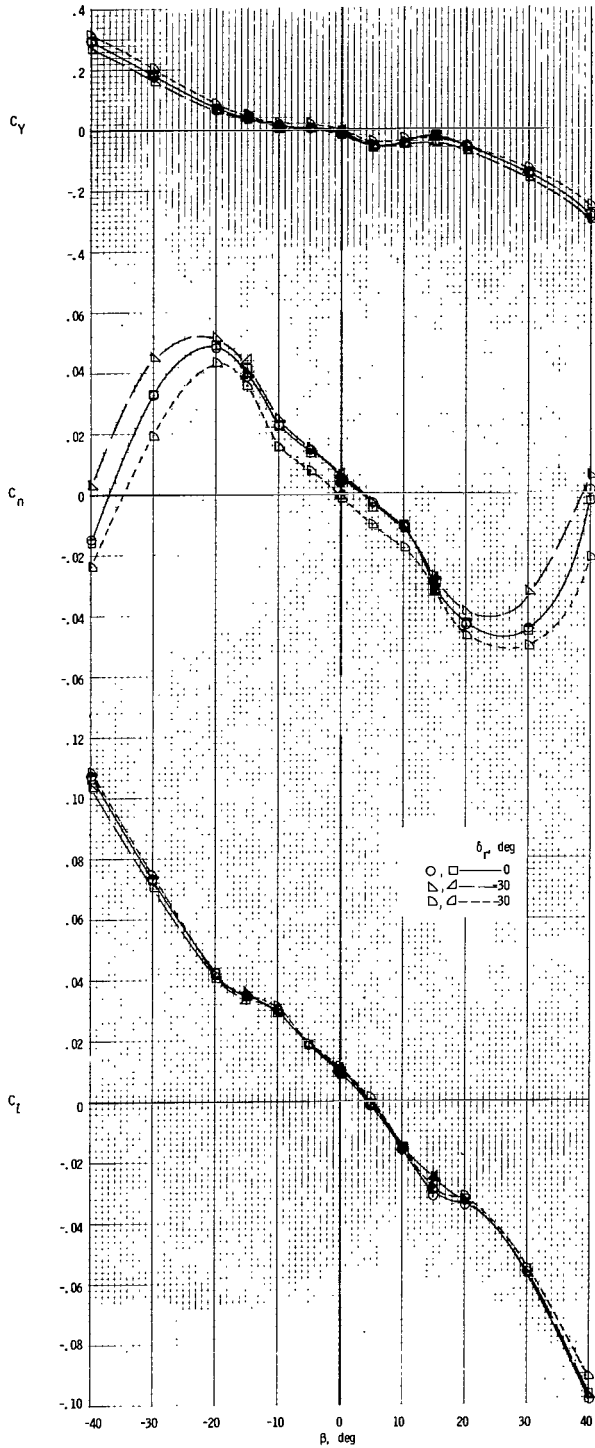


(m) $\alpha = 35^\circ$.

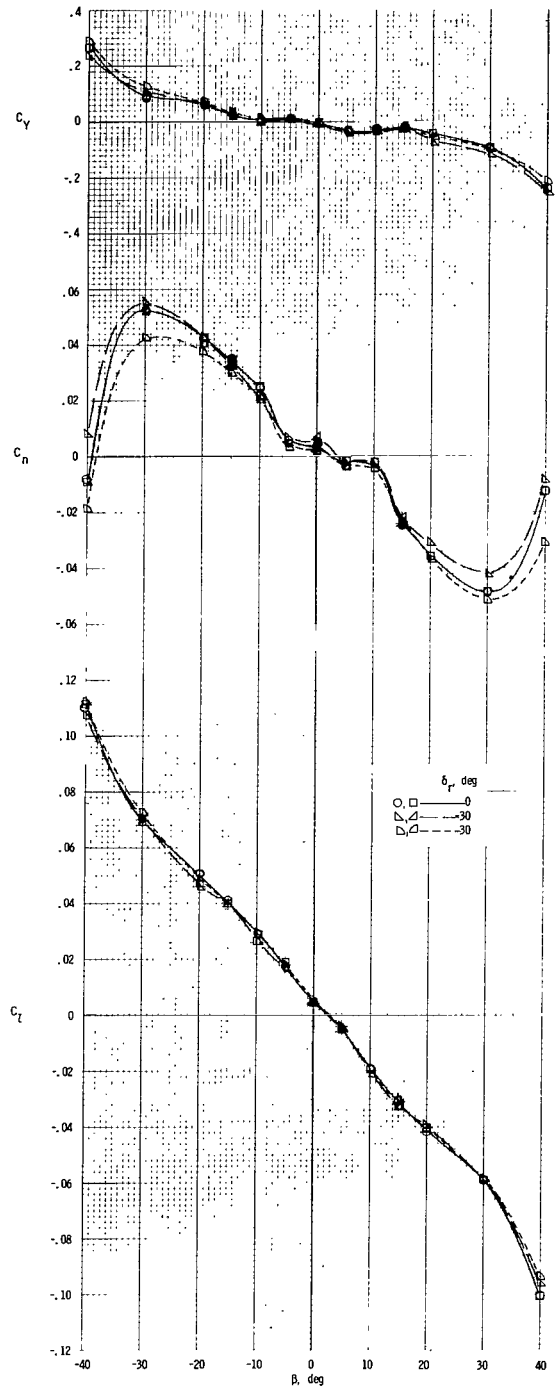


(n) $\alpha = 40^\circ$.

Figure 7.- Continued.

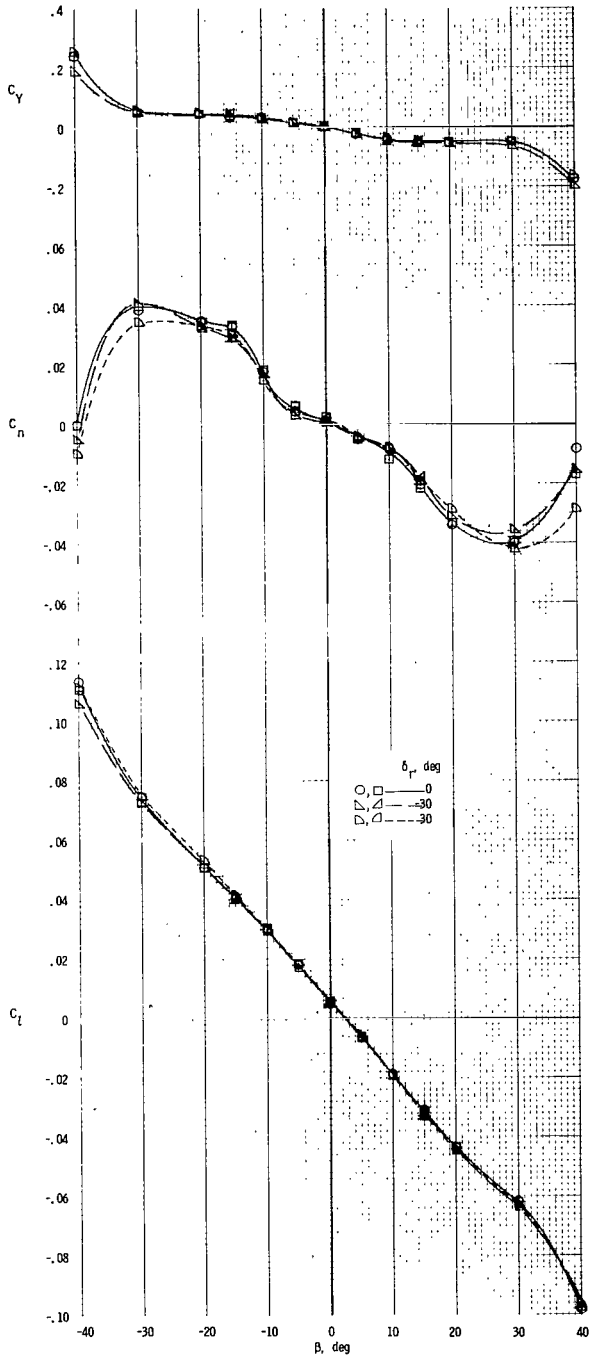


(o) $\alpha = 45^\circ$.

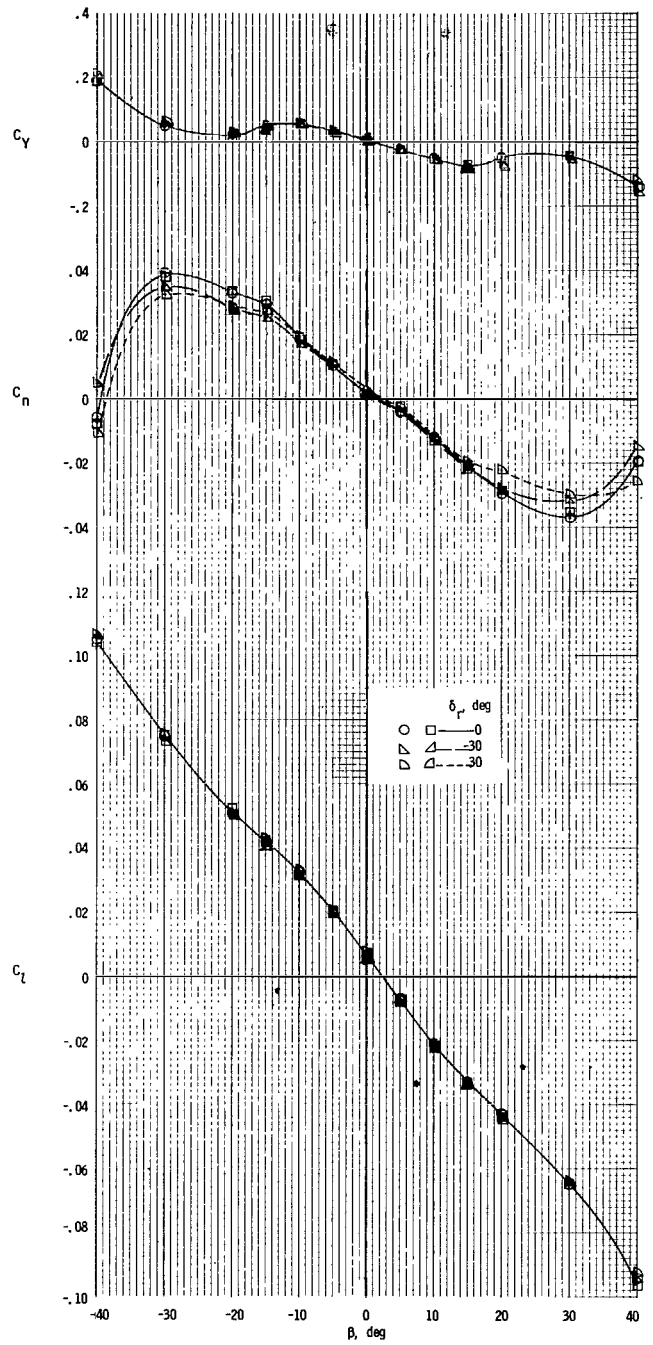


(p) $\alpha = 50^\circ$.

Figure 7.- Continued.

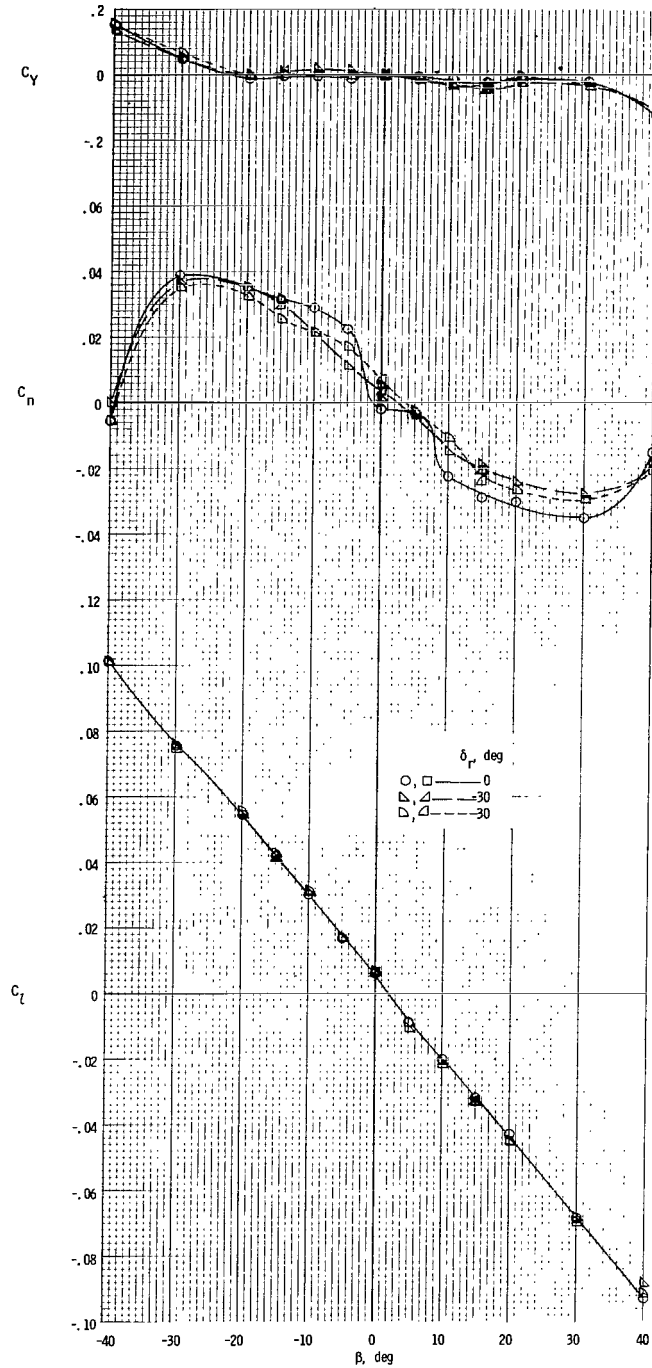


(q) $\alpha = 55^\circ$.



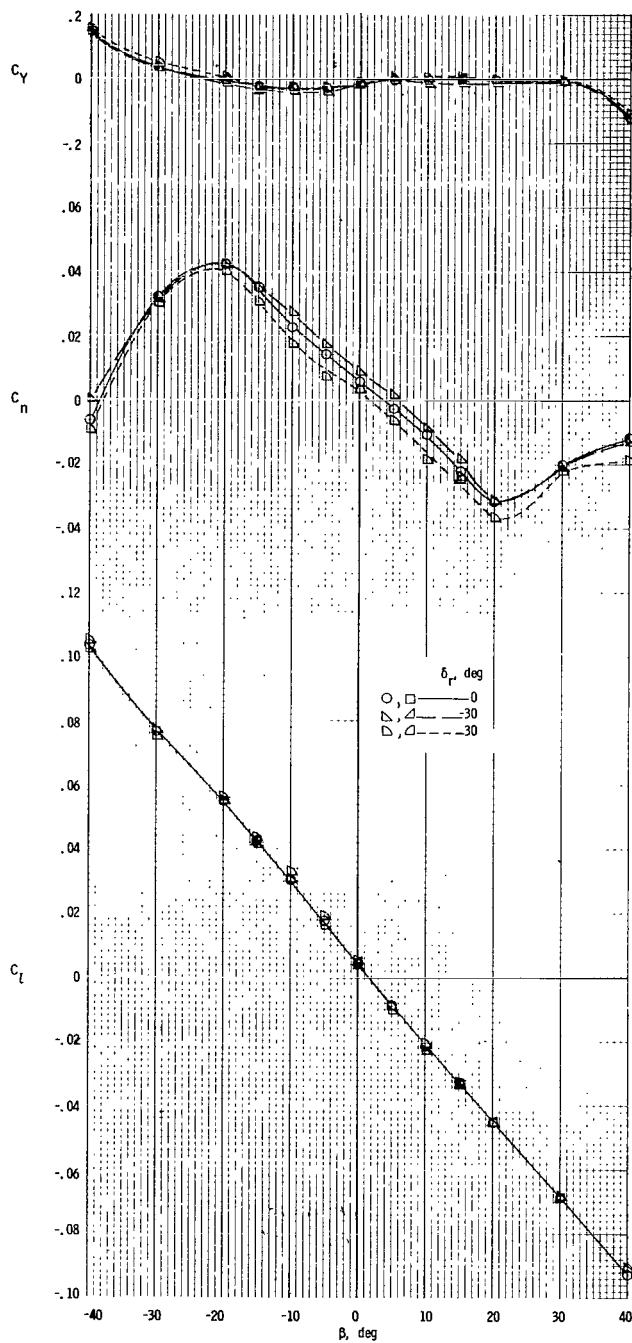
(r) $\alpha = 60^\circ$.

Figure 7.- Continued.

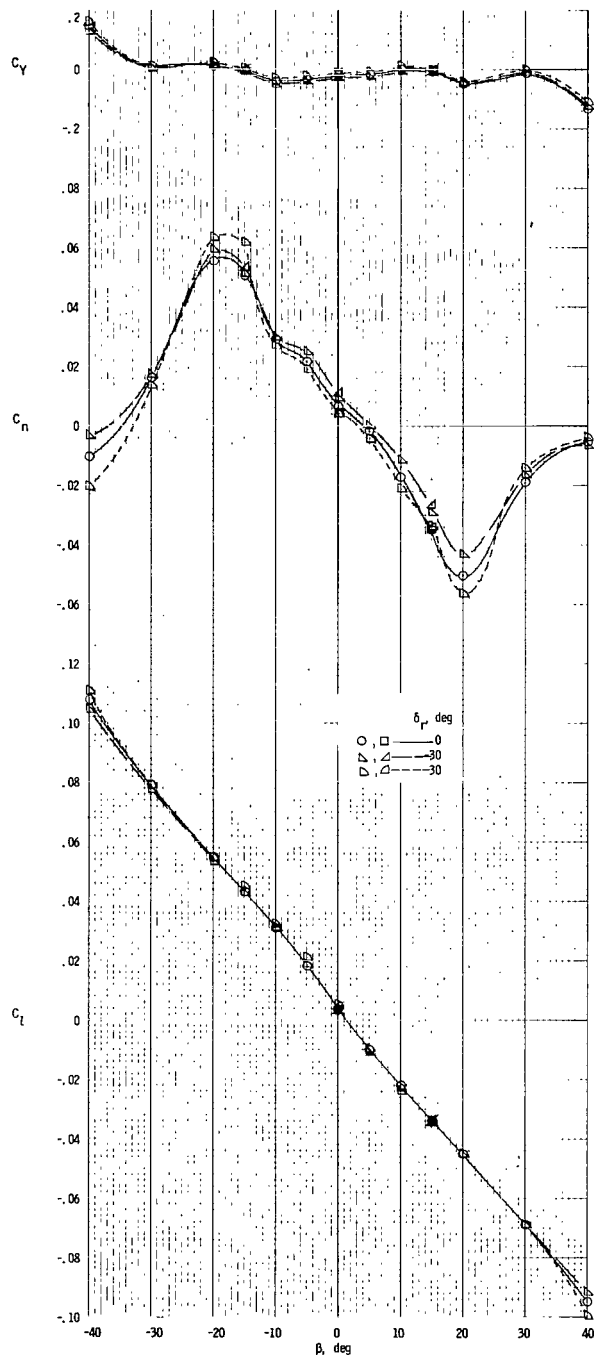


(s) $\alpha = 65^\circ$.

Figure 7.- Continued.

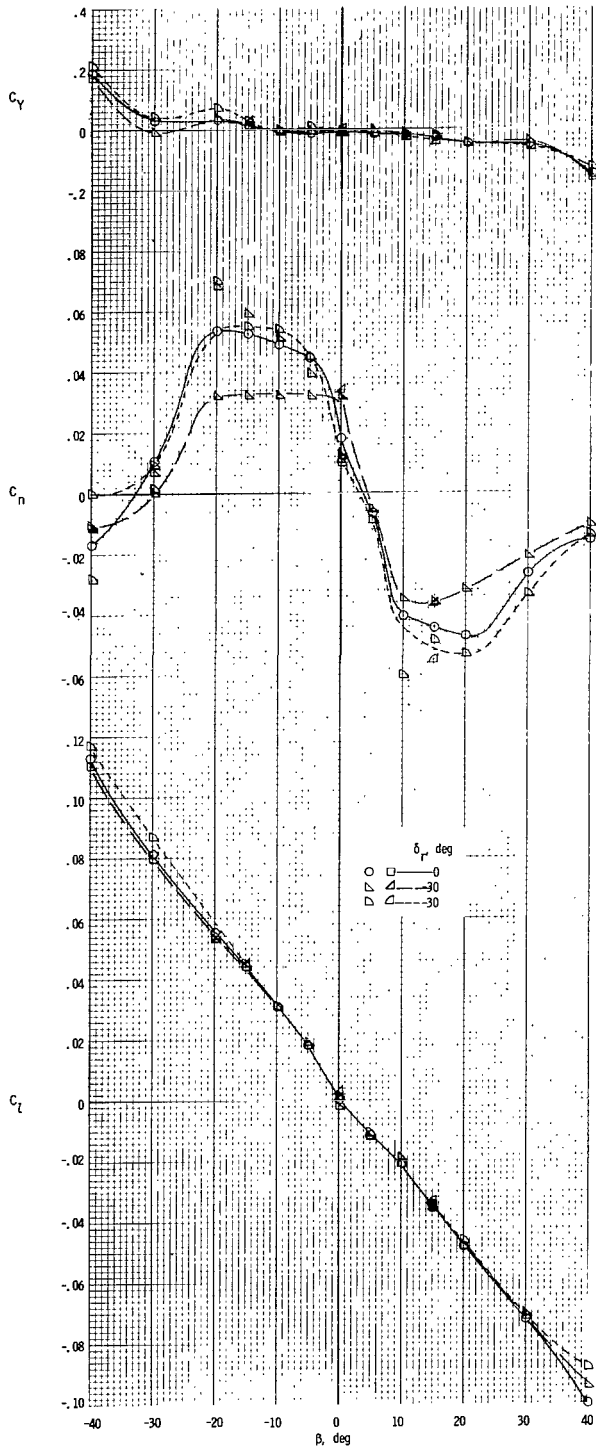


(t) $\alpha = 70^\circ$.

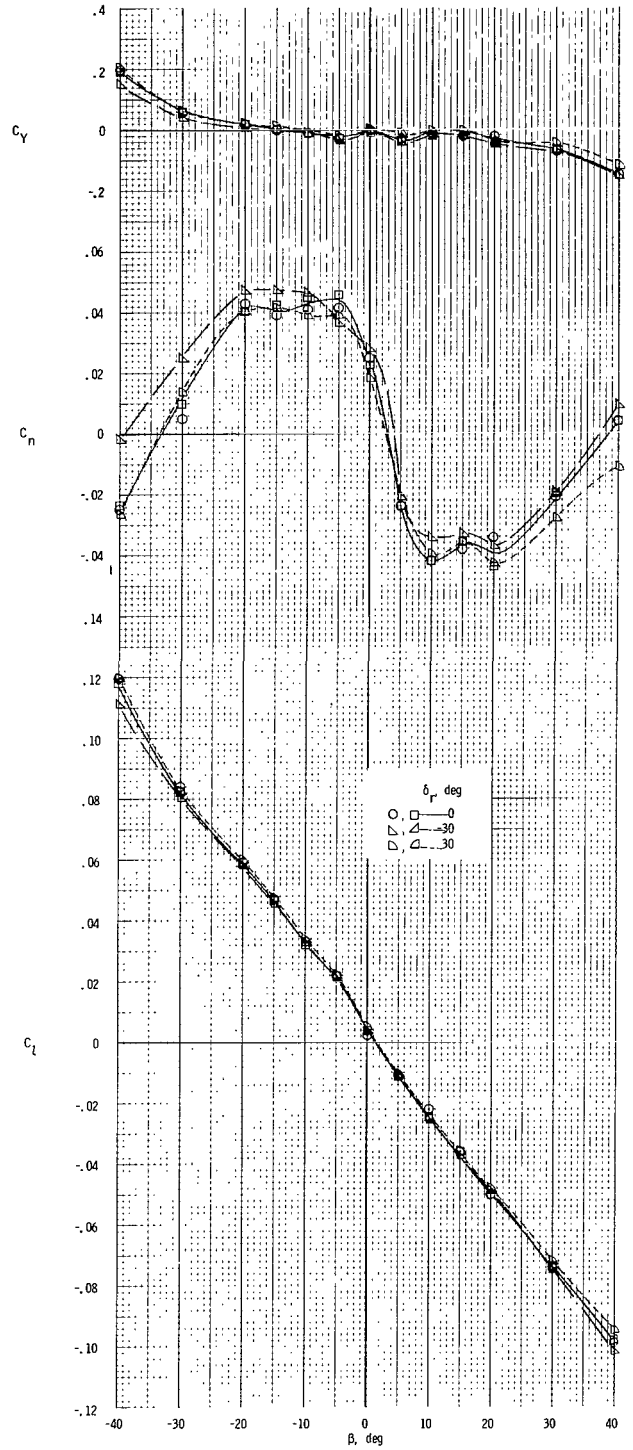


(u) $\alpha = 75^\circ$.

Figure 7.- Continued.

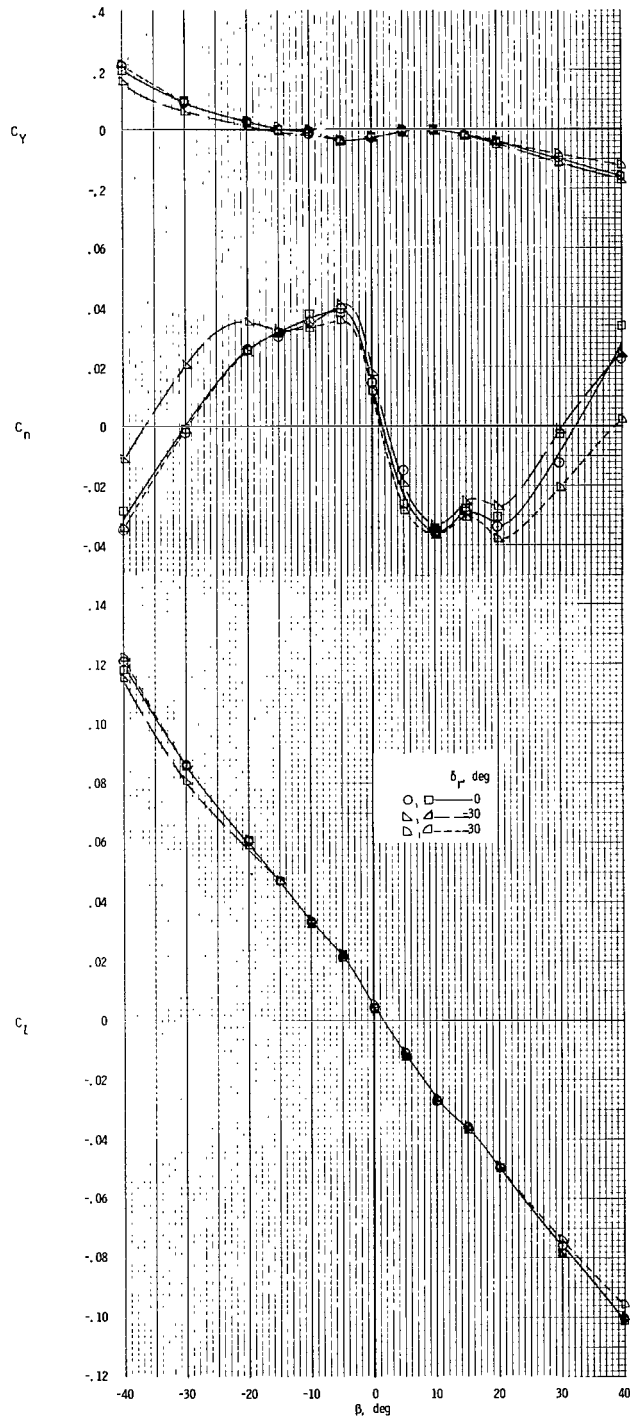


(v) $\alpha = 80^\circ$.



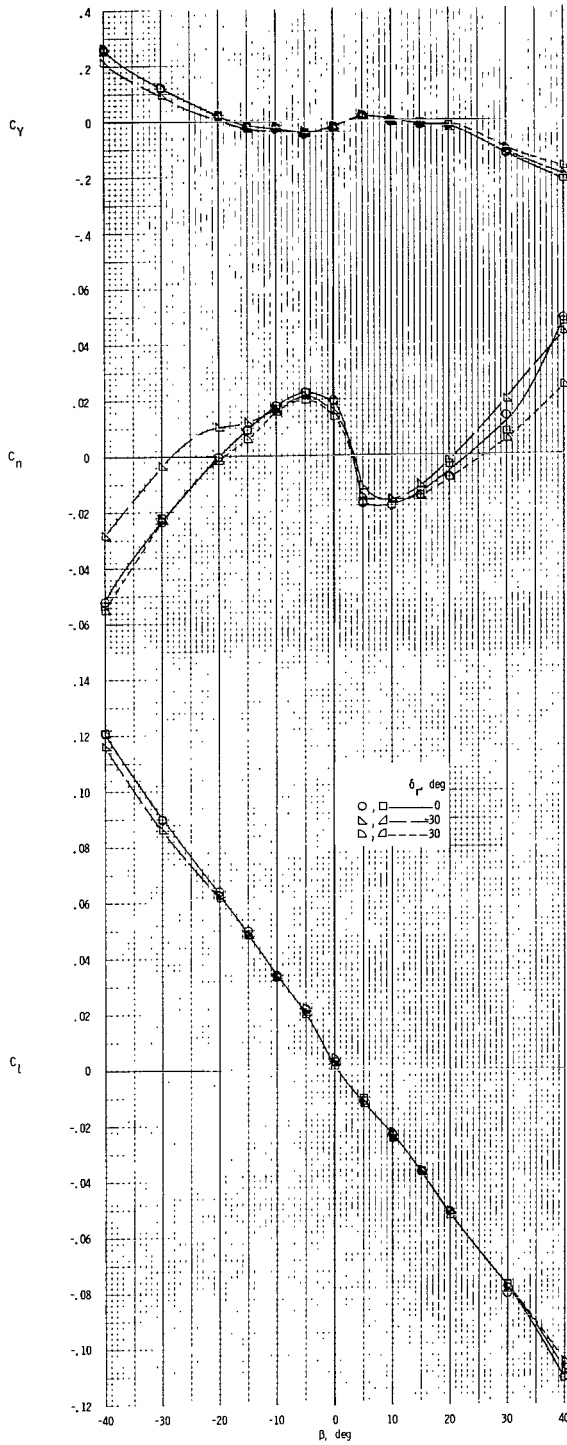
(w) $\alpha = 85^\circ$.

Figure 7.- Continued.

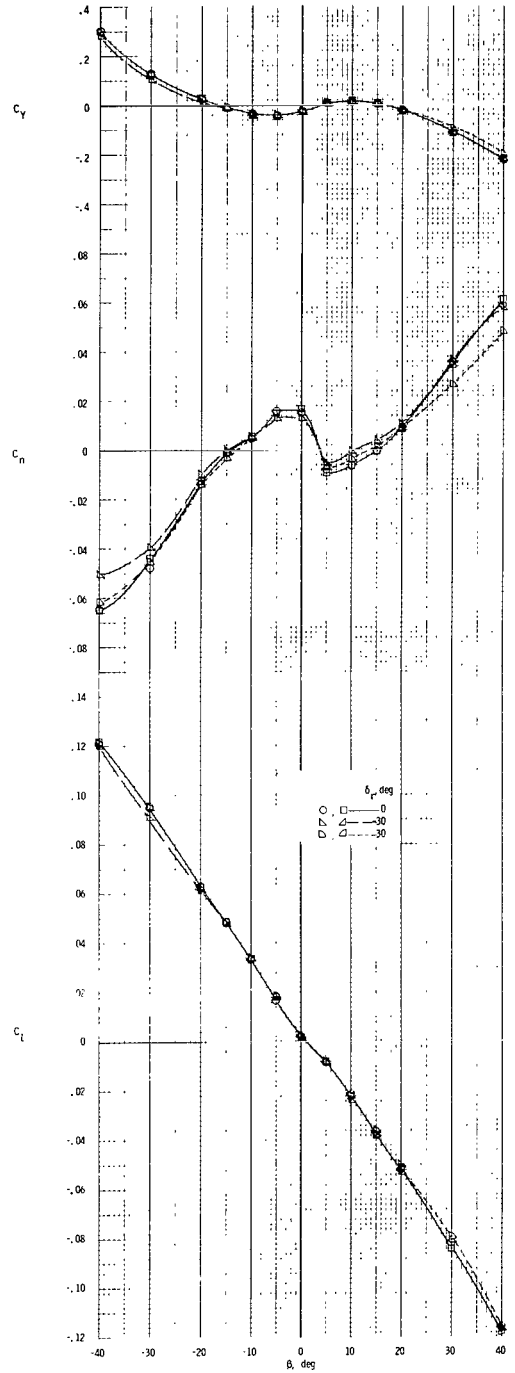


(x) $\alpha = 90^\circ$.

Figure 7.- Continued.



(y) $\alpha = 100^\circ$.



(z) $\alpha = 110^\circ$.

Figure 7.- Concluded.

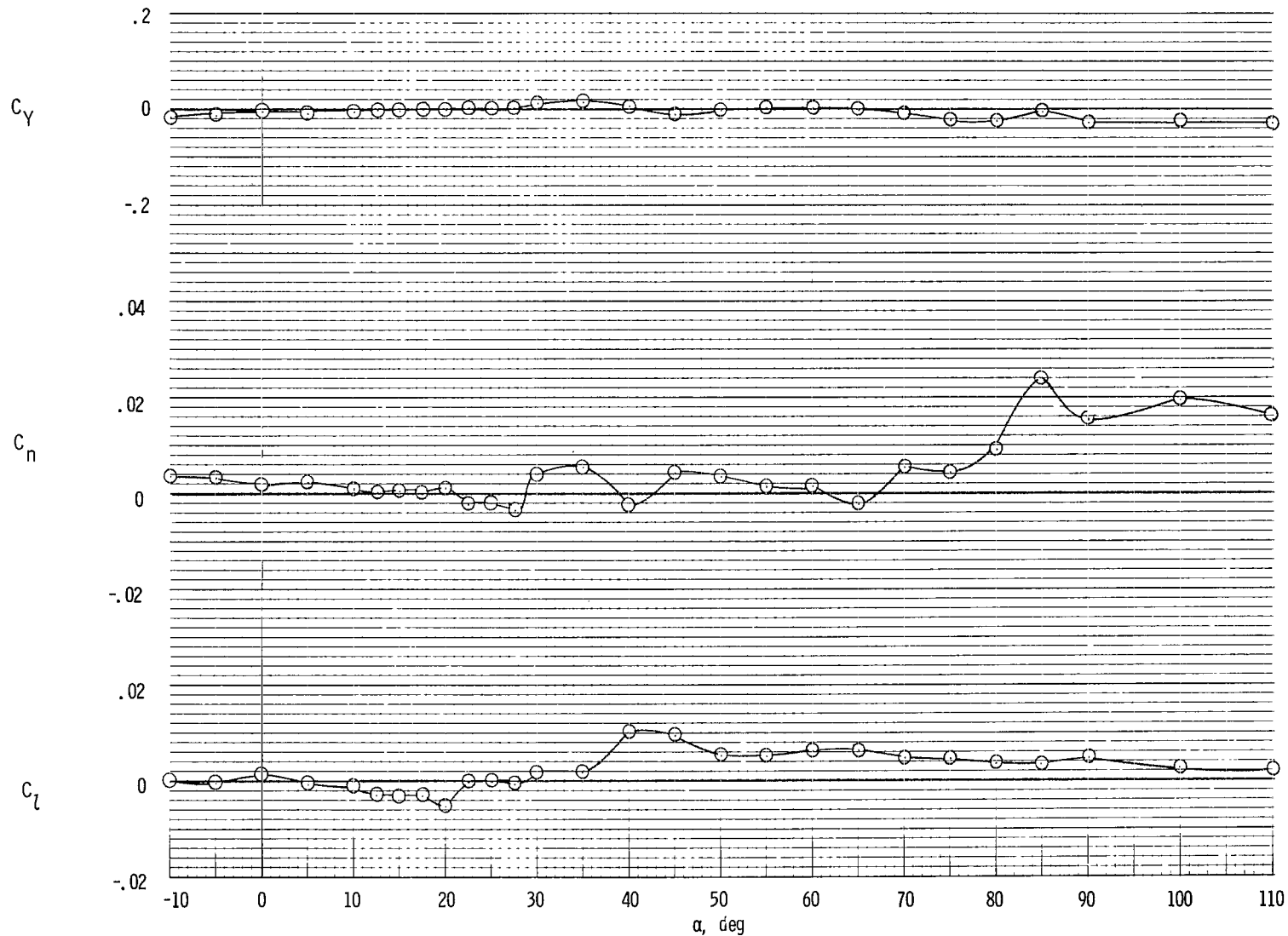
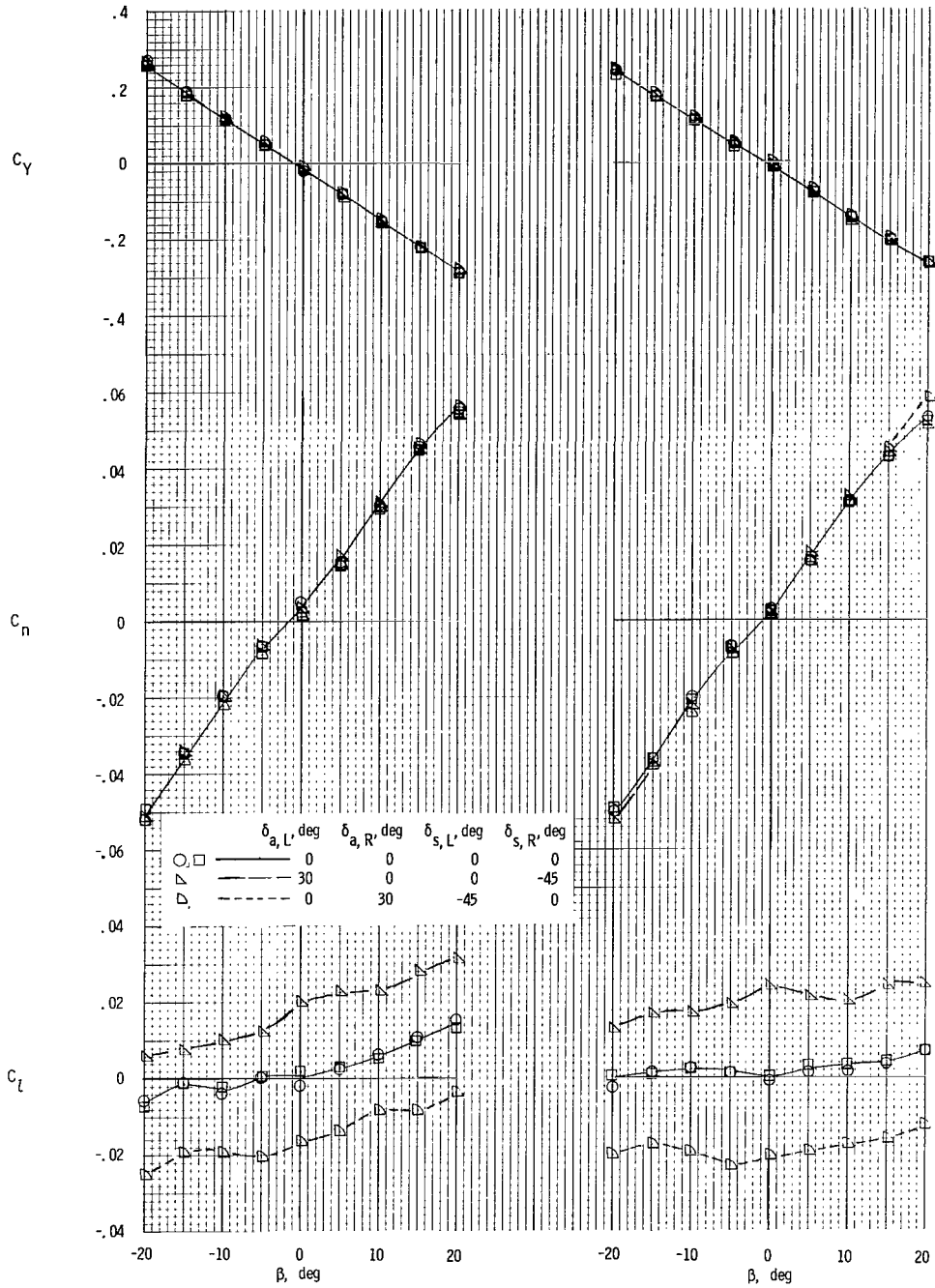


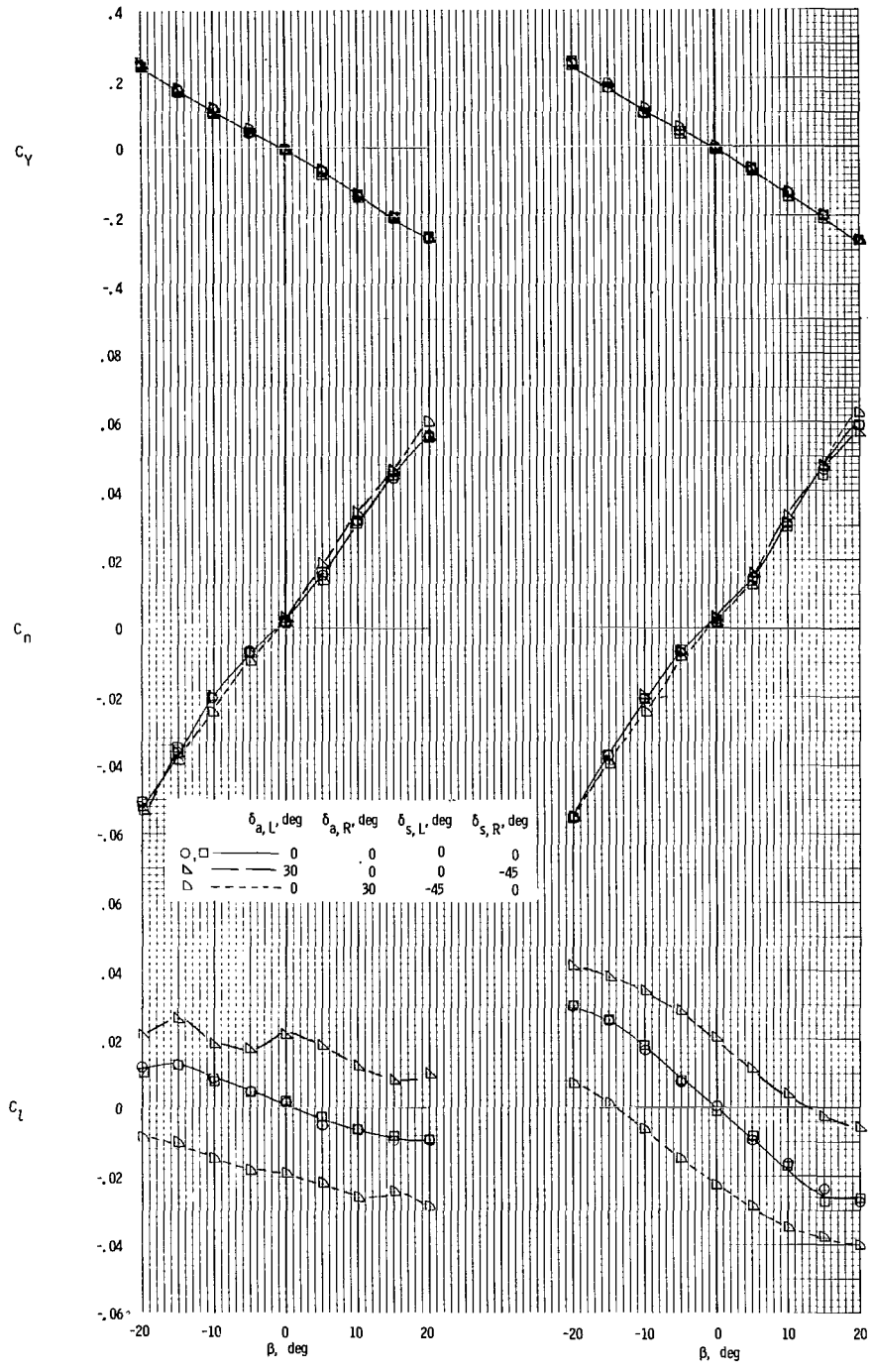
Figure 8.- Static lateral-directional stability coefficients plotted against angle of attack.
 $\beta = 0^\circ$; all controls neutral.



(a) $\alpha = -10^\circ$.

(b) $\alpha = -5^\circ$.

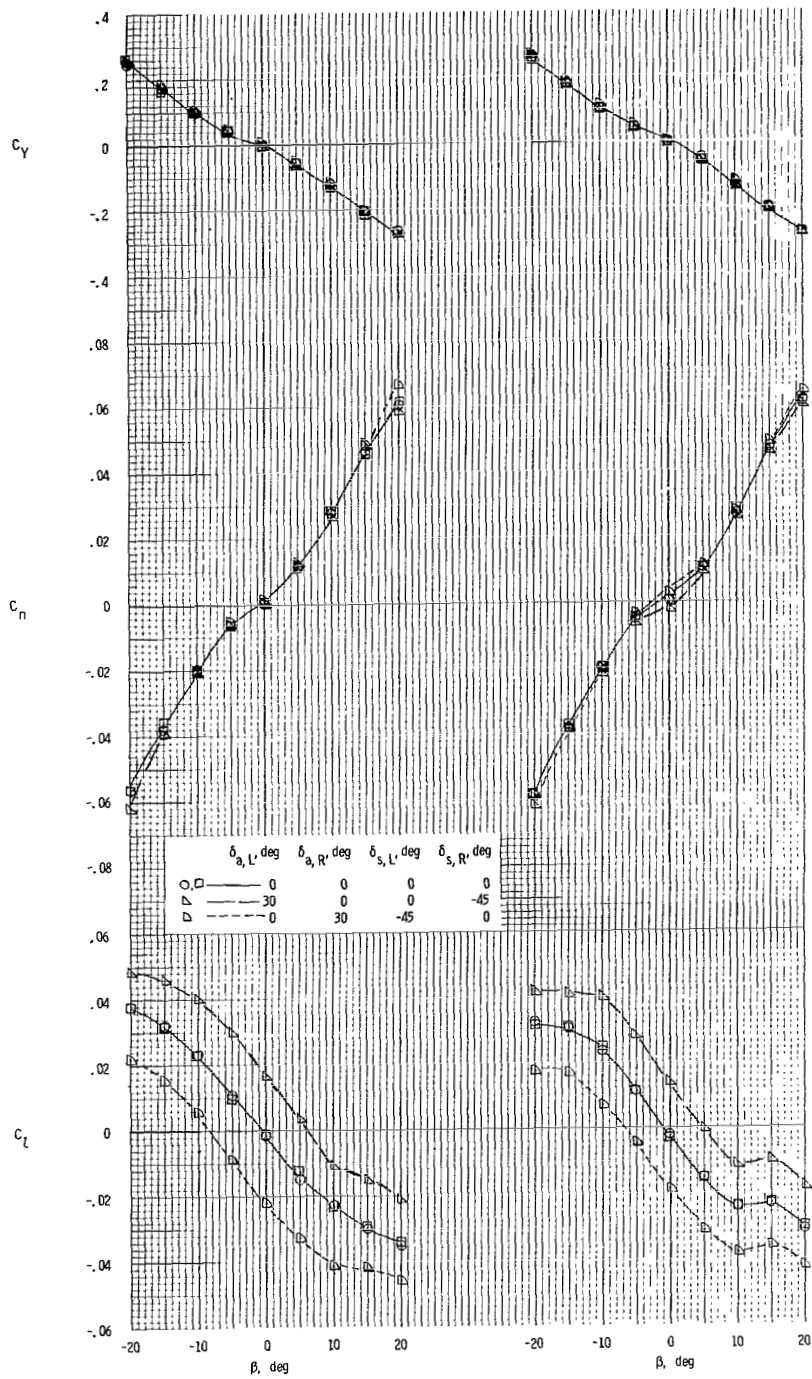
Figure 9.- Effect of roll control deflections (combined aileron and spoiler) on the static lateral-directional stability coefficients as a function of angle of attack and sideslip angle. $\delta_h = 0^\circ$. (Double symbols, when used, show repeat tests.)



(c) $\alpha = 0^\circ$.

(d) $\alpha = 5^\circ$.

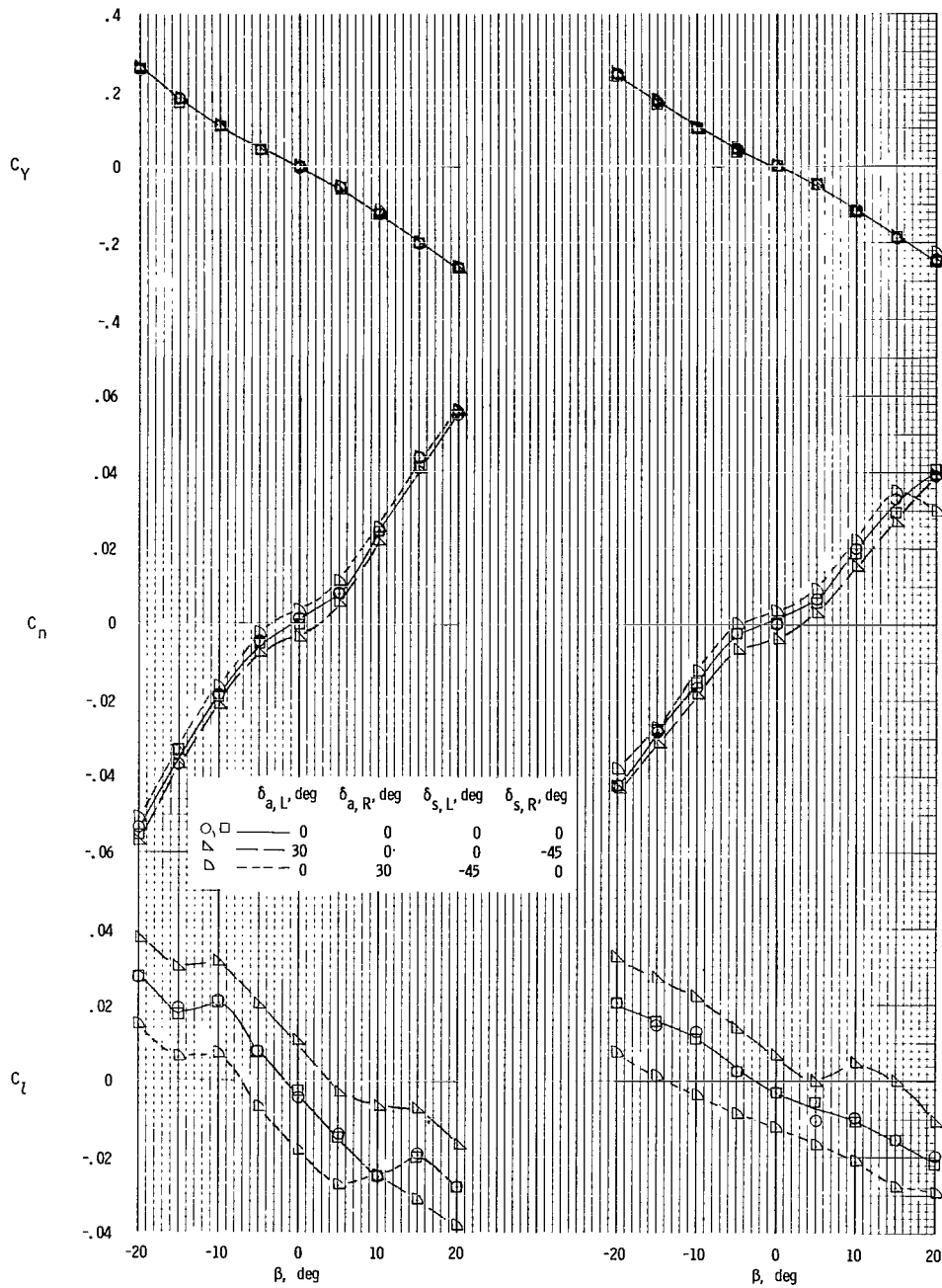
Figure 9.- Continued.



(e) $\alpha = 10^\circ$.

(f) $\alpha = 12.5^\circ$.

Figure 9.- Continued.



(g) $\alpha = 15^\circ$.

(h) $\alpha = 17.5^\circ$.

Figure 9.- Continued.

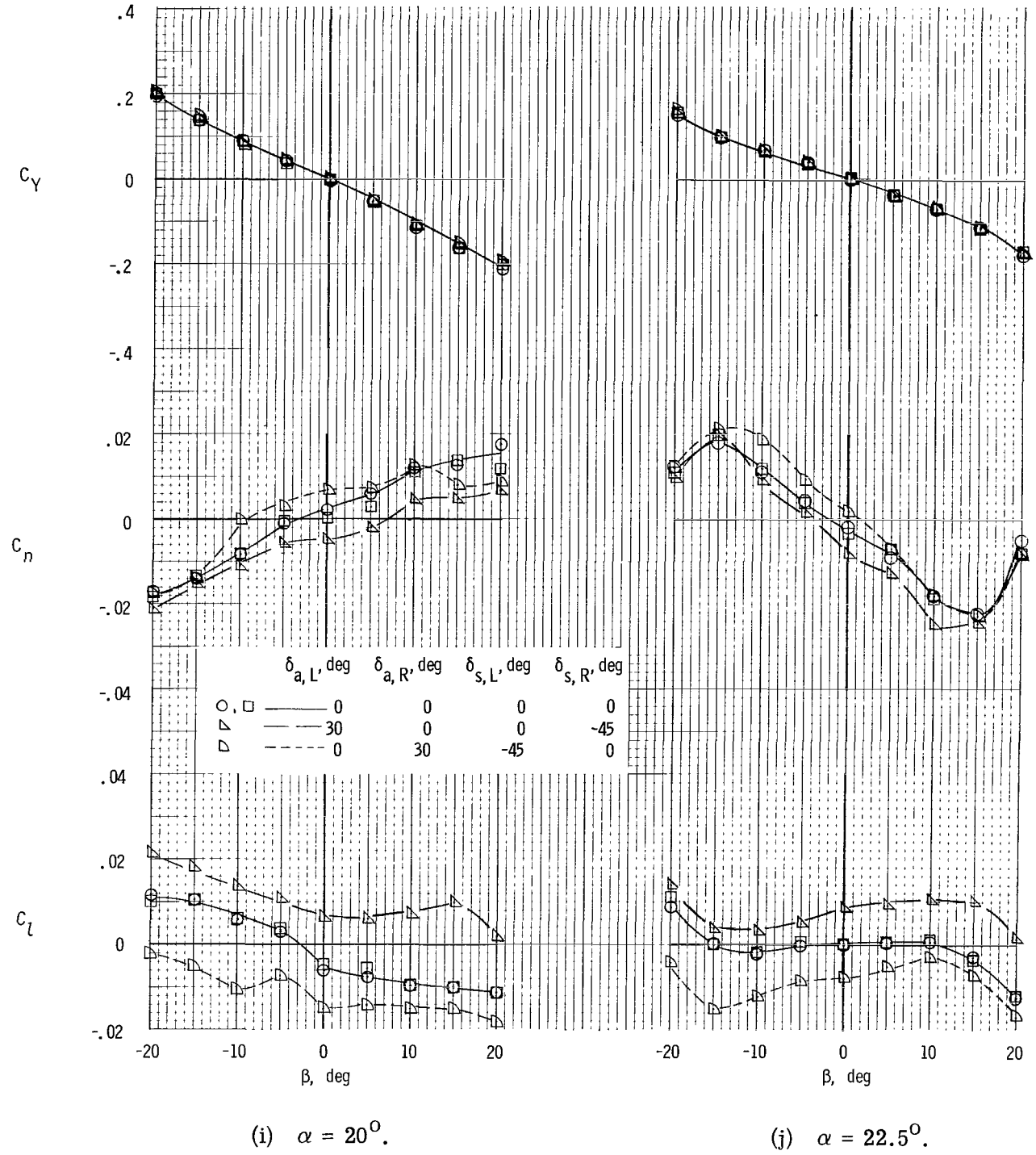
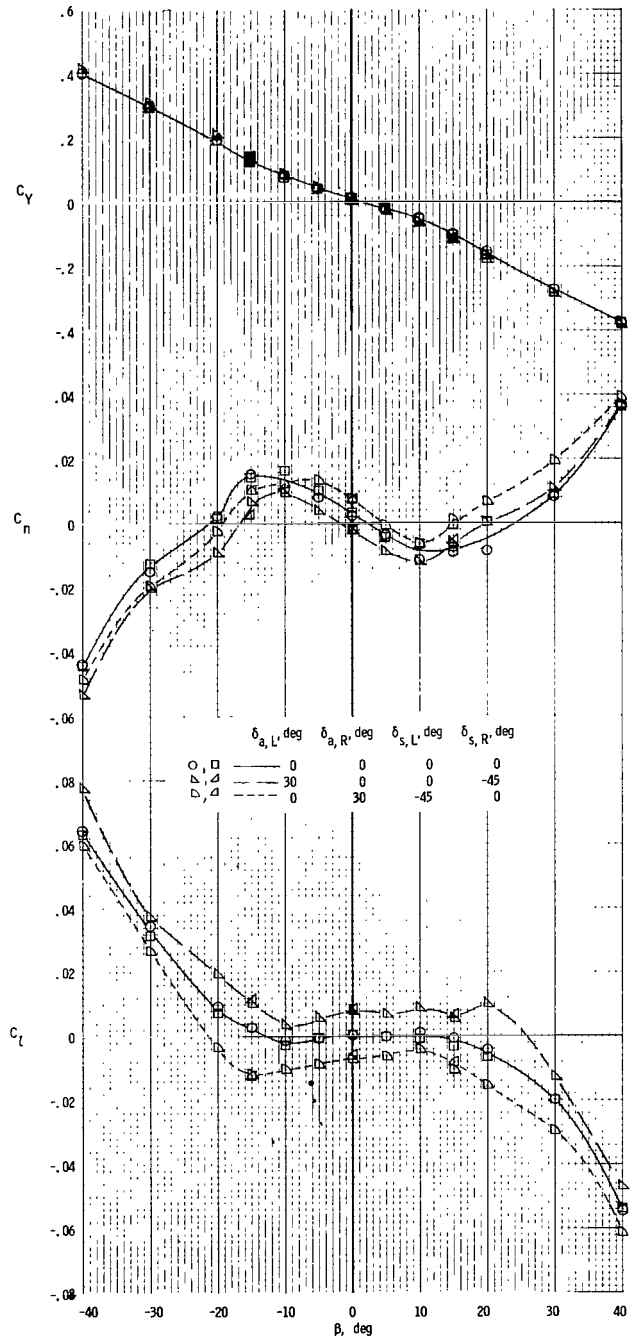
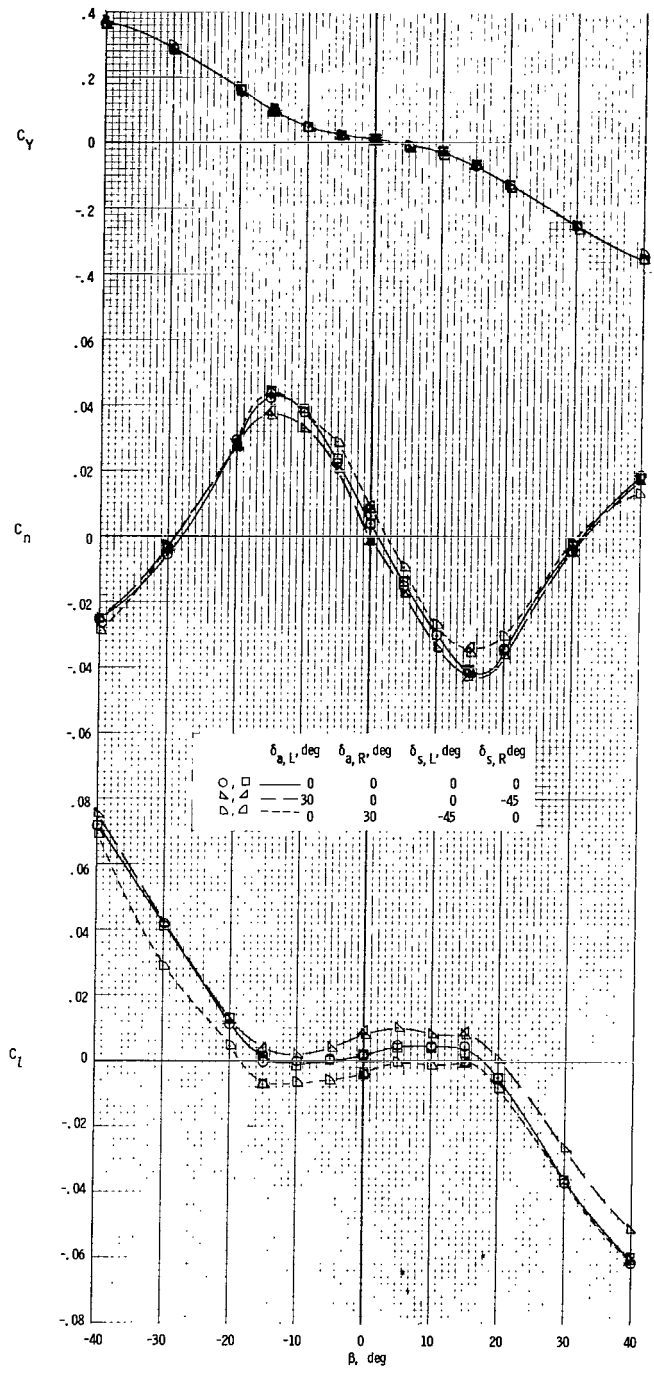


Figure 9.- Continued.



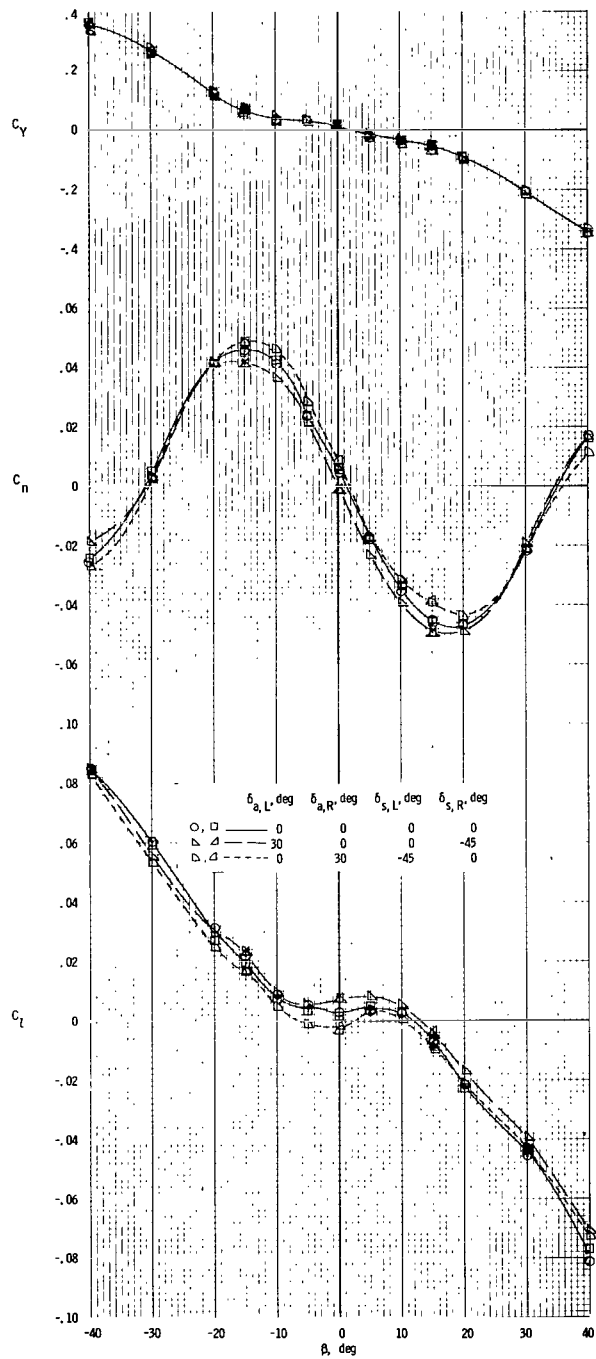
(k) $\alpha = 25^\circ$.

Figure 9.- Continued.

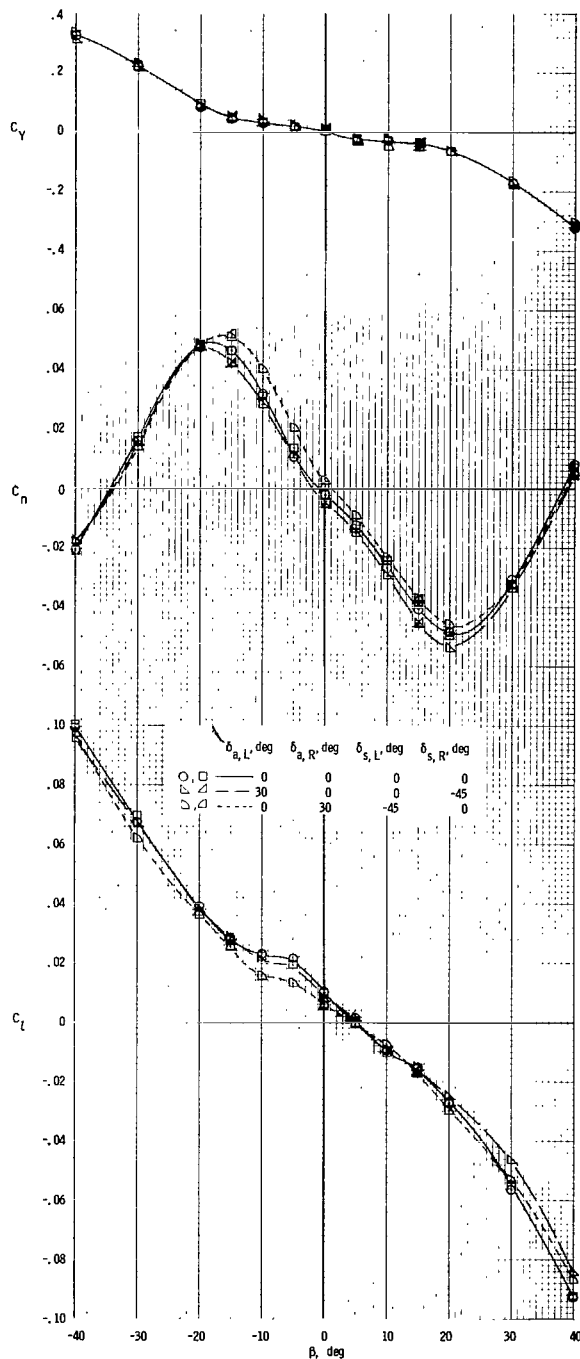


(l) $\alpha = 30^\circ$.

Figure 9.- Continued.

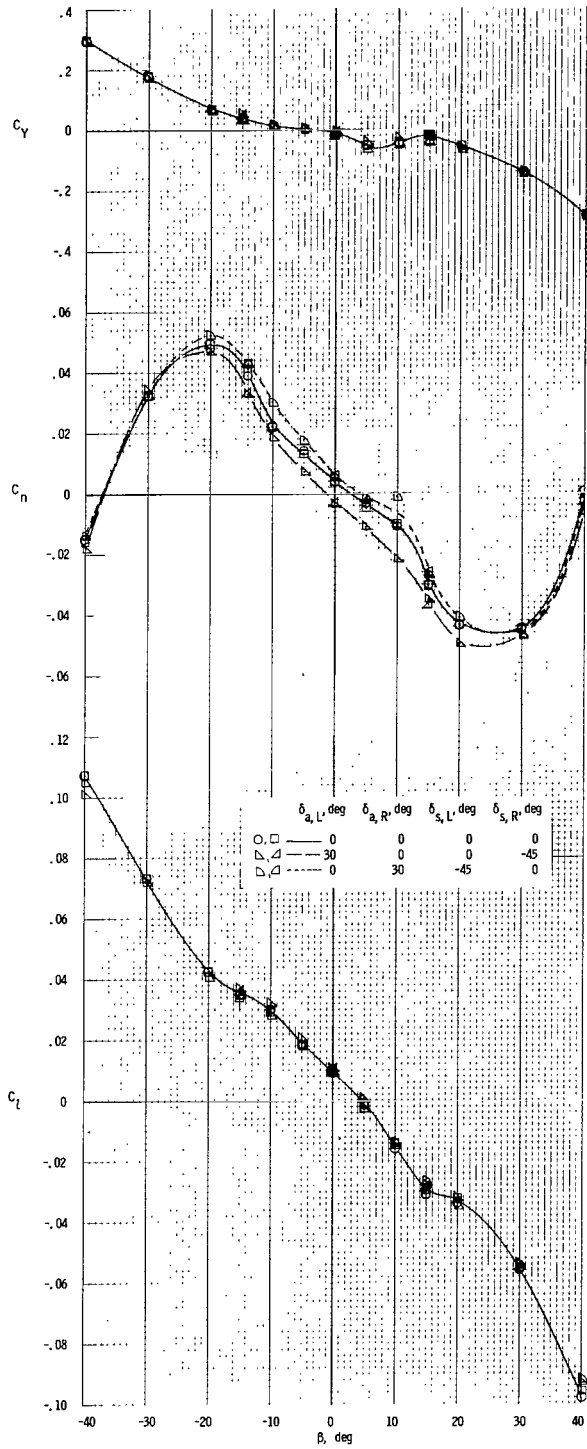


(m) $\alpha = 35^\circ$.

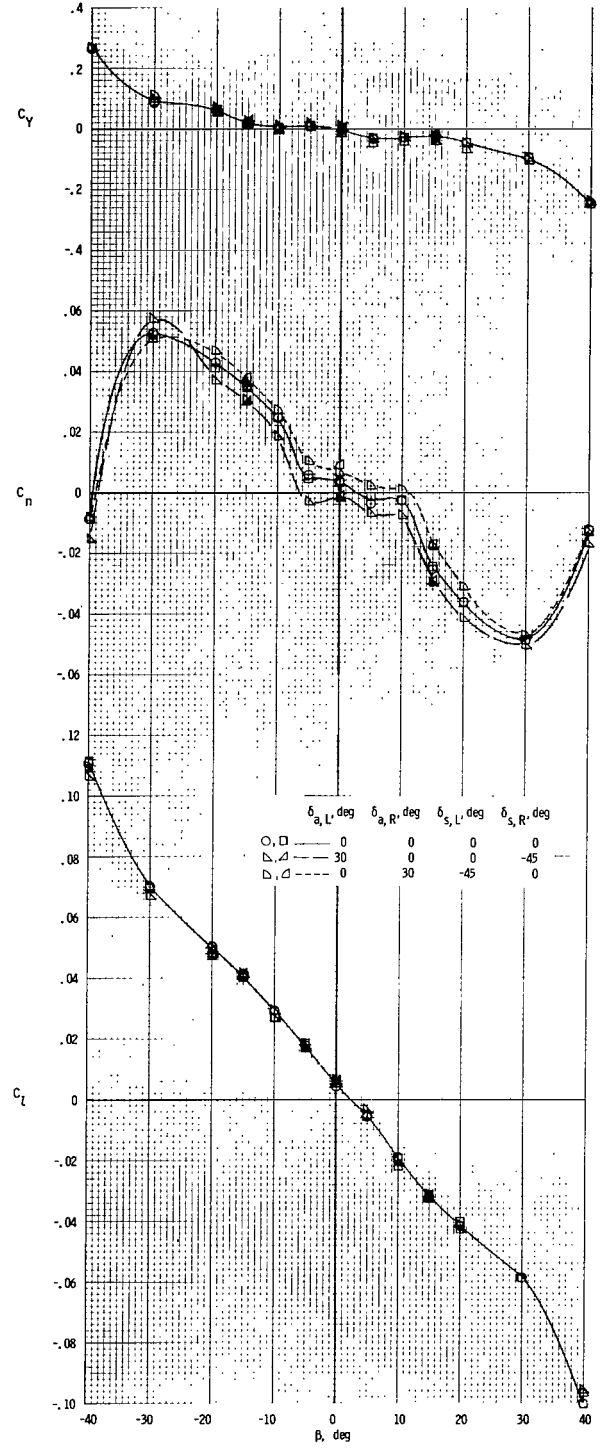


(n) $\alpha = 40^\circ$.

Figure 9.- Continued.

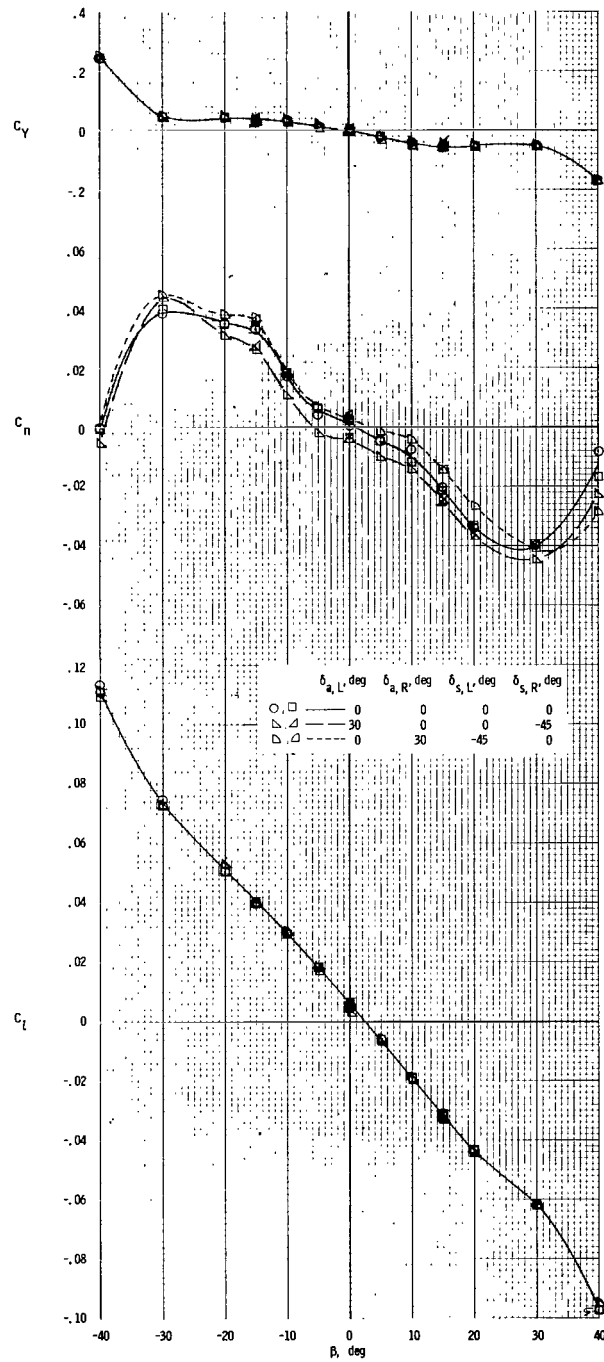


(o) $\alpha = 45^\circ$.



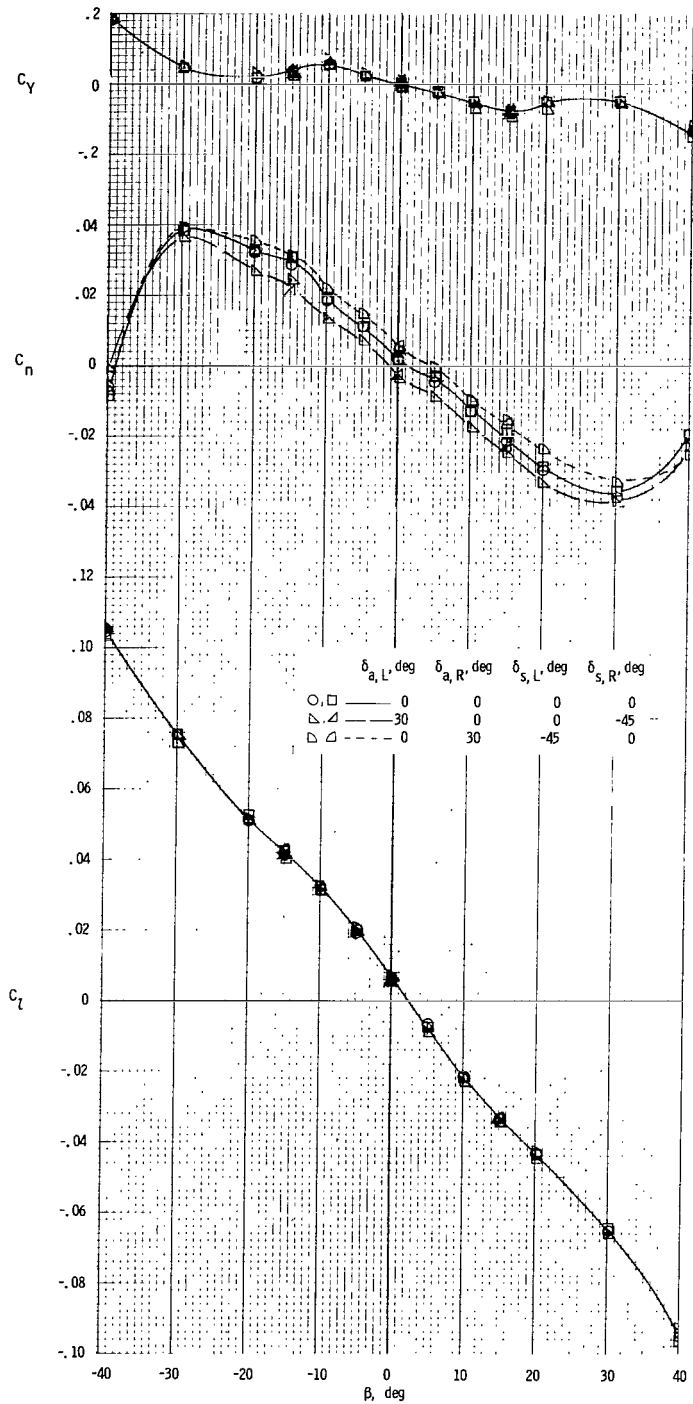
(p) $\alpha = 50^\circ$.

Figure 9.- Continued.



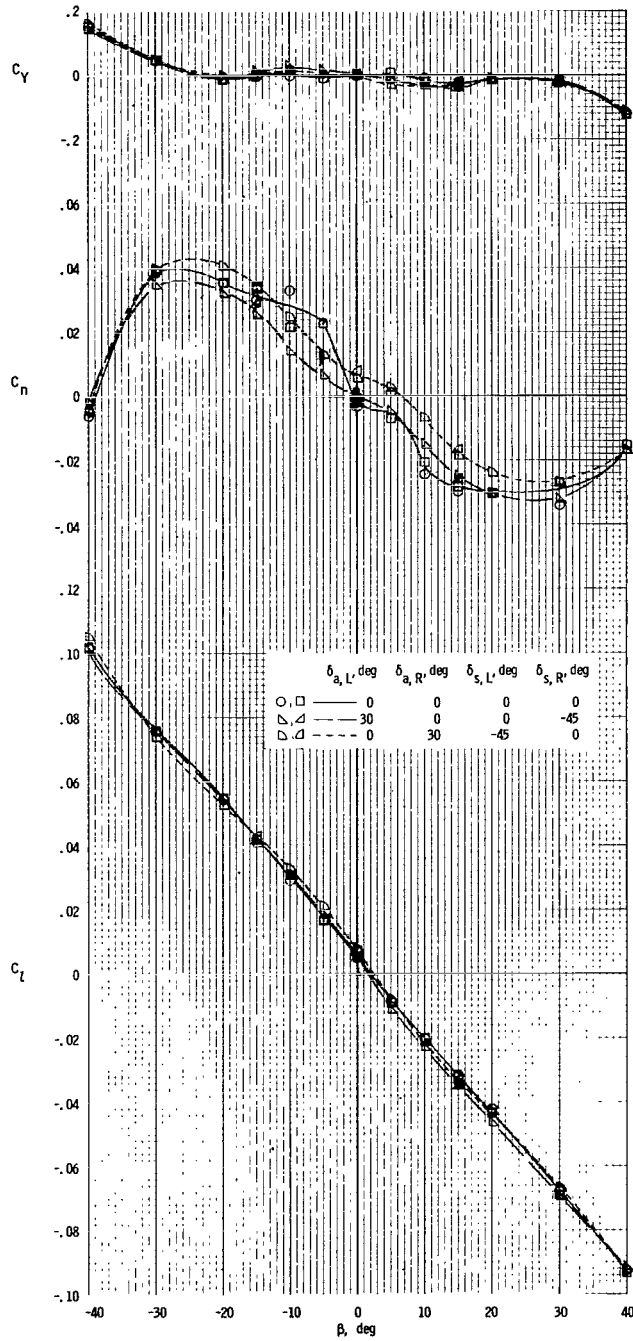
(q) $\alpha = 55^\circ$.

Figure 9.- Continued.



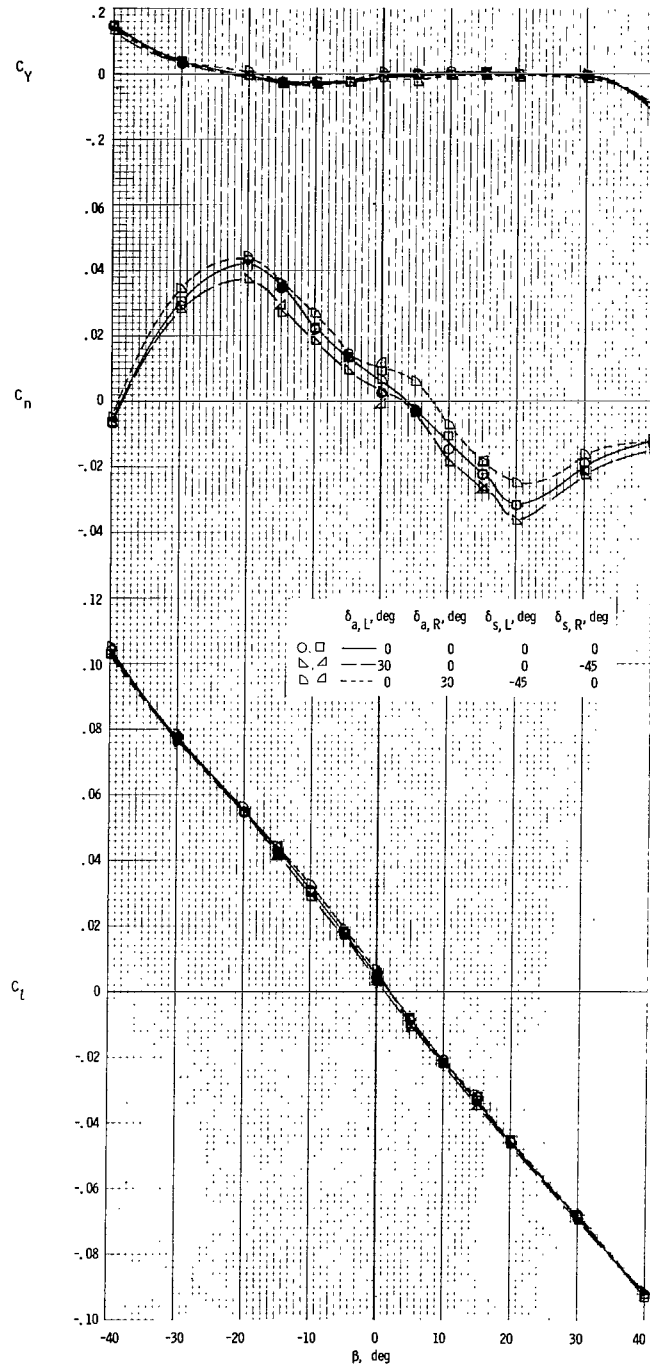
(r) $\alpha = 60^\circ$.

Figure 9.- Continued.



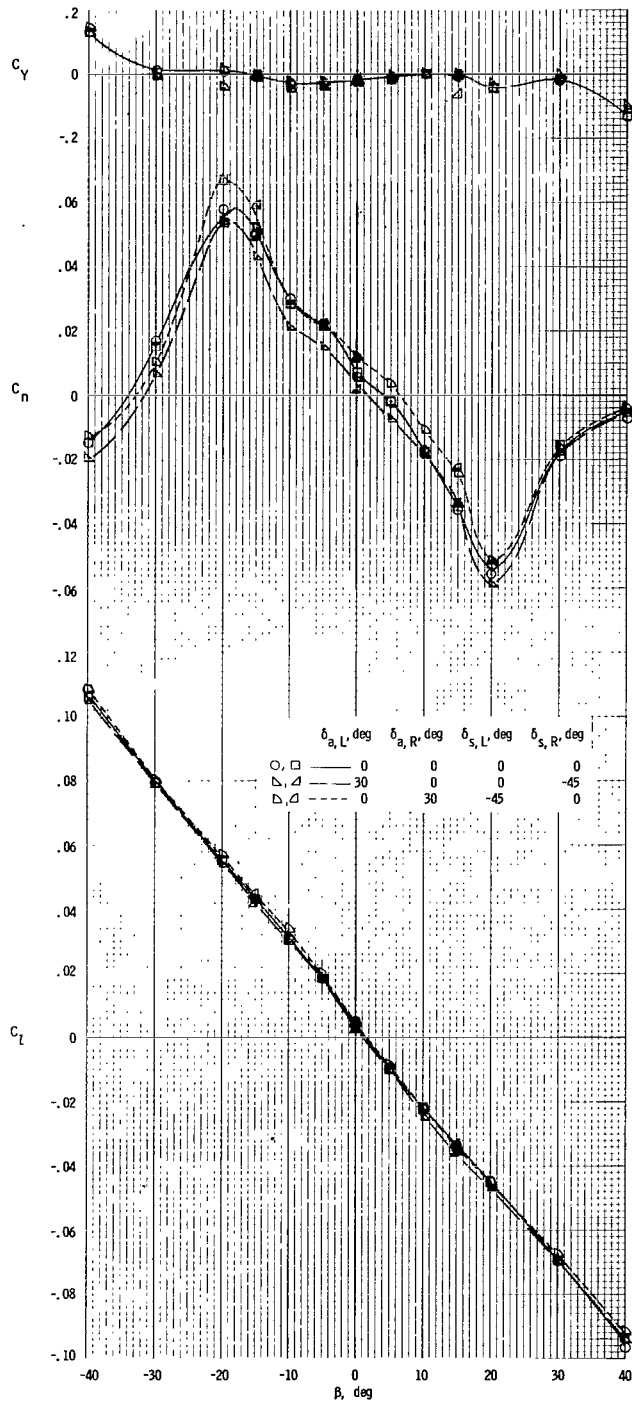
(s) $\alpha = 65^\circ$.

Figure 9.- Continued.



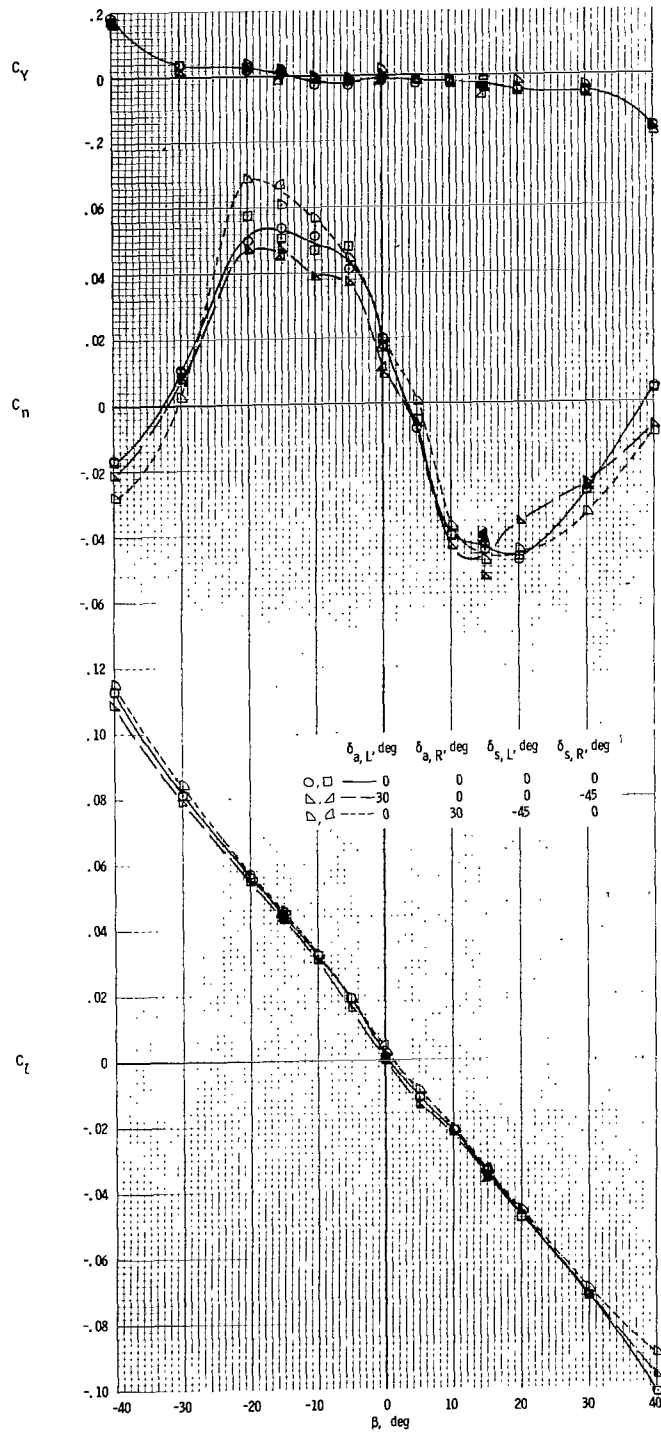
(t) $\alpha = 70^\circ$.

Figure 9.- Continued.



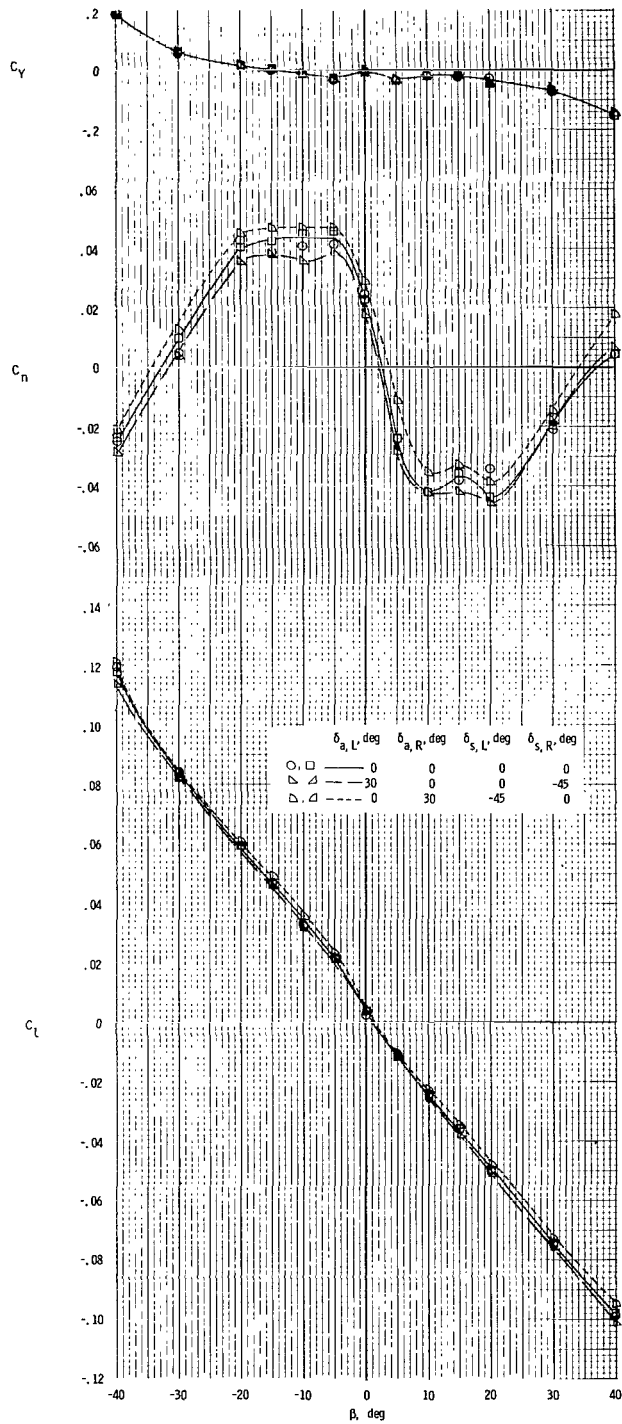
(u) $\alpha = 75^\circ$.

Figure 9.- Continued.

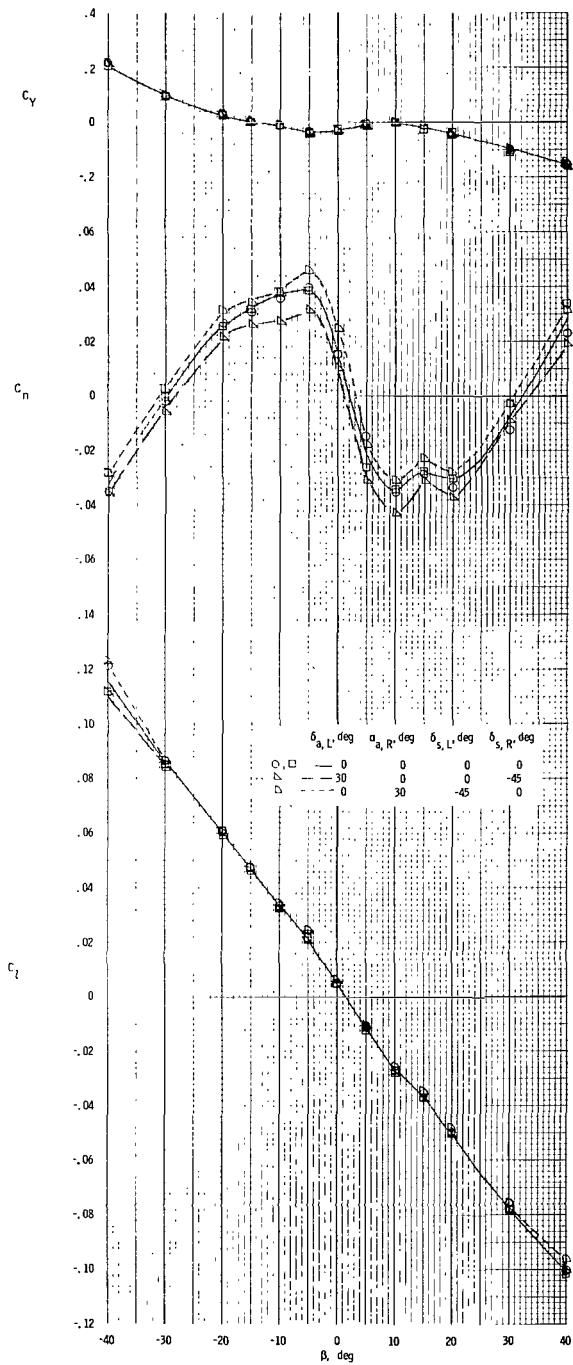


(v) $\alpha = 80^\circ$.

Figure 9.- Continued.

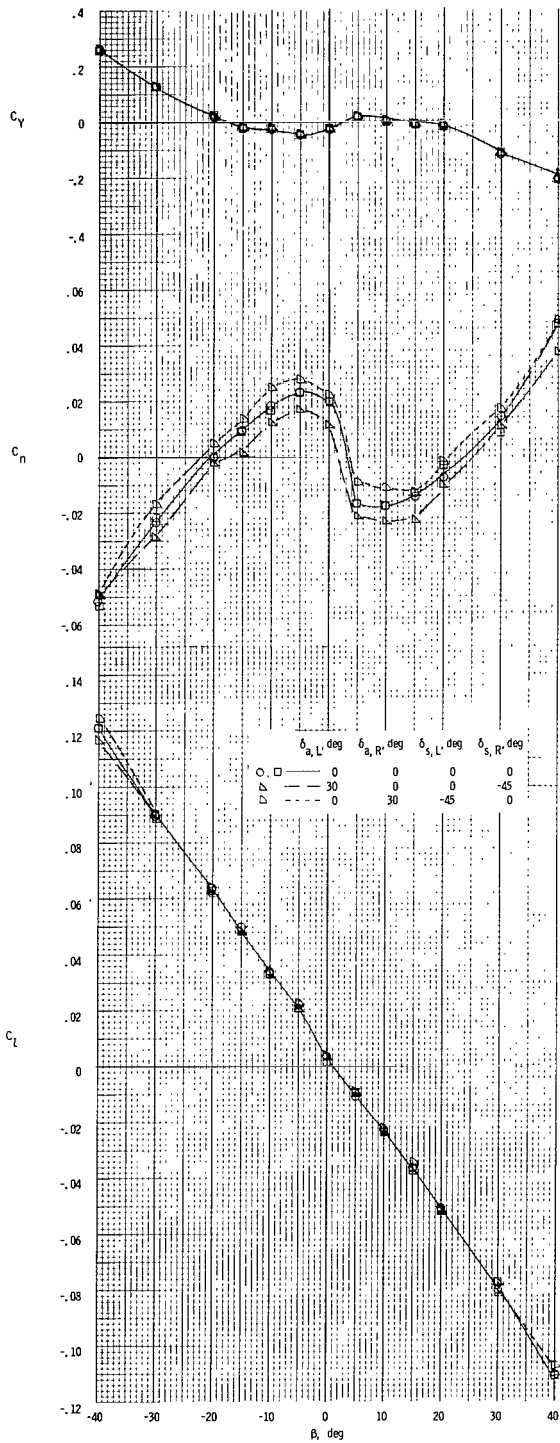


(w) $\alpha = 85^\circ$.

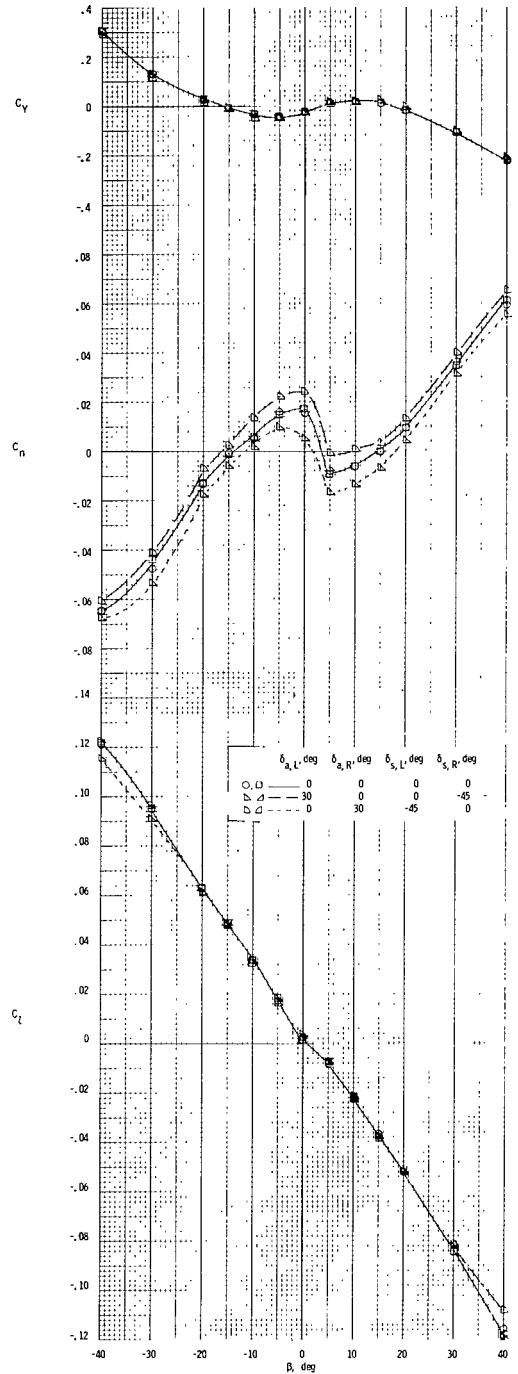


(x) $\alpha = 90^\circ$.

Figure 9.- Continued.

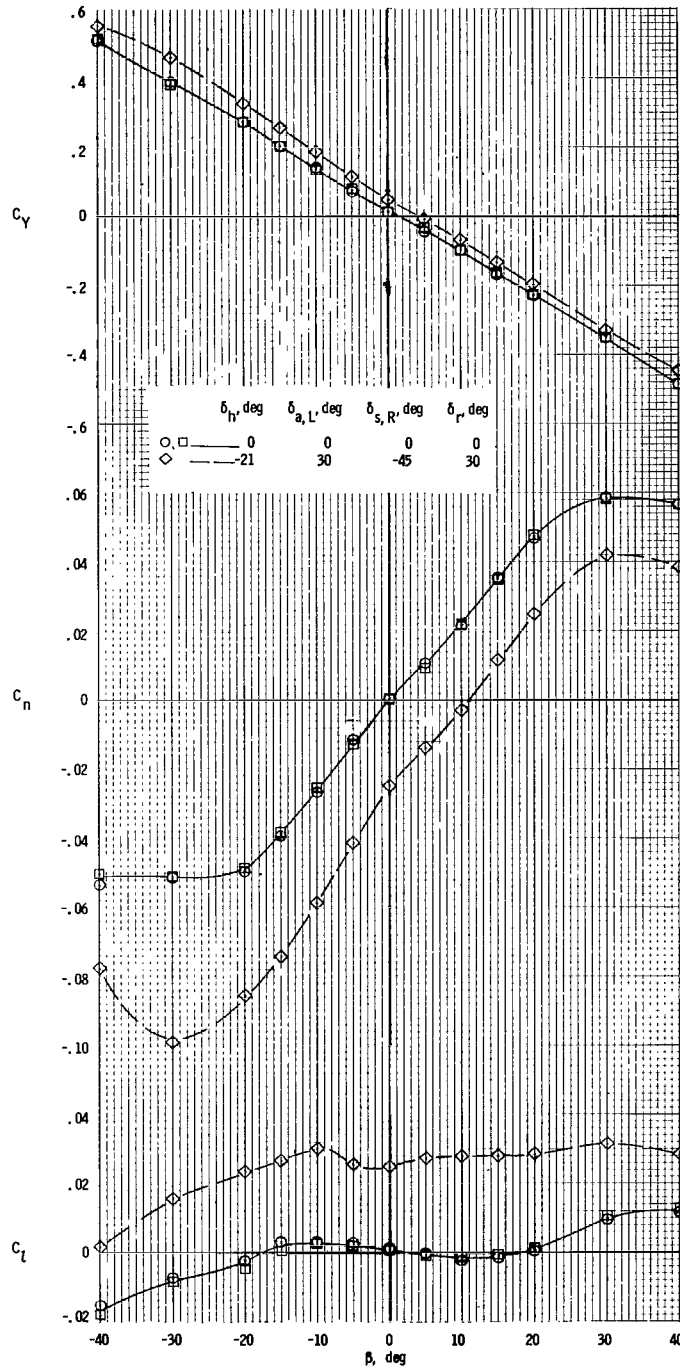


(y) $\alpha = 100^\circ$.



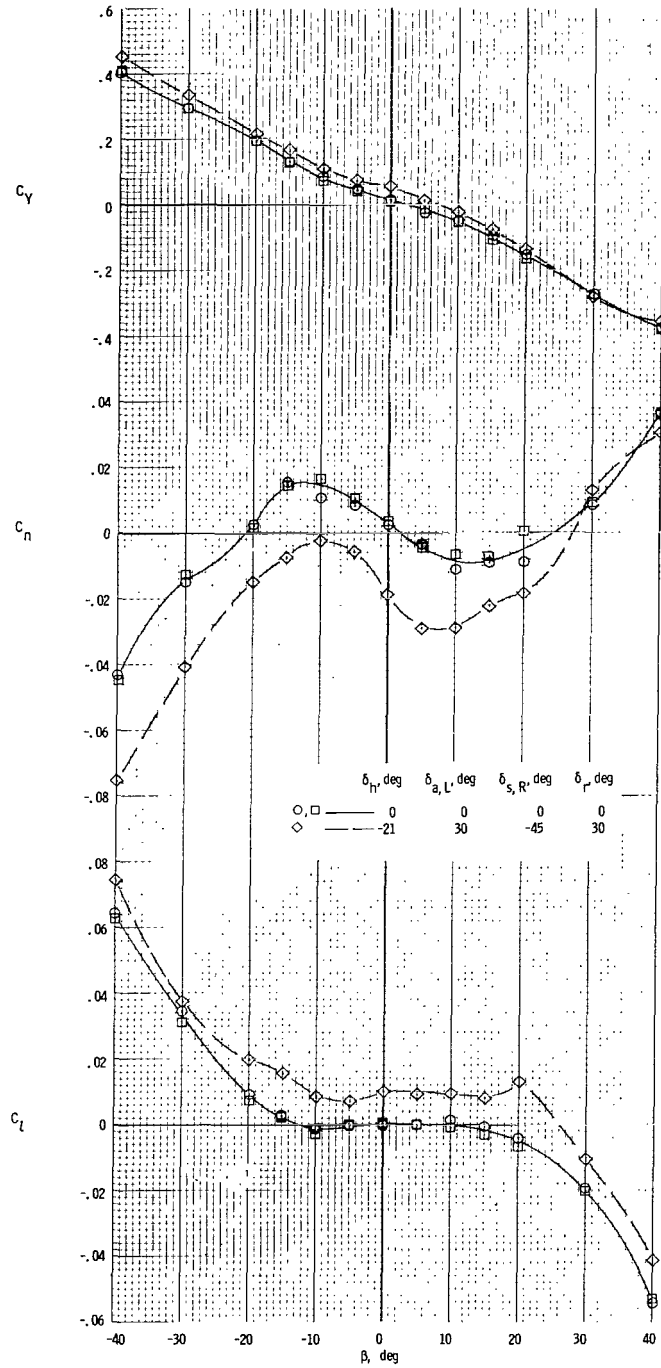
(z) $\alpha = 110^\circ$.

Figure 9.- Concluded.



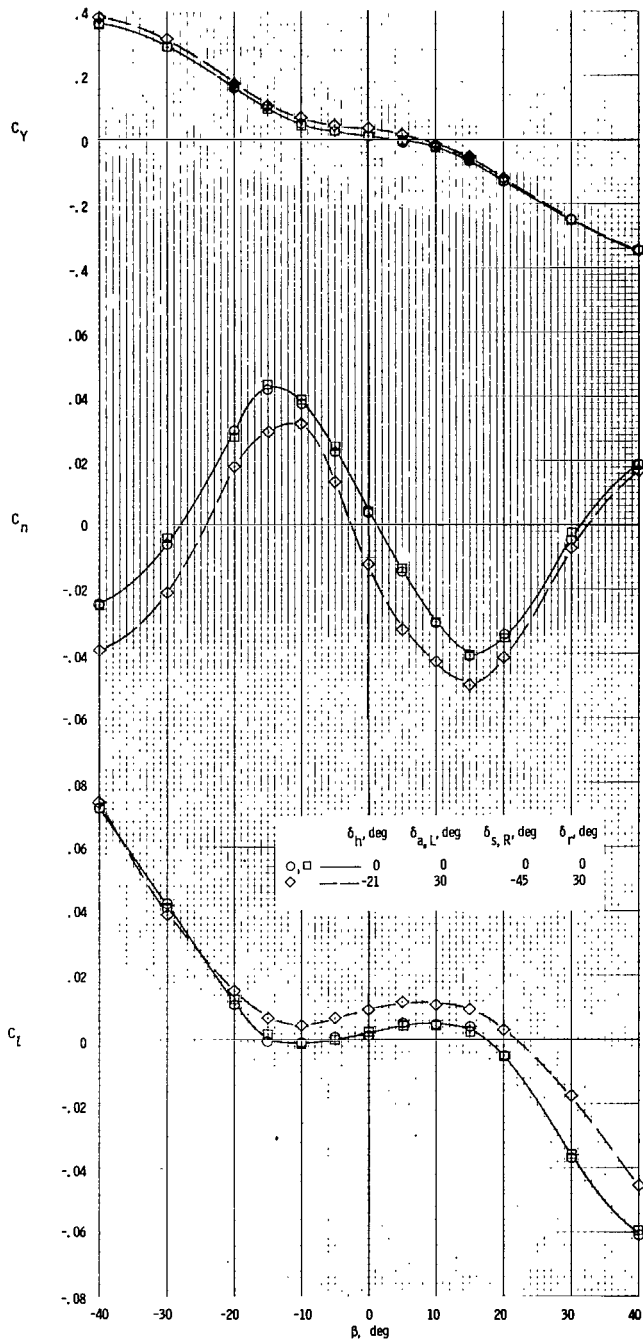
(a) $\alpha = 0^\circ$.

Figure 10.- Effect of combined left pro-spin controls on the static lateral-directional stability coefficients as a function of angle of attack and sideslip angle. $\delta_h = 0^\circ$. (Double symbols, when used, show repeat tests.)



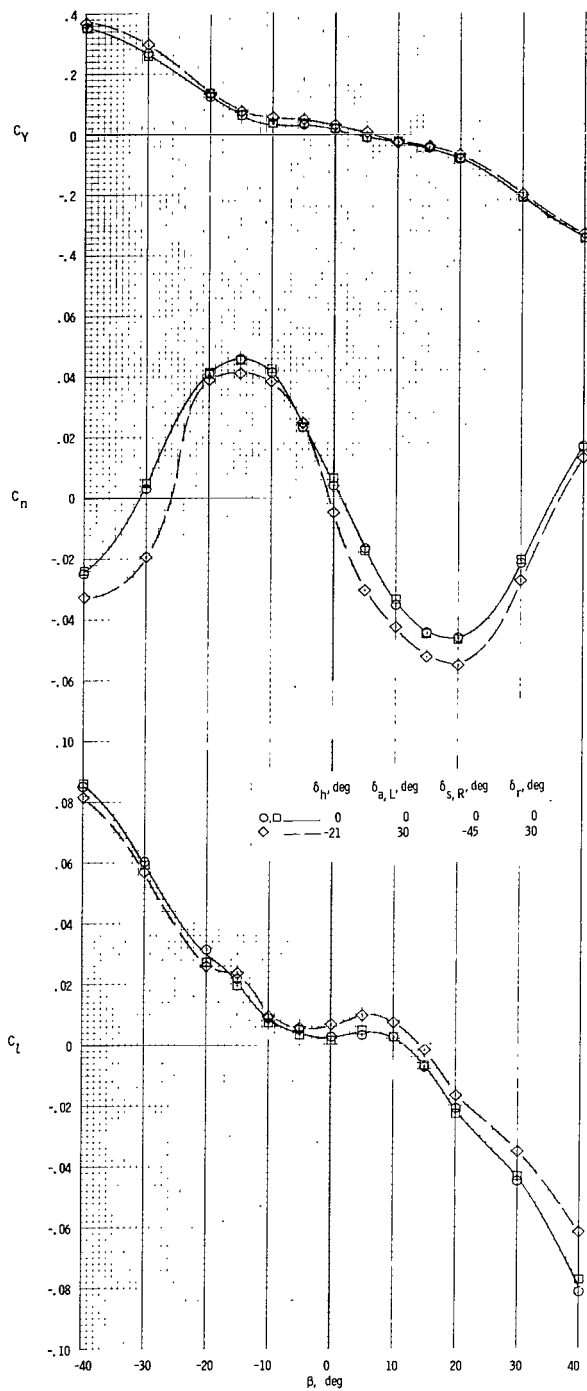
(b) $\alpha = 25^\circ$.

Figure 10.- Continued.

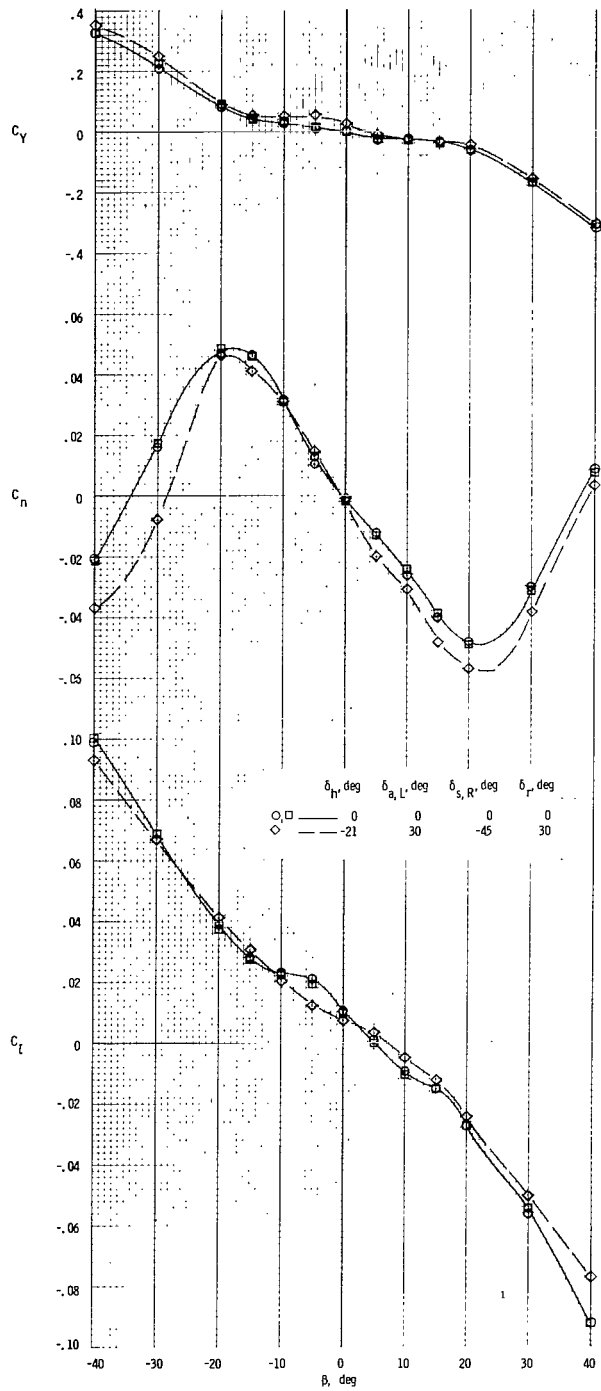


(c) $\alpha = 30^\circ$.

Figure 10.- Continued.

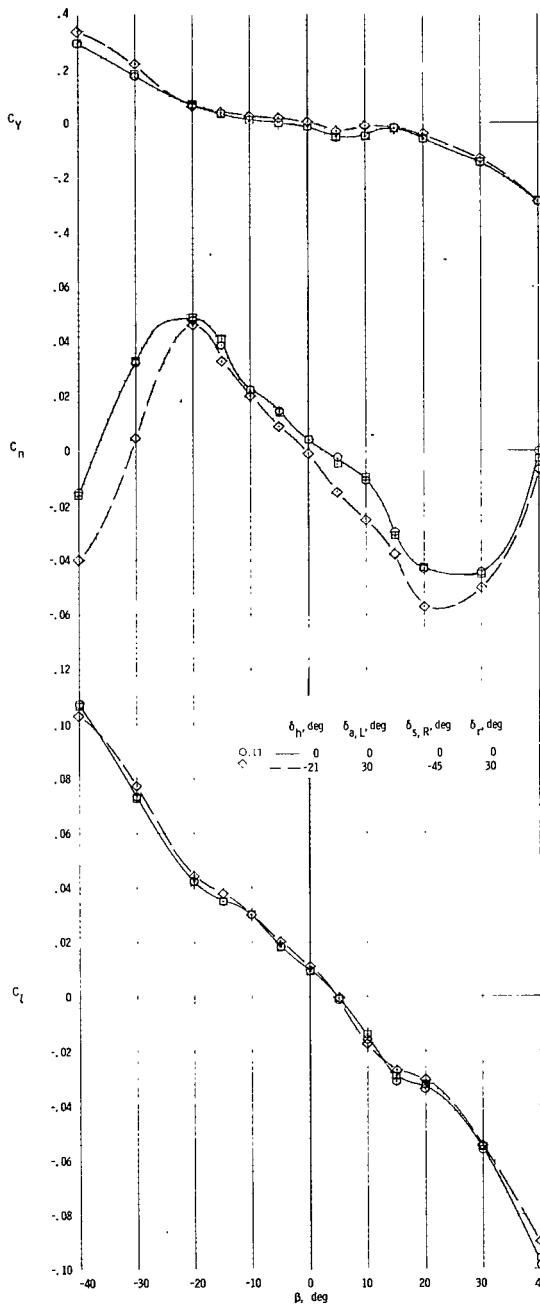


(d) $\alpha = 35^\circ$.

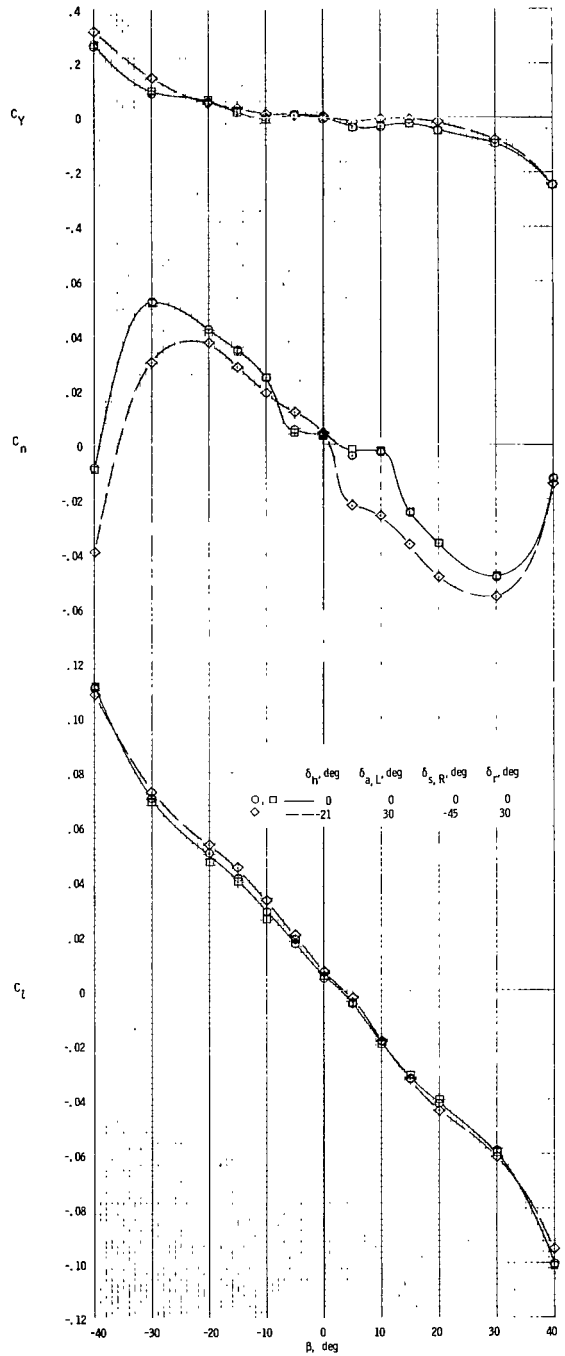


(e) $\alpha = 40^\circ$.

Figure 10.- Continued.

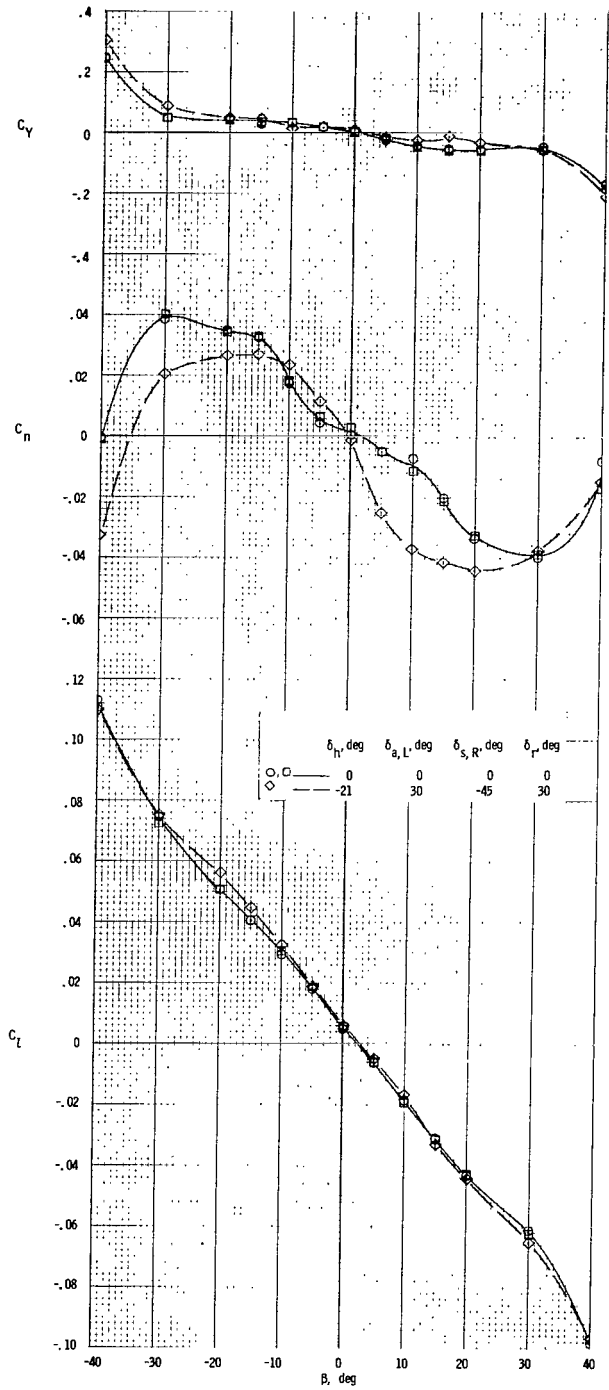


(f) $\alpha = 45^\circ$.



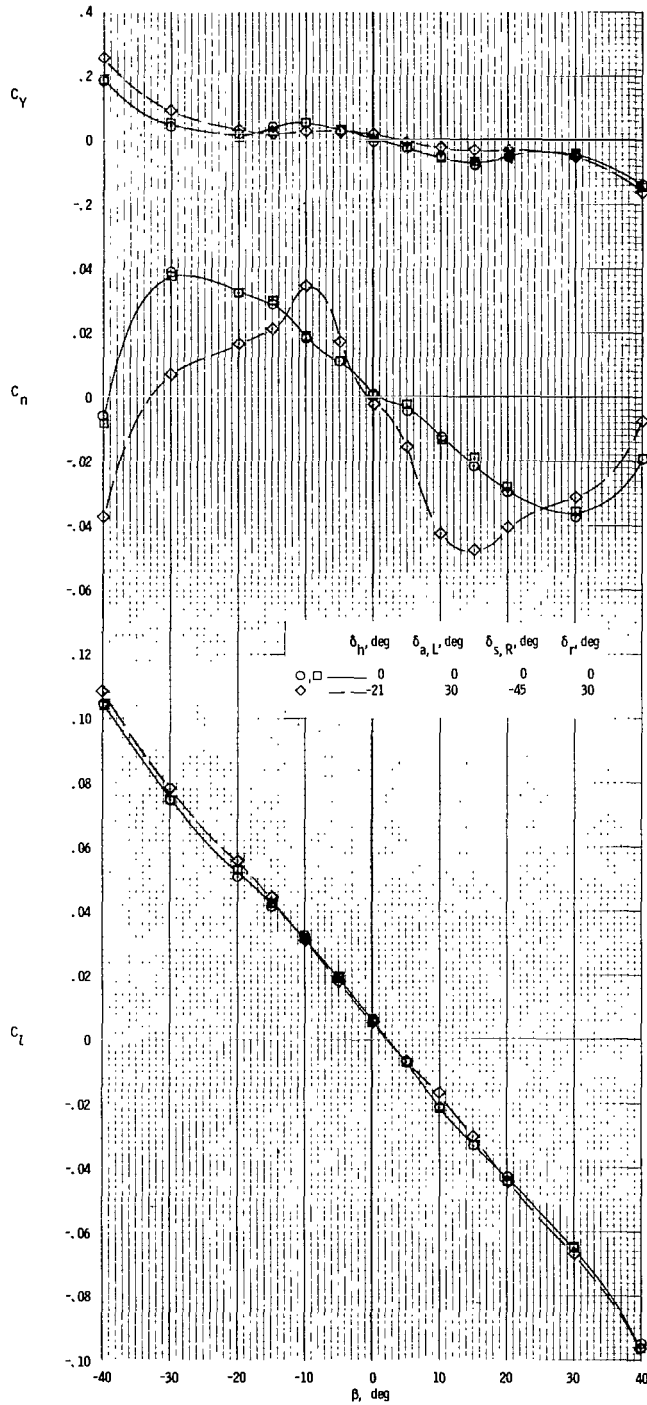
(g) $\alpha = 50^\circ$.

Figure 10.- Continued.



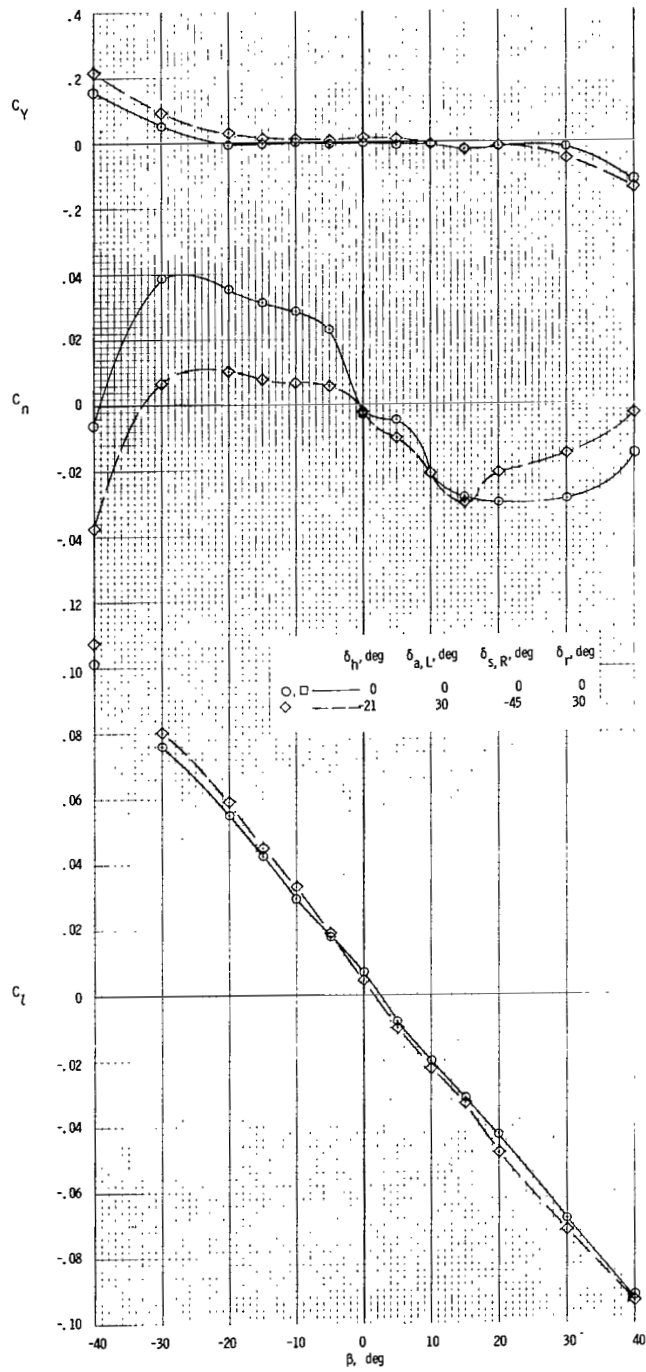
(h) $\alpha = 55^\circ$.

Figure 10.- Continued.



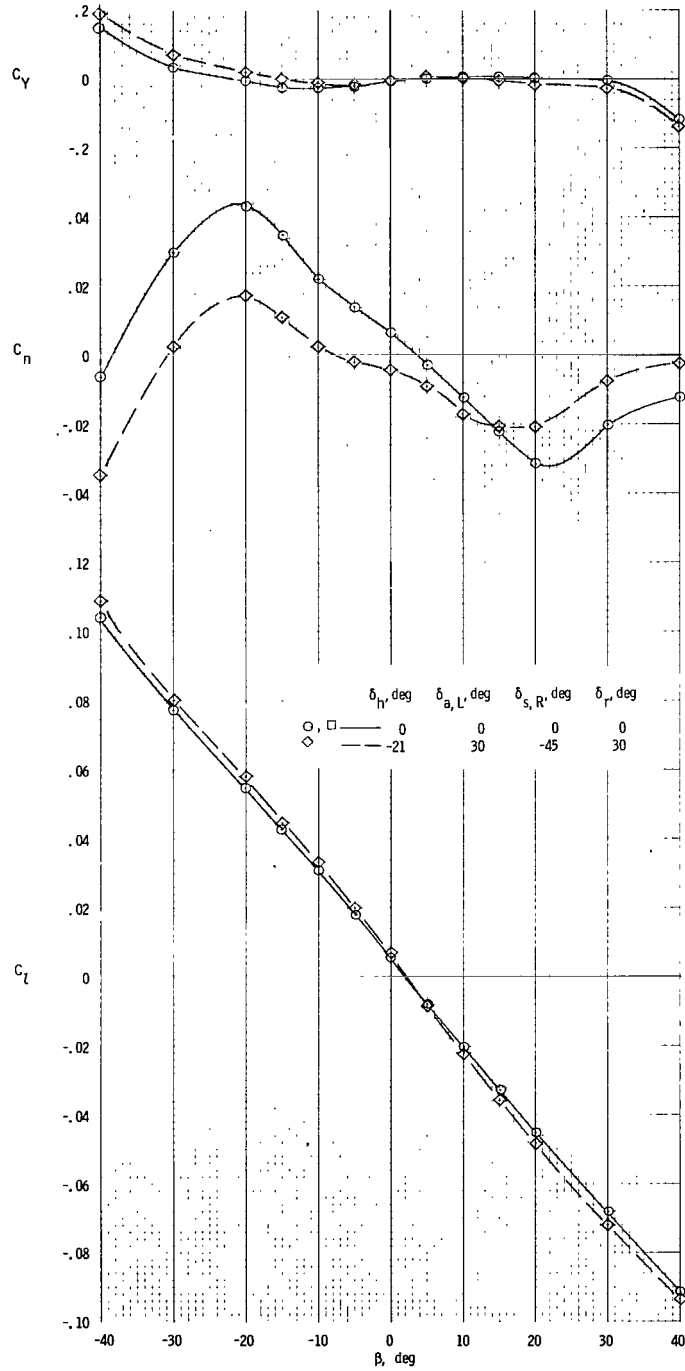
(i) $\alpha = 60^\circ$.

Figure 10.- Continued.



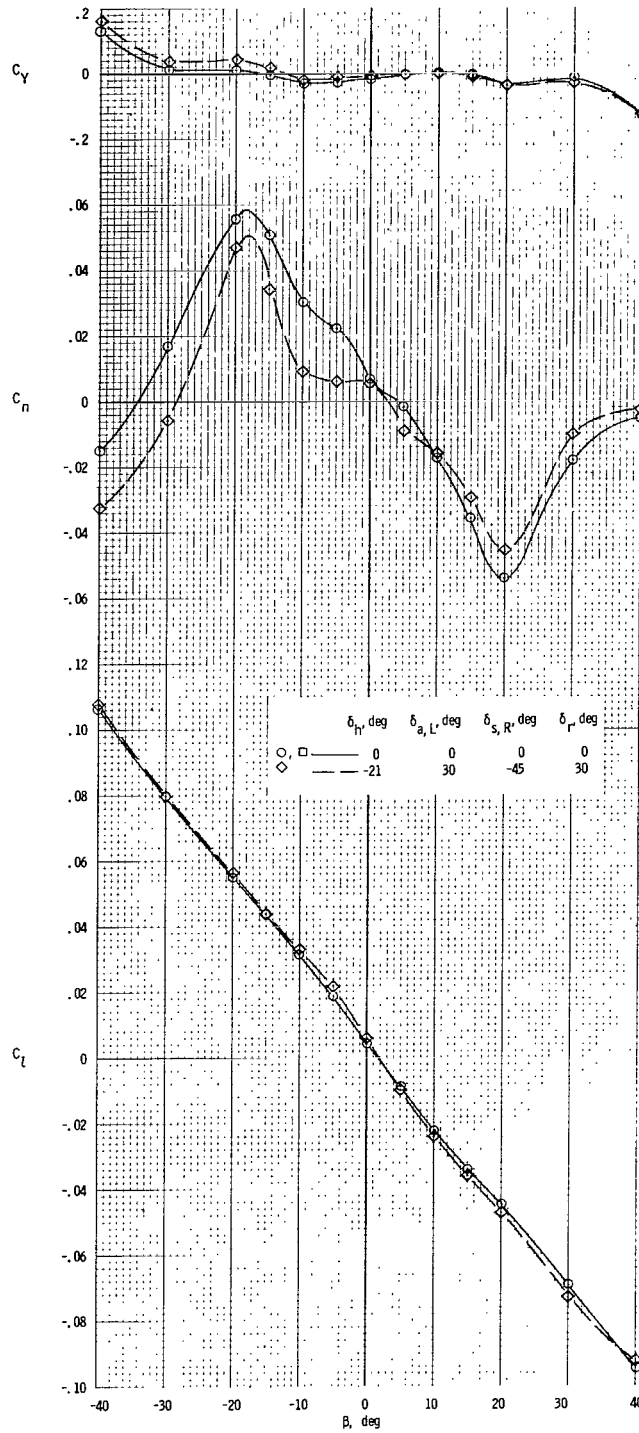
(j) $\alpha = 65^\circ$.

Figure 10.- Continued.



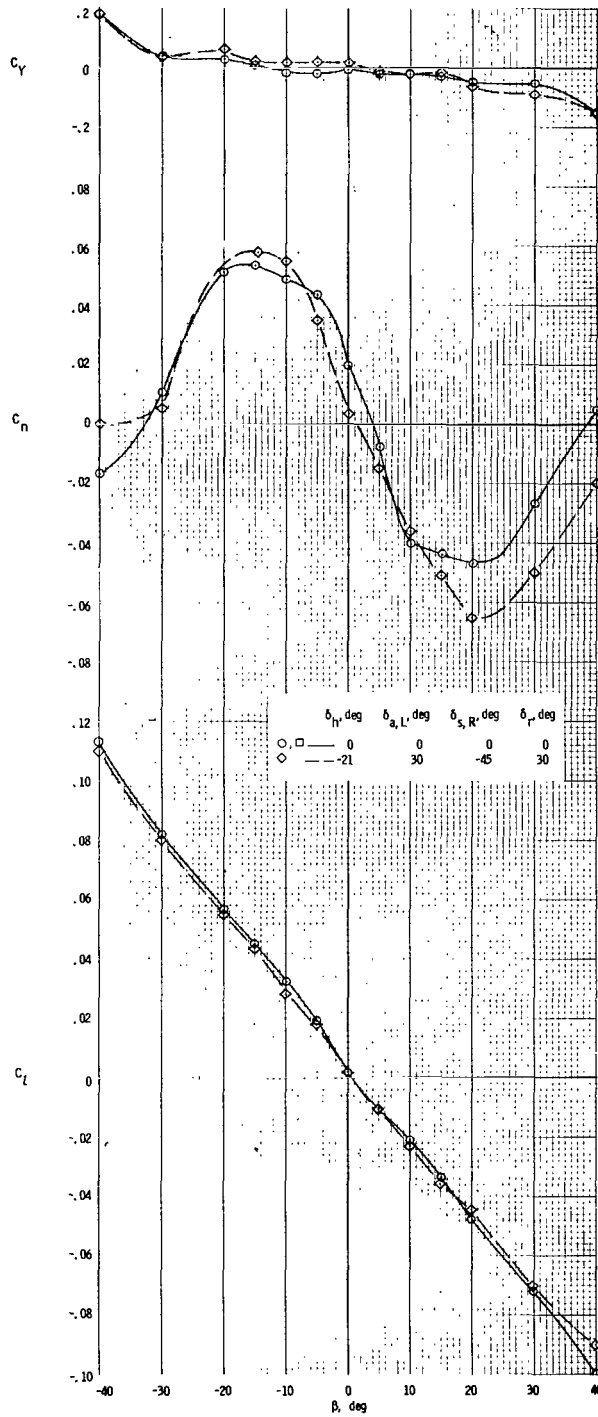
(k) $\alpha = 70^\circ$.

Figure 10.- Continued.



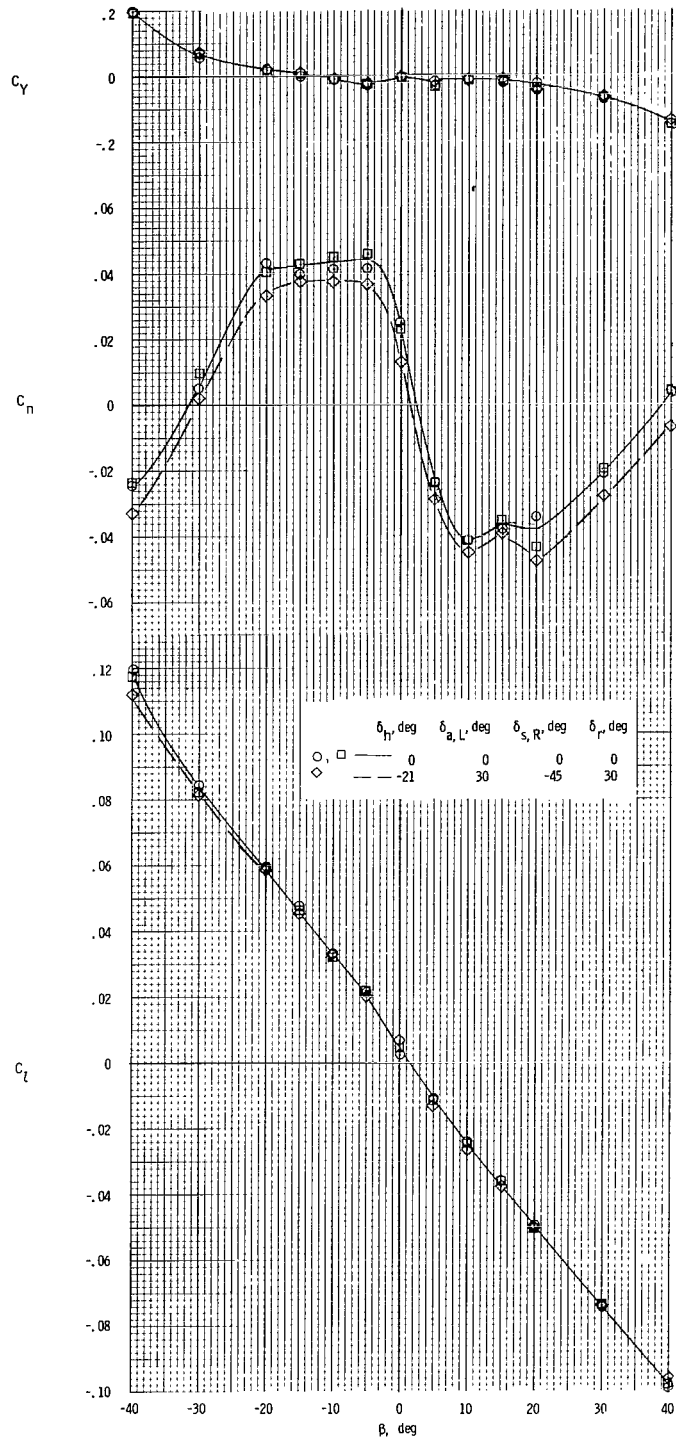
(l) $\alpha = 75^\circ$.

Figure 10.- Continued.



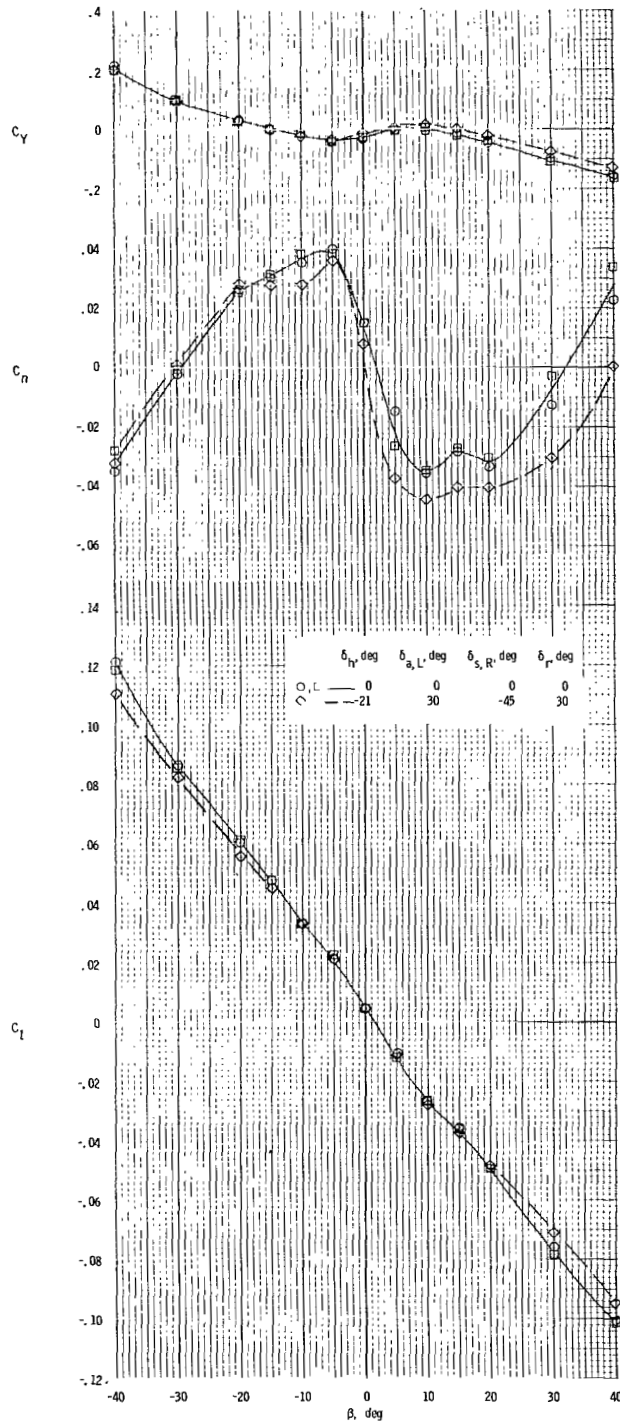
(m) $\alpha = 80^\circ$.

Figure 10.- Continued.



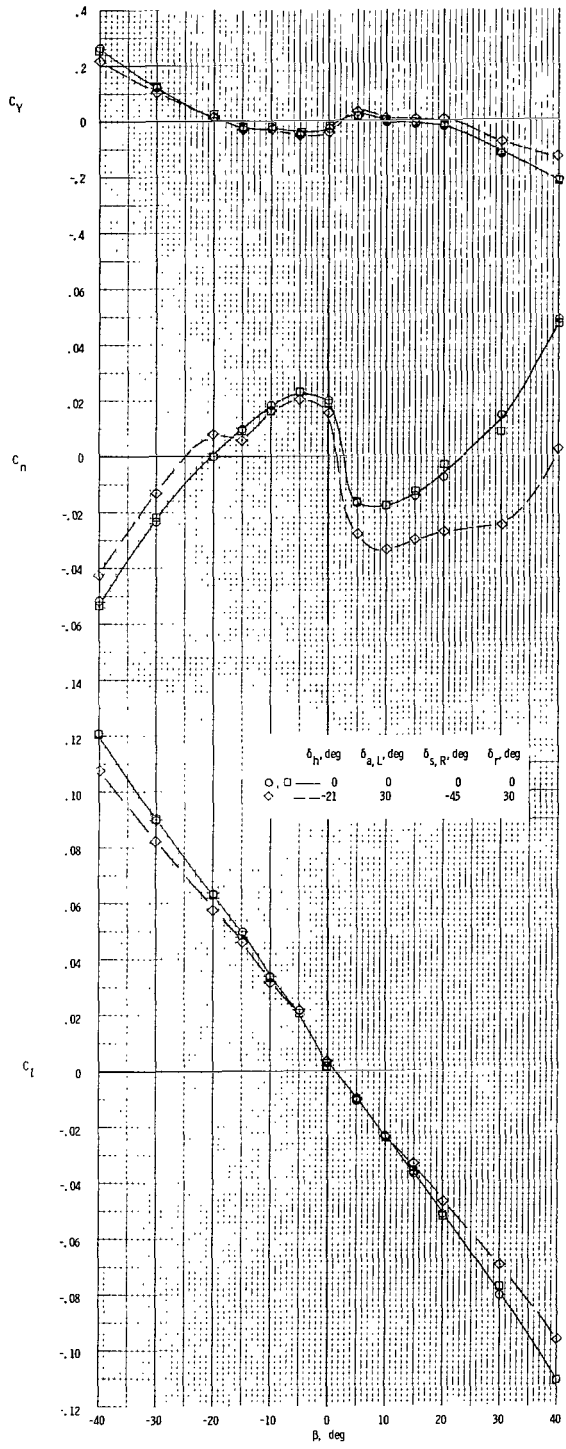
(n) $\alpha = 85^\circ$.

Figure 10.- Continued.

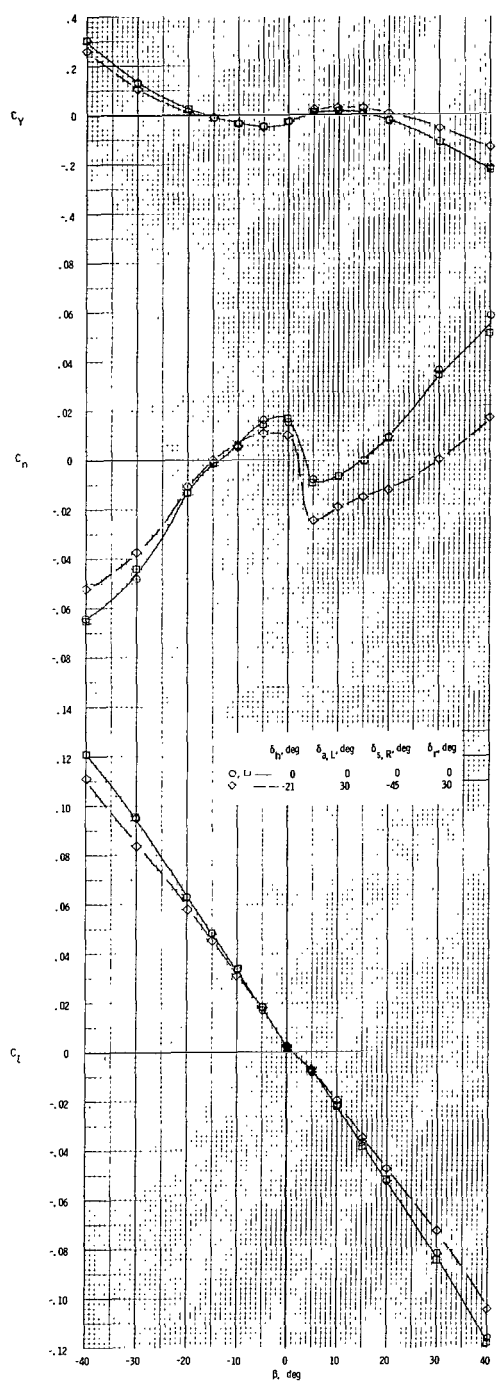


(o) $\alpha = 90^\circ$.

Figure 10.- Continued.

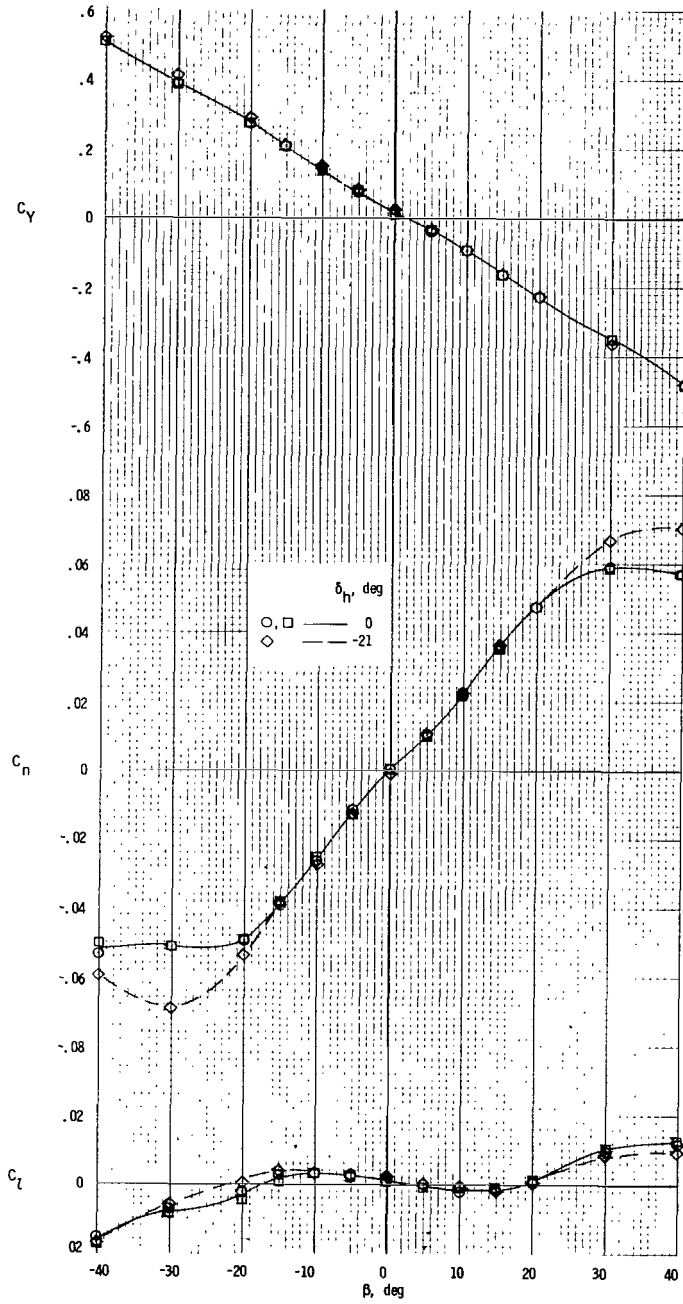


(p) $\alpha = 100^\circ$.



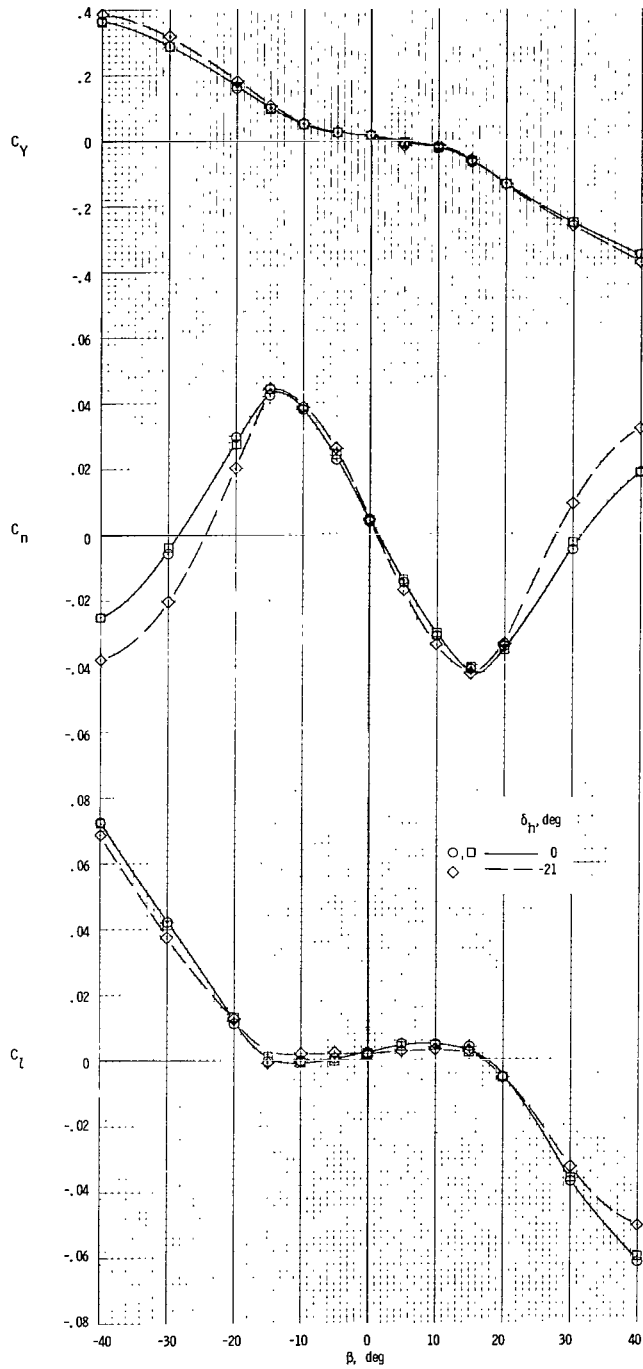
(q) $\alpha = 110^\circ$.

Figure 10.- Concluded.



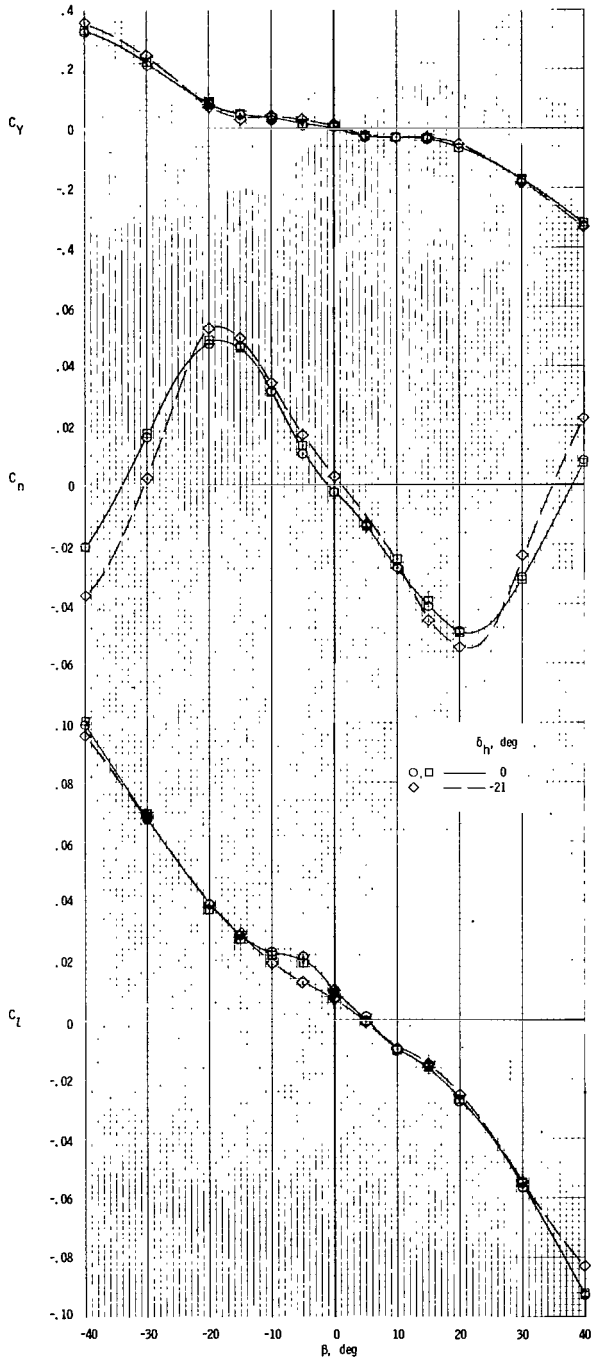
(a) $\alpha = 0^\circ$.

Figure 11.- Effect of elevator deflection on the static lateral-directional stability coefficients as a function of angle of attack and sideslip angle. $\delta_h = 0^\circ$. (Double symbols, when used, show repeat tests.)

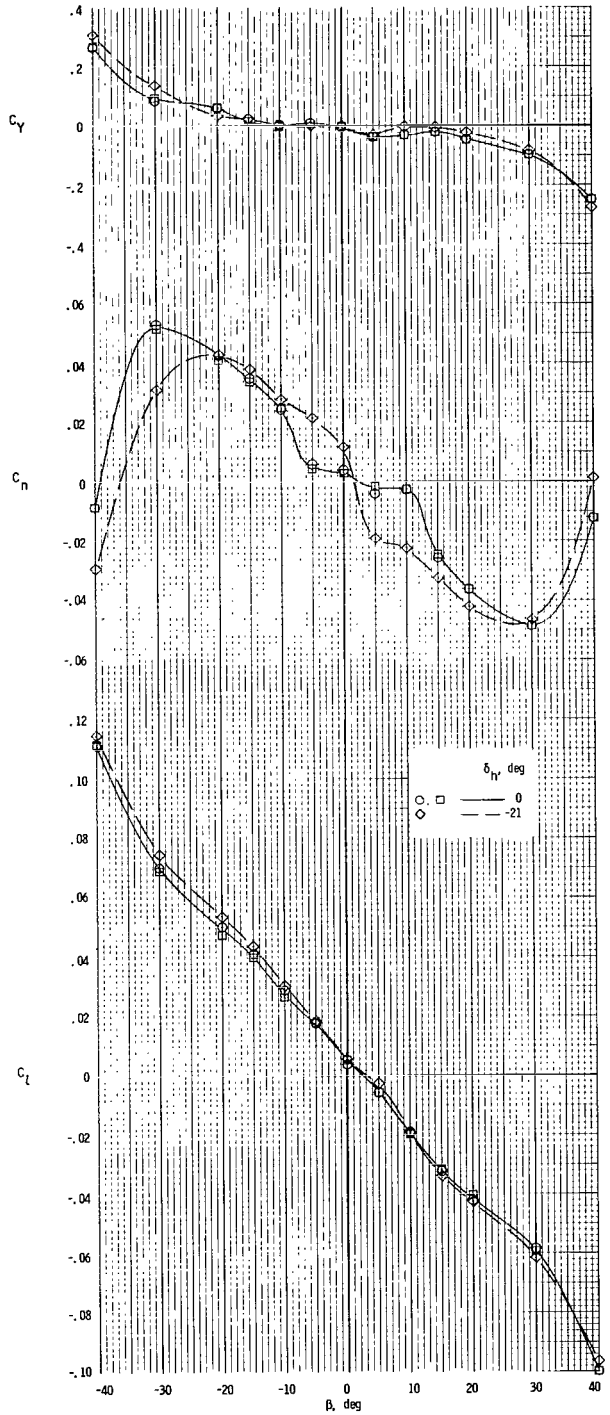


(b) $\alpha = 30^\circ$.

Figure 11.- Continued.

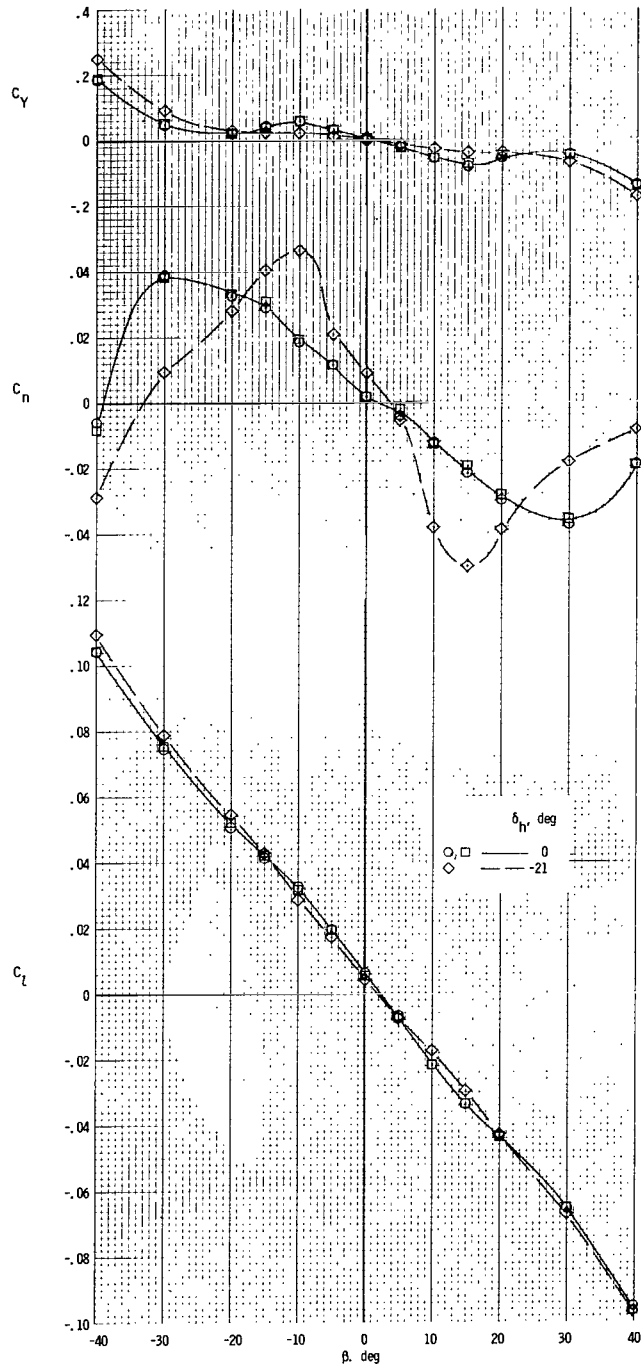


(c) $\alpha = 40^\circ$.



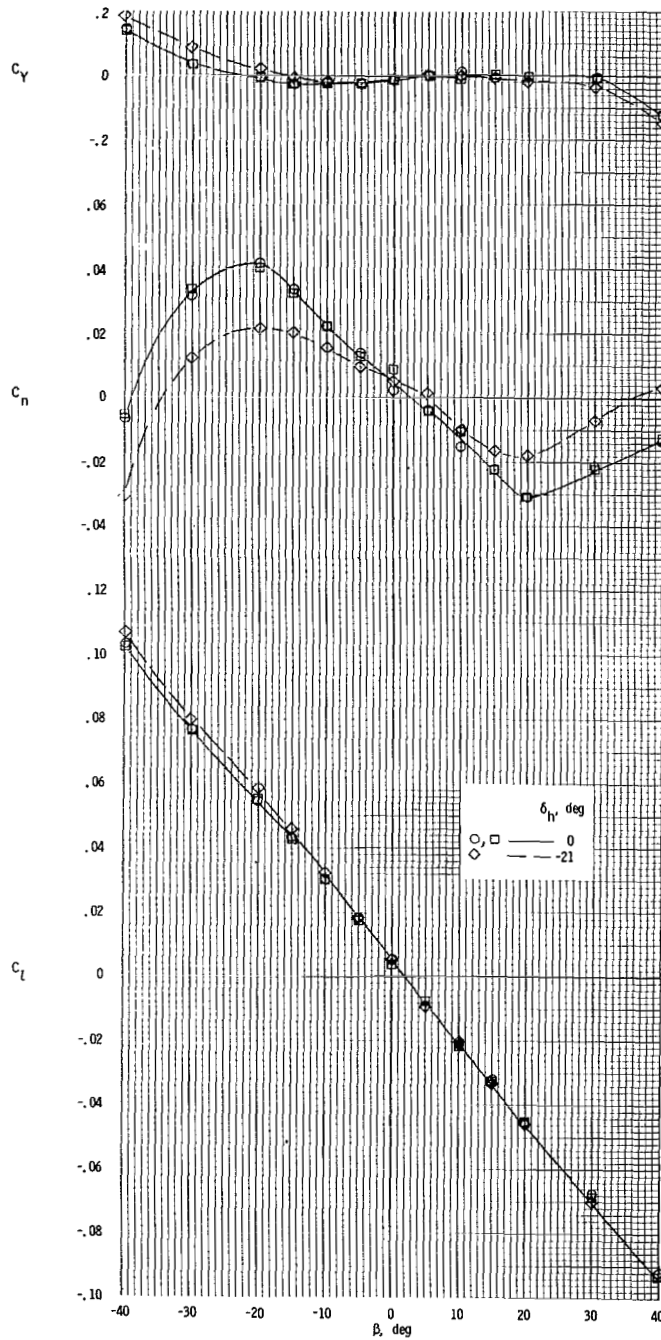
(d) $\alpha = 50^\circ$.

Figure 11.- Continued.



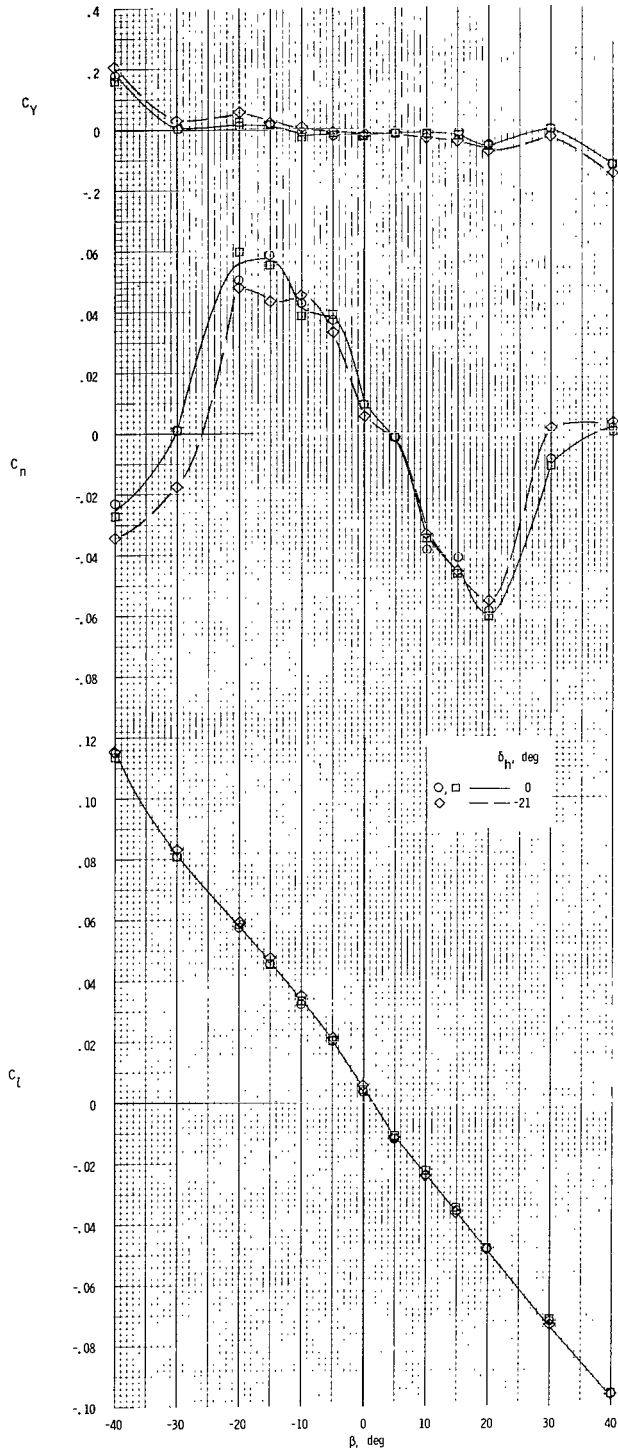
(e) $\alpha = 60^\circ$.

Figure 11.- Continued.

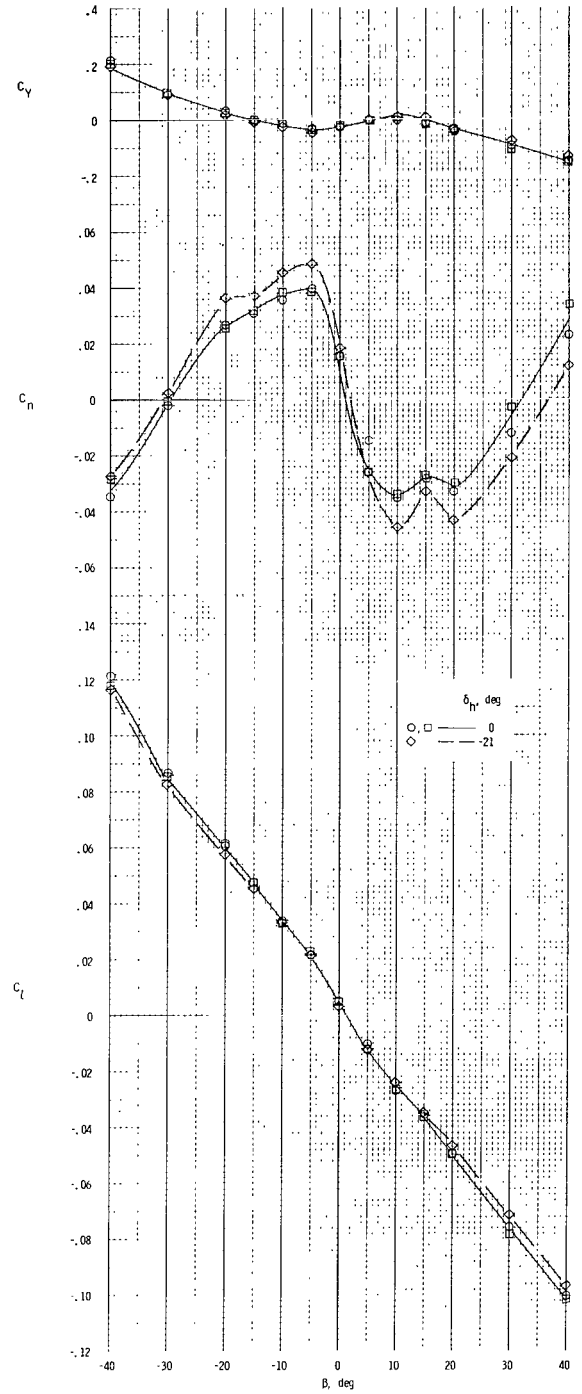


(f) $\alpha = 70^\circ$.

Figure 11.- Continued.

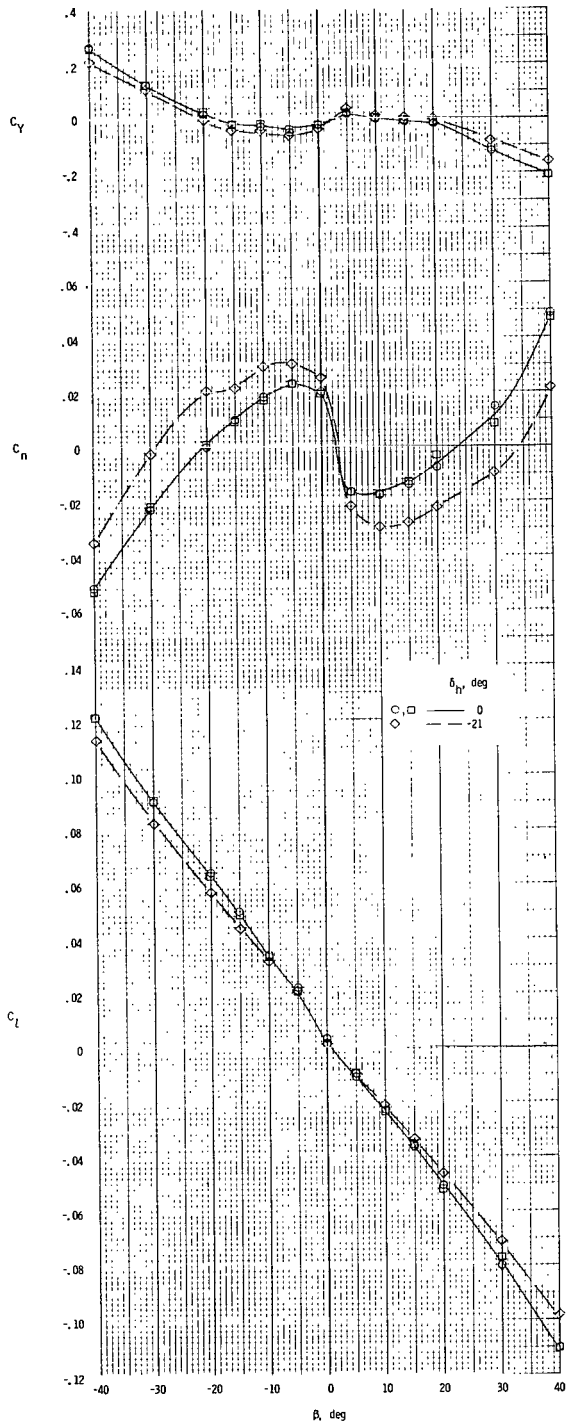


(g) $\alpha = 80^\circ$.

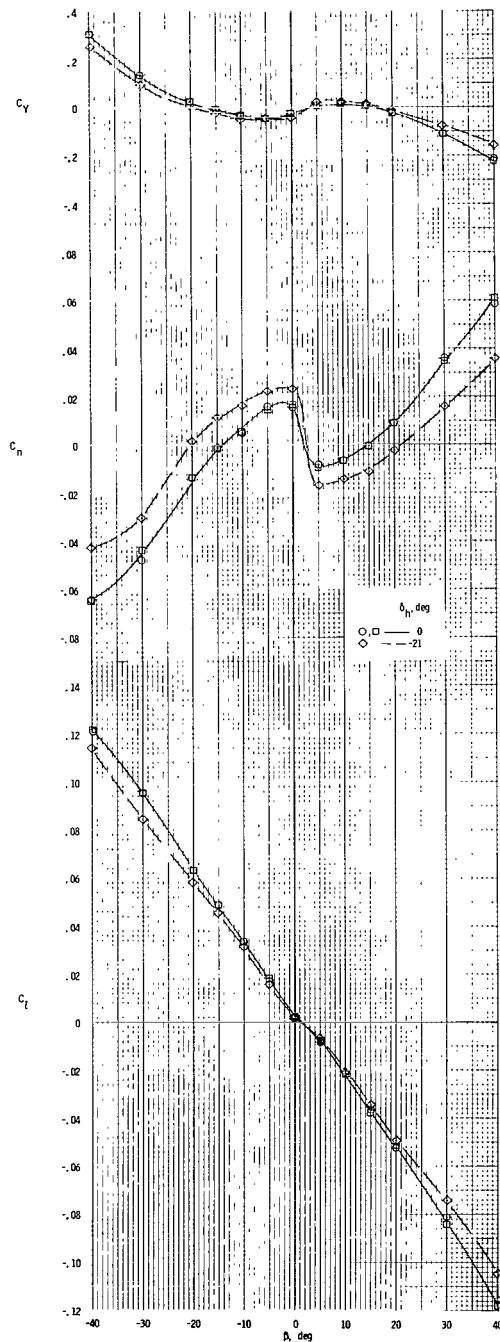


(h) $\alpha = 90^\circ$.

Figure 11.- Continued.



(i) $\alpha = 100^\circ$.



(j) $\alpha = 110^\circ$.

Figure 11.- Concluded.

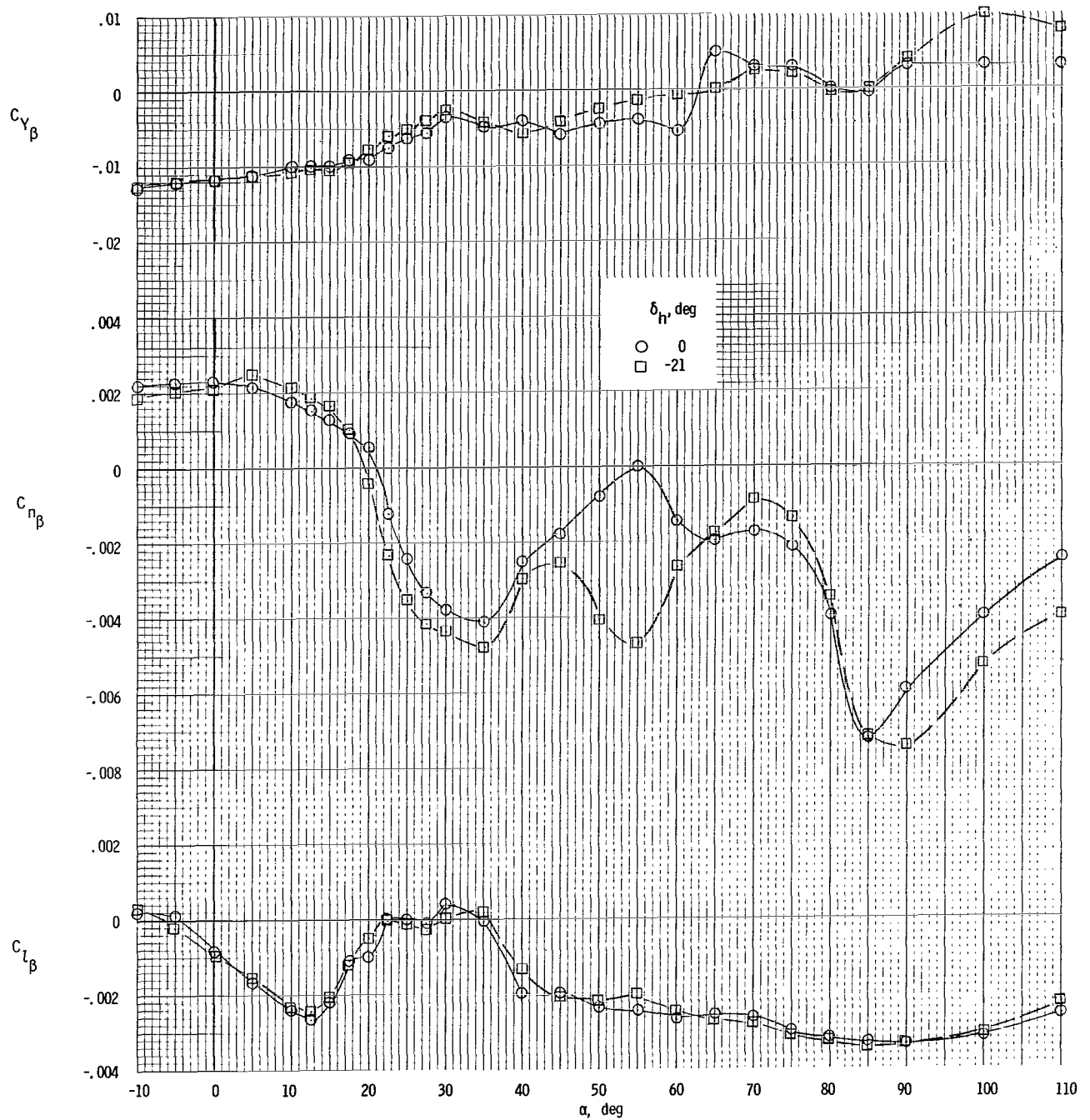


Figure 12.- Effect of horizontal-tail position on the static lateral-directional stability derivatives (data taken for $\beta = \pm 5^\circ$).

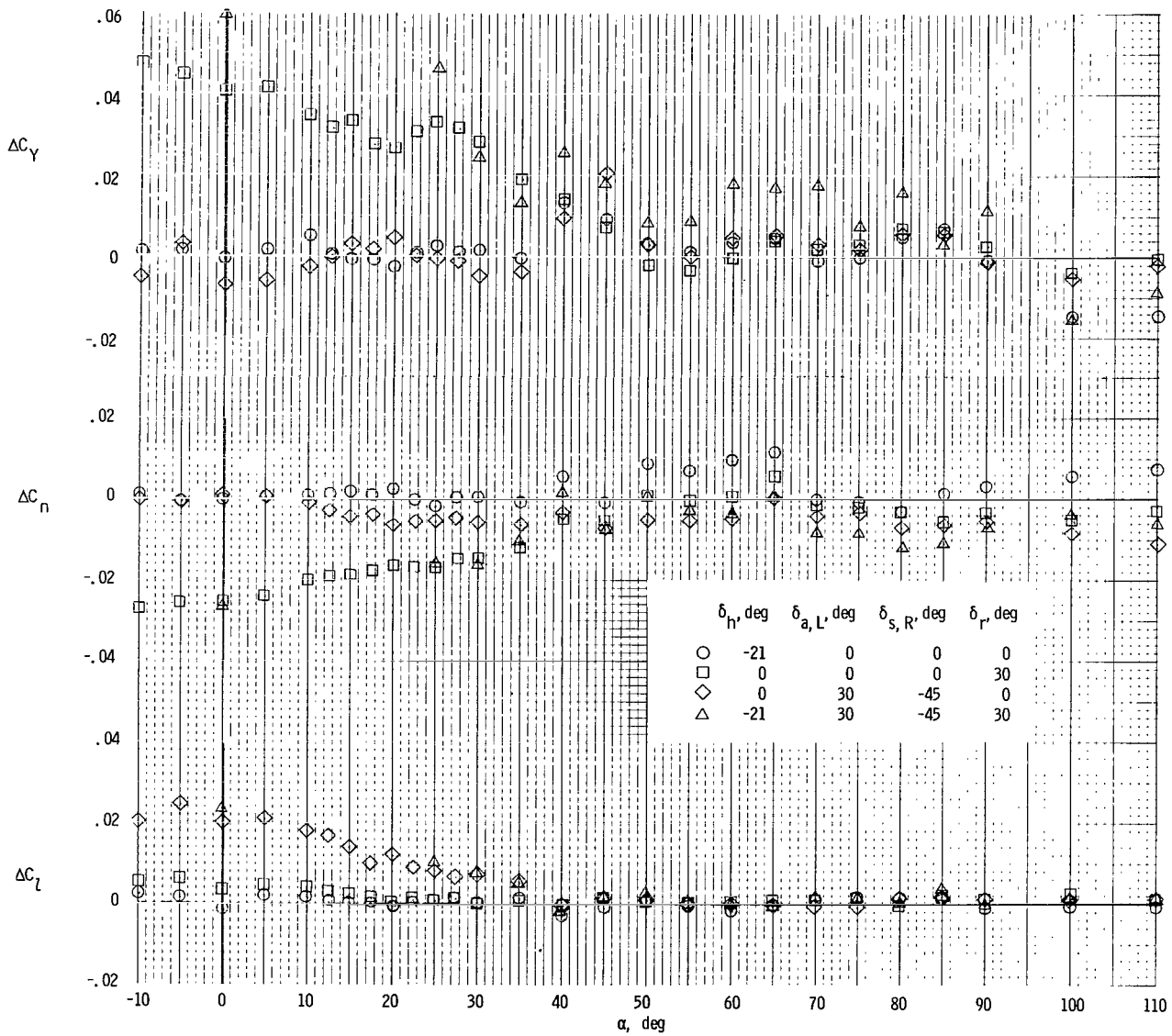


Figure 13.- Comparison of effectiveness of different control combinations on the static lateral-directional stability coefficient. $\beta = 0^\circ$.

NATIONAL AERONAUTICS AND SPACE ADMINISTRATION

WASHINGTON, D. C. 20546

OFFICIAL BUSINESS

PENALTY FOR PRIVATE USE \$300

FIRST CLASS MAIL



POSTAGE AND FEES PAID
NATIONAL AERONAUTICS AND
SPACE ADMINISTRATION

004 001 C1 U 02 710730 S00903DS
DEPT OF THE AIR FORCE
WEAPONS LABORATORY /WLOL/
ATTN: E LOU BOWMAN, CHIEF TECH LIBRARY
KIRTLAND AFB NM 87117

POSTMASTER: If Undeliverable (Section 158
Postal Manual) Do Not Return

"The aeronautical and space activities of the United States shall be conducted so as to contribute . . . to the expansion of human knowledge of phenomena in the atmosphere and space. The Administration shall provide for the widest practicable and appropriate dissemination of information concerning its activities and the results thereof."

— NATIONAL AERONAUTICS AND SPACE ACT OF 1958

NASA SCIENTIFIC AND TECHNICAL PUBLICATIONS

TECHNICAL REPORTS: Scientific and technical information considered important, complete, and a lasting contribution to existing knowledge.

TECHNICAL NOTES: Information less broad in scope but nevertheless of importance as a contribution to existing knowledge.

TECHNICAL MEMORANDUMS: Information receiving limited distribution because of preliminary data, security classification, or other reasons.

CONTRACTOR REPORTS: Scientific and technical information generated under a NASA contract or grant and considered an important contribution to existing knowledge.

TECHNICAL TRANSLATIONS: Information published in a foreign language considered to merit NASA distribution in English.

SPECIAL PUBLICATIONS: Information derived from or of value to NASA activities. Publications include conference proceedings, monographs, data compilations, handbooks, sourcebooks, and special bibliographies.

TECHNOLOGY UTILIZATION PUBLICATIONS: Information on technology used by NASA that may be of particular interest in commercial and other non-aerospace applications. Publications include Tech Briefs, Technology Utilization Reports and Technology Surveys.

Details on the availability of these publications may be obtained from:

SCIENTIFIC AND TECHNICAL INFORMATION OFFICE

NATIONAL AERONAUTICS AND SPACE ADMINISTRATION

Washington, D.C. 20546